Universidade de Aveiro
2021

NÉLIA PATRÍCIA VITORINO FERREIRA

SÍNTESE E ESTUDOS DE CITOTOXICIDADE DE PIRAZÓIS PARA REVERTER DANOS NO ADN E NEURODEGENERAÇÃO INDUZIDOS POR STRESS OXIDATIVO

SYNTHESIS AND CYTOTOXICITY STUDIES OF PYRAZOLES TO COUNTERACT DNA DAMAGE AND NEURODEGENERATION INDUCED BY OXIDATIVE STRESS

Universidade de Aveiro
2021

NÉLIA PATRÍCIA VITORINO FERREIRA

SÍNTESE E ESTUDOS DE CITOTOXICIDADE DE PIRAZÓIS PARA REVERTER DANOS NO ADN E NEURODEGENERAÇÃO INDUZIDOS POR STRESS OXIDATIVO

Dissertação apresentada à Universidade de Aveiro para cumprimento dos requisitos necessários à obtenção do grau de Mestre em Bioquímica, realizada sob a orientação científica da Doutora Vera Lúcia Marques da Silva, Professora Auxiliar do Departamento de Química da Universidade de Aveiro, e coorientação da Doutora Sandra Maria Tavares da Costa Rebelo, Professora Auxiliar do Departamento de Ciências Médicas da Universidade de Aveiro

“Deus não exige nada do Homem, sem oferecer-lhe ao mesmo tempo, a força para isso.”
(Santa Teresa Benedita da Cruz)

o júri

presidente

Prof. Doutor Mário Manuel Quialheiro Simões
professor auxiliar da Universidade de Aveiro

Prof. Doutora Vera Lúcia Marques da Silva
professora auxiliar da Universidade de Aveiro

Prof. Doutora Carla Alexandra Pina da Cruz Nunes
professora auxiliar da Universidade de Aveiro

agradecimentos

Às minhas orientadoras, professora Vera Silva e professora Sandra Rebelo, pela orientação deste trabalho e aconselhamento científico.

À aluna de Doutoramento, Sónia Lopes, pelo bom ambiente de trabalho no QOPNA/ LAQV-REQUIMTE e pela amizade criada.

À aluna de Doutoramento, Cátia Pereira pelos ensinamentos práticos que me transmitiu no iBiMED - Institute of Biomedicine.

À aluna de Doutoramento, Bárbara Sousa pela sua disponibilidade para ajudar e ensinar, com gosto, dedicação e simpatia.

À Dra. Mónica Pinho pela proximidade, disponibilidade e amabilidade com que me acompanhou nesta etapa.

Aos meus amigos da Residência Universitária, David, José, Inês, Marjorie e Rúben, por terem partilhado comigo este percurso e pela sua amizade.

Ao Marcelo, pela presença incondicional, disponibilidade, compreensão, força e carinho.

À minha irmã e ao meu cunhado, Susana e Carlos, pelas palavras de incentivo.

Aos meus pais, Helena e Agostinho, por terem dado sempre o melhor de si para me impulsionar o mais longe possível, por me terem ensinado a dar sempre o meu melhor em qualquer situação a que me proponha, e por me mostrarem continuamente que desistir nunca deve fazer parte das minhas opções.

palavras-chave

pirazóis, síntese, stress oxidativo, neurodegeneração, danos no ADN, citotoxicidade, histona H2AX

resumo

Atualmente, as doenças neurodegenerativas são as mais prevalentes e preocupantes na população idosa, sendo um importante foco de estudo da comunidade científica. Este conjunto de doenças é vasto e inclui, por exemplo, a doença de Alzheimer, a doença de Parkinson e a esclerose lateral amiotrófica. Dado que a esperança média de vida está a aumentar, surgem mais preocupações com as doenças relacionadas com a idade. Estas são genericamente caracterizadas por uma degeneração neuronal progressiva e irreversível, que culmina com a destruição e morte de certas populações de neurónios, surgindo complicações funcionais, como perda de memória e de outras funções cognitivas, disfunções motoras, dificuldades de linguagem e problemas respiratórios, que levam à morte.

Existem várias teorias para explicar a origem dessas doenças. Uma das mais importantes sugere que a neurodegeneração é causada pela existência de um ambiente oxidante, resultante de stress oxidativo, que é prejudicial a todos os tecidos do nosso organismo. Este define-se como um desequilíbrio entre a quantidade de espécies oxidantes e antioxidantes no organismo. Essas espécies oxidantes são prejudiciais por interagirem com proteínas e lípidos, resultando em danos nos tecidos, nomeadamente do sistema nervoso, um tecido particularmente sensível à neurodegeneração, e com os ácidos nucleicos podendo resultar em danos no ADN. Para reverter o stress oxidativo, o organismo produz antioxidantes, e para reverter o dano no ADN, vias de reparo do dano no ADN são ativadas. As vias de reparo mais importantes, em particular para o reparo de danos do tipo SSB, o dano mais comum induzido por ROS, são as vias BER e PARP. Quando o erro não é reparado, pode culminar em morte e degeneração celular.

Alvos de crescente atenção em investigação científica, os pirazóis são compostos sintéticos que possuem diversas atividades biológicas, nomeadamente anti-inflamatória, antioxidante e neuroprotetora. Este trabalho pretende, em primeiro lugar, apresentar uma análise dos mecanismos pelos quais o stress oxidativo interage com os tecidos vivos, nomeadamente no processo de neurodegeneração e no surgimento de dano do ADN bem como os mecanismos pelos quais o próprio dano do ADN é também capaz de conduzir à neurodegeneração. De seguida, apresentam-se os mecanismos moleculares de reversão desses danos e estudos que mostram a ação de compostos semelhantes aos estudados neste trabalho na reversão do stress oxidativo, atuando como antioxidantes e do dano de ADN atuando como potencializadores das vias de reparo. Em resumo, será estudada neste trabalho a possibilidade teórica de pirazóis serem eficazes na reversão da neurodegeneração e dos danos de ADN causados pelo stress oxidativo em organismos vivos. Assim, inicialmente foram sintetizados compostos do tipo estirilpirazóis e caracterizados por espetroscopia de ressonância magnética nuclear e espetrometria de massa de modo a confirmar a sua estrutura e pureza. Posteriormente, procedeu-se a estudos *in vitro* para avaliar a citotoxicidade dos compostos sintetizados, em células humanas, usando o método da resazurina e estes estudos foram ainda complementados por estudos de Western-Blot para avaliar o dano no ADN. Os resultados obtidos permitiram estabelecer alguns estudos de estrutura-atividade preliminares que são importantes para o desenho de novos compostos deste tipo e indicaram que, em geral, os compostos estudados não são citotóxicos ou apenas apresentam citotoxicidade significativa em concentrações mais elevadas, sendo assim promissores para o seguimento dos estudos iniciados neste trabalho.

keywords

Pyrazoles, synthesis, oxidative stress, neurodegeneration, DNA Damage, Cytotoxicity, H2AX Histone

abstract

Currently, neurodegenerative diseases are the most prevalent and worrying in the elderly population, being an important focus of study in the scientific community. This set of diseases is vast and includes, for example, Alzheimer's disease, Parkinson's disease and amyotrophic lateral sclerosis. Given that the average life expectancy is increasing, more concerns about age-related diseases arise. The latter are generally characterized by a progressive and irreversible neuronal degeneration, which culminates in the destruction and death of certain populations of neurons resulting in functional complications such as loss of memory and other cognitive functions, motor dysfunction, language difficulties and respiratory problems, which lead to death.

There are several theories to explain the origin of these diseases. One of the most important ones suggests that neurodegeneration is caused by the existence of an oxidizing environment, caused by oxidative stress, which is harmful to living tissues. The oxidative stress is defined as an imbalance between the amount of oxidant and antioxidant species in the body. These oxidizing species are harmful because they interact with proteins and lipids, resulting in tissue damage, namely in the nervous system, a particularly vulnerable tissue, and with nucleic acids leading to DNA damage. To counteract oxidative stress, body produces antioxidants and to counteract DNA damage, DNA damage repair pathways are activated. The most important repair pathways, in particular for single-strand chain damage repairing (SSB), the most common damage induced by reactive oxygen species (ROS), is the BER and the PARP pathways. When the error is not repaired, it might culminate in cell death and degeneration.

Targets of increasing attention in scientific research, pyrazoles are synthetic compounds that have several biological activities, including anti-inflammatory, antioxidant and neuroprotective. This work intends, firstly, to present an analysis of the mechanisms by which oxidative stress interacts with living tissues, namely in the neurodegeneration process and the occurrence of DNA damage, as well as the mechanisms by which DNA damage itself is also capable to cause neurodegeneration. Next, the molecular mechanisms for reversing these damages are presented and studies showing the action of compounds similar to those studied in this work in reversing oxidative stress, acting as antioxidants, and DNA damage by acting as activators of repair pathways. In summary, the theoretical possibility of pyrazoles being effective in reversing neurodegeneration and DNA damage caused by oxidative stress in living organisms will be studied in this work. Thus, initially styrylpyrazole-type compounds were synthesized and characterized by nuclear magnetic resonance spectroscopy and mass spectrometry in order to confirm their structure and purity. Subsequently, *in vitro* studies were carried out to assess the cytotoxicity of the synthesized compounds, in human cells, using the resazurin method and these studies were further complemented by Western-Blot studies to assess DNA damage. The results obtained allowed establishing some preliminary structure-activity studies that are important for the design of new compounds of this type and indicated that, in general, the studied compounds are not cytotoxic or only present significant cytotoxicity at higher concentrations, thus being promising for the follow-up of the studies initiated in this work.

ABBREVIATIONS LIST

$ABTS^{+\bullet}$	2,2′-Azinobis-(3-ethylbenzothiazoline-6-sulphonate)
AD	Alzheimer's Disease
ALS	Amyotrophic lateral sclerosis
AP	Abasic sites
APS	Ammonium persulfate
ATCC	American Type Culture Collection
BCA	Bicinchoninic acid assay
BER	Base excision repair
BSA	Albumin bovine serum
CAT	Catalase
CNS	Central nervous system
COX-2	Cyclooxygenase-2
CPD	Cyclobutane pyrimidine dimers
d	Doublet
DCC	Dicyclohexylcarbodiimide
dd	Double doublet
ddd	Double doublet of doublets
DDR	Damage Repair
DHA	Docosahexaenoic acid
DMEM	Dulbecco modified eagle medium
DMSO	Dimethylsulfoxide
DNA	Desoxyribonucleic acid

dNTPs	Desoxyribonucleotide triphosphate
DSB	Double strand break
dt	Double triplet
ECD	Electrochemical detection
EDTA	Ethylenediamine tetraacetic acid
EPA	Eicosapentaenoic acid
EPR	Electron paramagnetic ressonance
equiv	Molar equivalent
FBS	Fetal bovine serum
FRAP	Ferric reducing antioxidant power assay
GC	Gas chromatography
GPx	Glutathione peroxidase
GSH	Glutathione
h	hour
H2A.X	Histone from the H2A family encoded by the H2AFX gene
HD	Huntington's disease
HMBC	Heteronuclear Multiple Bond Coherence
HRP	Horseradish peroxidase
HR	Homologous recombination
HSQC	Heteronuclear single quantum coherence
IR	Ionizing radiation
IUPAC	International Union of Pure and Applied Chemistry
J	Coupling constant
LC	Liquid chromatography

LGB	Lower gel buffer
Lit.	Literature
m	Multiplet
MDA	Malondialdehyde
min	Minute
MMR	Mismatch repair
mp.	Melting point
MS	Mass spectrometry
MS/MS	Tandem MS
NER	Nucleotide excision repair
ND	Neurodegenerative diseases
NHEJ	Non-homologous end joining
NMR	Nuclear magnetic resonance spectroscopy
NO	Nitric oxide
NOS	Nitric oxide synthase
ORAC	Oxygen radical absorbance capacity
PARP	Poly [ADP-ribose] polymerase 1
PBS	Phosphate buffered salin
PD	Parkinson's disease
4-PPy	4-Pirrolidinopyridine
RNS	Reactive nitrogen species
ROS	Reactive oxygen species
r.t.	Room temperature
SAR	Structure-activity relationship

SCGE	Single cell gel electrophoresis assay
SDS	Sodium dodecyl sulfate
SNP	Single nucleotide polymorphism
SOD	Superoxide dismutase
SSB	Single strand break
TAS	Total oxidant status
TBARS	Thiobarbituric acid reactive substances
TBS	Tris-buffered saline
TBS-T	Tris-buffered saline with tween
TDP43	Transactive response DNA binding protein 43
TEMED	Tetramethylethylenediamine
TLC	Thin layer chromatography
UGB	Upper gel buffer
UV	Ultraviolet
ϒH2A.X	Phosphorylated H2A.X
WB	Western blotting
^{1}H NMR	Proton nuclear magnetic resonance spectroscopy
5-HMdU	5-Hydroxymethyl-2'-deoxyuridine
8-OHdG	8-Hydroxy-2' -deoxyguanosine
8-oxoG	8-Oxo-7,8-dihydroguanine
^{13}C NMR	Carbon-13 nuclear magnetic resonance spectroscopy
δ	Chemical shift

FIGURES LIST

SCHEMES LIST

TABLES LIST

INDEX

CHAPTER 1

INTRODUCTION

CHAPTER 1: INTRODUCTION

1.1. Neurodegenerative Diseases

Nowadays, cases of neurodegenerative diseases (ND) are increasing significantly, and they represent a major threat to human's health. Since the onset of these diseases is closely related to aging, this predominance may be due to the increase of the elderly population in recent year[1,2]. Besides that, the current prevalence is alarming, being estimated that around 50 million people worldwide suffer from conditions like this and it is predicted that the number of affected people with more than 60 years old will double each 5 years[3]. Therefore, although life expectancy is better, the observation that almost all older brains exhibit characteristic changes, probably linked to neurodegenerative diseases, makes these as the most feared kind of diseases for the elderly[2,4]. The increase of elderly population and the fact that neurodegenerative diseases are very disabling makes the study of these diseases a major issue between the scientific community[5].

ND are a very heterogeneous group of disorders, where the main events are progressive, irreversible and selective, affecting particular brain areas of anatomically or physiologically related neuronal systems[6], meaning that there is a neuronal vulnerability for degenerative mechanisms in brain specific regions, causing neuronal populations damage and/or dead[7]. Alzheimer's disease (AD), Parkinson's disease (PD), Huntington's disease (HD), amyotrophic lateral sclerosis (ALS) and frontotemporal dementia are well known examples of ND[2,8–13]. For example, in AD, hippocampal and cortical neurons progressively die, in PD the dopaminergic midbrain neurons of the *substantia nigra pars compacta* are the most affected, while in HD and ALS specifically the striatum neurons and motor neurons are injured, respectively[14].

Despite all these ND present different pathophysiological mechanisms, they all share common characteristics, namely protein misfolding and aggregation, and their specific and distinct brain hallmarks are characterized by formation, aggregation and deposition of abnormal insoluble filamentous brain proteins[2,7,9,10,12,13,15]. These abnormal protein accumulations are responsible for neuronal cell toxicity, leading to cell function impairment and death, being the major cause of ND[4]. In AD, there is an increase in beta-amyloid (Aβ) generation and accumulation as extracellular deposits-amyloid plaques.

Further, there is also an hyperphosphorylation of Tau protein forming the intracellular neurofibrillary tangles. Both amyloid plaque and neurofibrillary tangles are the two main AD hallmarks. The presence of alpha- synuclein in Lewy bodies composition is one of the hallmarks of PD. The transactive response DNA binding protein 43 (TDP43) is the hallmark of both frontotemporal dementia and ALS[16–18]. As a result, many functional complications occur leading to different symptoms, including cognitive and memory impairments, motor disorders, decline in language, breathing problems, among others[2,9,10,12].

Nevertheless, there are many and distinct clinical phenotypes and genetic etiologies for ND[7]. Beyond the age, the onset of this diseases is mainly due to the environment (lifestyle, diet, exposure to substances, etc.) and stochastic events, and controlled by genetics. Many genetic and epigenetic studies have been made to understand the molecular pathways of neurodegeneration, and genetics seems to make a major contribution. In that sense, neurodegeneration may be considered a consequence of an accelerated aging, being a dramatic and intensified manifestation of characteristics that are proper to aging, especially epigenetic modifications, like DNA methylation, among others[2,19,20].

In fact, it is known that aging is characterized by many individual processes, like loss of protein homeostasis, DNA damage, lysosomal dysfunction, epigenetic changes, and immune dysregulation, most of them being due to oxidative stress[21]. The genetic predisposition of the individual together with the exposure to the environment seems to determine each specific ND that will be developed. Despite the accurate pathophysiological mechanisms are not to date well established, researchers aim to understand how environmental factors and genetics contribute to a particular disease (AD, PD, HD, ALS, frontotemporal dementia) with different aging hallmarks[21]. Nonetheless, it is important to study the molecular mechanisms of these diseases, but also to study the mechanisms of physiological aging[19].

Despite of genetics importance, the etiology of different neuropathologies is not exactly known, but efforts to understand it have led to some hypotheses that may explain its origin and progress. Studies have been carried out to identify the risk factors that mediate several of these diseases, as a strategy to find ways to get around them. These studies showed that the main mediators of ND in general are excitotoxicity (glutamate

mediated), presence of reactive oxygen species and protein aggregates and even the presence of inflammatory processes and some defects in energy metabolism[22–25].

Among ND, AD is the most prevalent disease, being responsible for 60-80% of all cases of dementia[26]. AD is the third major cause of disability and death among the elderly population, after cardio and cerebrovascular diseases and cancer which occupy the first places (OMS data, 2019). Besides that, it is expected that the global prevalence of dementia doubles every 20 years, reaching 74.7 million cases in 2030, 81 million in 2040 and 131.5 million in 2050[26,27]. Being the most prevalent, we will focus our attention on AD throughout this work. To explain the origin and progress of AD, several hypotheses have been suggested[28] like the cholinergic hypothesis[29], the amyloid hypothesis[30], tau propagation hypothesis[31], mitochondrial cascade hypothesis[32], oxidative stress hypothesis[33,34] and metal ion hypothesis[35]. In addition, several factors have been associated to an increased risk of developing AD, like sleep disorders[36], some already identified Single Nucleotide Polymorphisms (SNPs)[37] and midlife hypertension[38].

1.2. Oxidative Stress

1.2.1. Introduction to Oxidative Stress

Oxygen is essential for living tissues once it is used by eukaryotic cells for performing their normal functions. It has a high redox capacity, so it can easily accept electrons from oxidized substrates, contributing for vital functions, including aerobic respiration. Of note, an hyperoxia state is a very dangerous situation for the tissues, because oxygen can be quite toxic[39,40] depending on its structure. The reduced oxygen forms, generated from the molecular oxygen (O_2), are more energetic than oxygen and, this way, they are very unstable and tend to interact with many molecules by accepting or giving electrons towards its stabilization. These active forms of oxygen, generated by oxidation/reduction reactions, are the most toxic, and are designated as reactive oxygen species (ROS). Examples of ROS are the superoxide anion radical ($O_2^{\bullet -}$), the hydroxyl radical ($HO^{\bullet}$), the hydrogen peroxide (H_2O_2) and the singlet oxygen ($^1O_2$)[41].

Besides oxygen, there is another molecule in the body responsible for several vital functions, including signaling processes. Nitric oxide ($NO^{\bullet}$) is formed endogenously by

the enzymatic oxidation of L-arginine by NO synthase (NOS) and, after that, it can directly induce signaling processes or can be converted by redox reactions into other nitrogen oxide species[42]. When it reacts with O_2 or with its radicals, it can lead to formation of other dangerous molecules, known as Reactive Nitrogen Species (RNS), of which NO_2 (nitrogen dioxide) and N_2O_3 (dinitrogen trioxide) are two examples. Therefore, ROS and RNS act together causing damage to the cell in a process named of oxidative and nitrosative stress[43].

Due to their high reactivity, ROS and RNS interact chemically with body biomolecules, inducing cell modifications and cell death and ultimately tissue damage. To overcame ROS and RNS toxicity, aerobic organisms have antioxidant defense systems that can block reactive species and prevent its toxic action in the body. Essentially, the antioxidant defense systems consist of stable molecules (antioxidants) having the ability to donate (oxidation) an electron to chemically unstable species (free radicals) and remain stable while this electron is given over to radical species (reduction) to stabilize them, so they lose the ability to interact with other molecules, for example body tissues causing damage[44].

Oxidative stress is a concept that was firstly described in 1985, by Helmut Sies, in the first introductory book chapter called “Oxidative Stress”[45]. In 1986 was published a review presenting oxidants, antioxidants, and showing their endogenous and exogenous sources[46]. Since then, this redox-biology research area has growing massively in areas like chemistry, biology and biochemistry, and also medicine[47]. Recently, in January 2020, there were 21 5120 results matching the expression "Oxidative Stress" in and in December 2021 there were 26 867 correspondent results.

Oxidative stress is defined as an imbalance between oxidant and antioxidant species in the human body. Oxidant species are products from aerobic metabolism, and in healthy conditions, antioxidant systems are capable to counteract them and keep the balance between oxidant and antioxidant species. Moreover, antioxidants are capable to adapt according to the needs. However, in pathophysiological conditions, for some reasons, antioxidants cannot counteract oxidants and an imbalance between them occurs. When the ROS production overcomes the antioxidant capacity, there is an excessive accumulation of ROS and oxidative stress arises[45,46,48,49]. The latter may cause tissue injury, since oxidative stress can cause lipid peroxidation, protein oxidation and nucleic acids damage. Hence, oxidative stress can damage cell membranes, inflict protein

structure and function changes and causes structural damages on DNA[50]. For that reason, oxidative stress is implicated on the onset and progression of diseases like cancer[51], neurodegenerative diseases[52,53], atherosclerosis, diabetes[54] and aging[55].

1.2.2. Oxidants and Antioxidants

Our body produces many types of ROS working as oxidants. In one hand, they can be considered oxidants that are produced in a deliberated way, meaning that there is a purpose for its production. One example is the production of $O_2^{\bullet-}$ and H_2O_2 by neutrophils, monocytes, macrophages, and eosinophils in a very important defense mechanism for killing bacteria and fungi and also for inactivating viruses. But in the other hand, they can be considered oxidants that are produced accidentally, when they are generated from some molecules through their direct reaction with oxygen. One example is the formation of $O_2^{\bullet-}$ and H_2O_2 in the presence of epinephrine hormone. Other and very significant example is the production of $O_2^{\bullet-}$ and H_2O_2 in mitochondria during cell respiration. There is a electrons transport chain from where a percentage of them directly escape forming $O_2^{\bullet-}$[56,57]. Besides that, there is also a biological production of NOS, especially in vessels, as a relaxing factor, and also in the brain by phagocytes for defense[58].

Interestingly, our body has their own antioxidant defense mechanisms to protect itself, always trying to achieve a perfect balance between oxidant and antioxidant species. The body antioxidant species can be divided in two groups: enzymes and non-enzymatic compounds. In the first group comprises substances able to participate in enzymatic responses that block oxidants activity, like superoxide dismutase (SOD) enzyme, glutathione peroxidase (GPx) and catalase (CAT)[59]. The second group includes non-enzymatic compounds as glutathione (GSH) and some antioxidants found in food or nutraceuticals as vitamin C (ascorbic acid), vitamin E (alfa-tocoferol) and vitamin A (beta-carotene)[56,57,59].

1.2.3. Oxidative Stress Contribution for Neurodegeneration

Although oxygen is essential for living tissues, being the major player in aerobic metabolism, each tissue has different oxygen requirements. The brain is one of the largest

oxygen consumers of whole body. In fact, brain represents only about 2% of the human body weight and is responsible for about 20% of total oxygen consumption. The main cells responsible for this consumption are neurons and astrocytes, the two major brain cell type[60]. For this reason, brain is particularly exposed to oxygen-derived dangers. In addition, neurons have a long life over which stress and damage will accumulate, and, when neurons are damaged, they have a low ability to regenerate[61].

Several studies associating oxidative stress with neurodegenerative diseases in general, and with AD, in particular, have been performed and are reviewed[40,52,62]. Many of them aim to explain the mechanisms behind each change that leads to cell death and neurodegeneration. Nowadays, it is very well-established that oxidative stress plays an important role in cell and tissue degeneration. ROS can interact with proteins, lipids and nucleic acids and, despite of it is a trigger for these processes, it is also a consequence for them. This means that ROS interact with molecules to cause damage or destruction of these biomolecules, and at the same time this destruction process generates more ROS, increasingly enhancing a cycle of high levels of ROS and high level of tissue destruction, that may culminate in neurodegeneration[51,63,64].

1.2.4. Antioxidant Therapies in Neurodegenerative Diseases

Since brain is highly exposed and sensitive to ROS damage, the antioxidant protection is extremely needed. When oxidative stress causes damage, such as neurodegeneration, it is possible to formulate the idea that this is not being counteracted sufficiently, that is, the antioxidant defenses are not enough, or they are not acting properly. Considering that oxidative stress is an important cause of neurodegeneration, thinking about fighting these diseases using therapies based in antioxidants has been an option all over the years.

The most studied antioxidants for clinical applications were vitamin E, that acts as a scavenger of radicals inhibiting brain lipid peroxidation; vitamin C, that works as an intracellular reducer molecule; and coenzyme Q10, that has an important role in the electrons transport along the electron transport chain in respiration[65,66]. Also some nutraceutical antioxidant experiments were conducted using ginseng, curcumin and garlic[67–70]. Later, compounds like polyphenols were also tested[71]. Besides that, some in vitro and in vivo animal studies have shown some neuroprotective activity and ability to

inhibit protein aggregation, characteristic in AD, for example, but results were not very effective when studies were performed in humans[66,72].

1.2.5. Oxidative Stress Induction and Measurement Methodologies

Given the important contribution of oxidative stress for developing ND, the identification of methodologies to induct and measure oxidative stress were mandatory. In terms of inducing oxidative stress in the laboratory, this can be done in different ways, namely by exposure to chemical substances. The most widely used method resorts hydrogen peroxide, which works as an oxidizer, reducing oxygen. This is fat-soluble and can therefore pass-through biological membranes[73].

In terms of measurement, essentially there are two different strategies to measure oxidative stress levels in laboratory: direct methods, where free radicals are directly quantified, and indirect methods, where the researcher looks for the levels of well-established oxidative stress markers. In the first group, electron paramagnetic resonance method (EPR) is considered the least ambiguous methodology and it allows to measure directly by spectroscopy the formation of radicals[74]. In the second group, it is possible to monitor the levels of several biomarkers, namely oxidation derivatives of lipids, proteins, and nucleic acids. Additionally, several biomarkers of antioxidant capacity, like TAS (Total oxidant status), FRAP (Ferric Reducing Antioxidant Power Assay) and ORAC (Oxygen radical absorbance capacity) could also be monitored[59]. A summary of the biomarkers used to evaluate the oxidative stress are resumed in **Table 1**.

Table 1: Biomarkers to evaluate oxidative stress. Adapted from Barbosa et al.[75]

Type of Biomarker	Biomarker	Description
Derivatives of lipids oxidation	MDA	Malondialdehyde. One of the most abundant lipid oxidation products. Mainly results from the oxidation of EPA and DHA.
	TBARS	Thiobarbituric acid reactive substances. By-product of lipid oxidation. It allows to quantify the formation of MDA.
Derivatives of proteins oxidation	Carbonyls	Results from the action of reactive species on amino acid side chains.
	3-Nitrosamine	Results from the action of reactive species on proteins.
Derivatives of nucleic acids oxidation	8-OHdG	Results from the guanine base oxidation.
	5-HMdU	Results from the thymine base oxidation.
Antioxidant Capacity	TAS	Allows the quantification of the total antioxidants present in the sample.
	FRAP	Allows the quantification of antioxidants that do not have S-H bonds present in the sample.
	ORAC	Allows the quantification of a specific antioxidant using fluorescence.

Since the current work of cytotoxicity studies is part of a larger project that aims to study the ability of these compounds to reverse neurodegeneration caused by oxidative stress, it is later planned to use the hydrogen peroxide method to induce oxidative stress in neuronal cells and apply the commercial kit named ROS-ID® Total ROS detection kit ENZ-51011 (Enzo Life Sciences) to measure its levels. This kit allows the direct

measurement of ROS and RNS production in living cells using fluorescence microscopy or flow cytometry. It directly detects radicals such as peroxynitrite ($ONOO^-$) and hydroxyl radicals ($^{\cdot}OH$), or molecules as hydrogen peroxide (H_2O_2). When radicals are present in cells, the kit reagents react with the radicals originating a green fluorescent product that can be observed using a wide-field fluorescence microscope equipped with standard green filter (490/525 nm), or a flow cytometer equipped with a blue laser (488 nm)[76].

1.3. DNA Damage

1.3.1. Introduction to DNA Damage Response

DNA consists in two polynucleotide chains coiled around each other by hydrogen bonds between the base portions of the nucleotide. Each cell contains around two meters of DNA interacting with histones in the nucleus[77]. This organelle is delimited by the nuclear envelope and regulates gene expression, replication, and cell proliferation and division and protects the DNA from reactive species present in the cell cytoplasm. Although the nucleus is an organelle separated from the rest of the cytoplasm by a double membrane, this membrane is permeable to small molecules, that cross and interact with DNA[78,79]. Given the crucial role of genome for the cell healthy maintenance and consequently perpetuation of healthy life, problems associated with genomic instability resulting from extensive damage represent a major issue to the scientific and medical community.

Every day our cells and DNA are exposed to several aggressions via endogenous and exogenous agents, or otherwise the DNA damage can be caused by internal or external factors. The first ones are associated with metabolism, like ROS (that are physiological in a certain level) or some spontaneous chemical reactions. The second ones are related with environmental factors, such as radiation, chemical agents, pollution or even some viruses[80]. Independently of the origin of the aggressive factors, they can lead to many alterations. In one hand, it can cause nucleotide sequence alterations, involving deletions, insertions, substitutions, or rearrangements of base pairs, what can lead to dysfunctional proteins. This type of genetic material alterations is called mutations[81]. It

can be caused by an agent or being simply spontaneous lesions occurred during normal DNA replication, what happens due to a deficient incorporation of deoxyribonucleotide triphosphate (dNTPs), interconversion between DNA bases caused by deamination, loss of DNA bases following DNA depurination and modification of DNA bases by alkylation[82]. In contrast, when we are talking about DNA damage, we refer to physical or chemical alterations in the tridimensional structure of the double helix. Sometimes, DNA damage ends in mutations when there is no capacity to repair the damage[81].

In overall, DNA damage results from endogenous processes (normal cellular replication[83,84] and metabolism[85,86] or from exogenous exposures (ultraviolet (UV)[87,88] and ionizing radiation (IR)[89,90], or to various genotoxic compounds[91,92]). Depending on the type of stress, different types of DNA damage are generated (**Figure 1**). For example, the normal replication process induces mismatch of nucleotide leading to mutations[93–96]. In turn, the oxidative stress will generate ROS from either the normal metabolism or from exposition to a genotoxic compound originating DNA breaks (single strand breaks (SSB) or double strand breaks (DSB))[97–99]. These alterations lead the activation of DNA damage repair mechanisms (**Figure 1**).

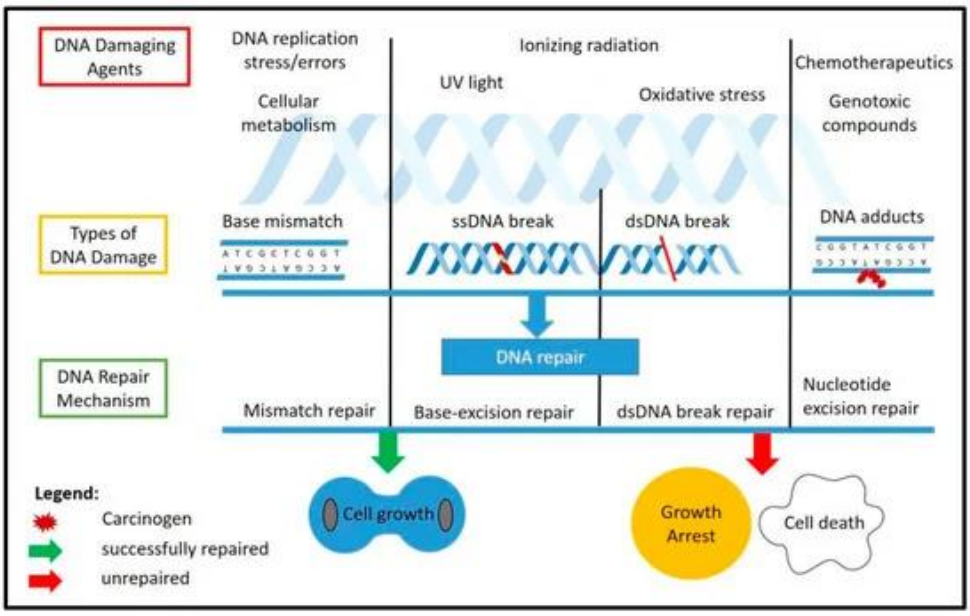

Figure 1: Summary of DNA damaging agents, types of DNA damage caused by the mentioned agents, and mechanisms of DNA repair activate. Taken from Imran et al.[100]

Another type of DNA damage called abasic sites (APs) occurs when a base (pyridine or pyrimidine) is lost from the DNA by cleavage of a *N*-glycosyl bond, leaving the sugar-phosphate chain intact[101], though a process is called depurination or depyrimidination, respectively. Further the deaminations, characterized by the loss of amino groups from DNA bases, producing bases that naturally do not exist[102]. There are also cyclobutane pyrimidine dimers (CPDs), in which covalent linkages between adjacent pyrimidines occur in the same DNA strand, and they are the most frequent type of DNA lesion derived by UV light exposure[103].

1.3.2. DNA Damage caused by Oxidative Stress on Neurodegenerative Diseases

The DNA damage repair (DDR) and damage-bypass mechanisms are detrimental to protect DNA and to ensure cell survival. There is a perfect balance between DNA repair and tolerance mechanisms and when they are altered, they will destabilize cellular metabolic homeostasis, leading to devasting diseases like cancer an ND, where disruption or deregulation of DDR results in genomic instability. The DDR will be responsible for detection of any type of DNA damage that occurs and will activate a repair signaling cascade at the damage site. Consequently, the cells will continue proliferating if the repair successfully occurs or will activate cell apoptosis if the damage was too extensive and the repairing mechanisms are not able the repair the damage[104].

There are several mechanisms of DNA repair reviewed in Imran et al.[100] (**Figure 2**), including mismatch repair (MMR)[105], base excision repair (BER)[106], nucleotide excision repair (NER)[107], homologous recombination (HR)[108] and non-homologous end joining (NHEJ)[109]. Interestingly, several DNA damage types can be repaired though activation of an important repair factor named ATM kinase, being the major factor associated to dsDNA break repair via NHEJ[109]. In overall, DNA damage will activate a series of damage sensors, them the transduction of damaged signal to the DDR mediators and downstream effectors and finally the DDR effectors coordinate and regulate the appropriate response according to the severity of DNA damage. DDR is a phosphorylation-driven signaling event that leads to the activation of both ATM and ATR, as two crucial DDR transducers that in turn interacts with several proteins namely p53, checkpoint kinase 1 and 2 and decrease the activity of cyclin-dependent kinase[110].

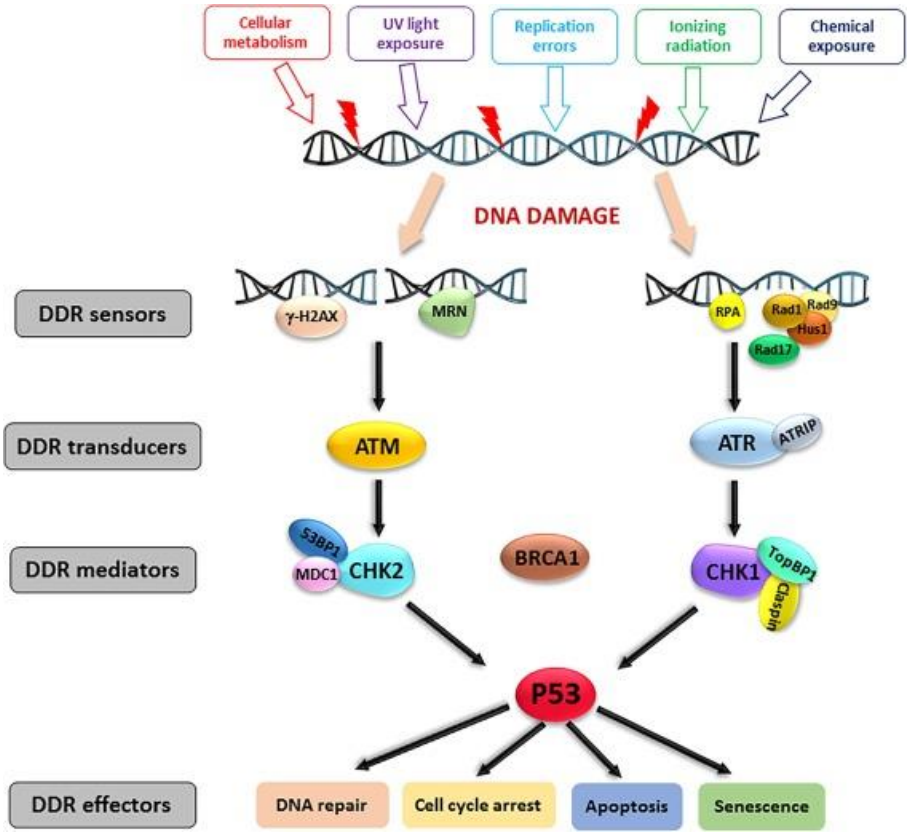

Figure 2: DNA damage response network. Taken from Mirza et al.[111]

1.3.3. DNA Damage Repair Pathways

Brain neurons are the most susceptible cells to DNA damage caused by oxidative stress once brain have a high O_2 consumption, what generates a huge amount of ROS[112]; brain has a weak level of antioxidant enzymes[113]; the free radical NO· is an important biological messenger highly diffusible and playing a prominent in CNS[114]; there is a high transcriptional demand in post-mitotic neurons, what causes a huge dependency of these cells on SSBs; and they have limited regenerative capacity. This way, they are particularly susceptible of DNA error, and consequently to function loss and death[115].

This way, nucleotides are constantly subjected to oxidation. The most possible oxidized studied base is guanine. As it has a low oxidation potential, it is particularly susceptible to singlet oxygen, forming 8-oxo-7,8-dihydroguanine (8-oxoG). This base alteration can guide to APs formation or lead itself to many alterations. It can lead to disruption of many cellular functions, like affect how proteins bind to the DNA, what can disrupt DNA binding and promote transcription; and its APs can alter DNA secondary

structure, forming stacked groups of guanines that affect genome stability, replication, and gene regulation through enforcing single stranded DNA and providing protein binding sites[116,117].

To solve the APs and SSBs, Damage Repair Pathways (DDRs) are implicated, particularly BER and PARP-1. There are evidence that this pathways are deregulated in ND, particularly BER-genes are less expressed and PARP-1 more activated in AD[116].

1.3.4. DNA Induction and Measurement Methodologies

To induct DNA damage in laboratory, techniques such as exposure to chemicals (such as methylphenidate[118], Tributyltin[119], bleomycin[120], among others) or ionizing radiation (such as UV)[87] are widely used.

To identify and measure DNA damage in laboratory, nowadays there are many techniques and it is even possible to search for each specific type of damage caused by oxidative stress. In our case, we are most interested in search for APs and SDBs damages.

To identify and measure AP sites, we can follow for example 8-oxo-G, or other oxidative base modification. This can be done by Gas chromatography (GC) and liquid chromatography (LC), simultaneous with electrochemical detection (ECD) or mass spectrometry (MS). Between these techniques, LC with Tandem MS (MS/MS) have been the most used and considered as the standard method to measure oxidative DNA base lesions in biological samples. As an advantage for this one, the information obtained includes lesion structural information, but it has disadvantages like it is needed a high DNA amount (around 30 mg) and it is needed a previous DNA preparation by enzymatic digestion what can cause artefactual oxidative lesions[121,122]. On the other hand, there is also search for 8-oxo-guanin (8-oxo-G) or others by immunoassays, using antibodies against lesions. The big disadvantage is its lack of specificity between oxidized lesion and undamaged bases[123].

To identify and measure strand break type lesions, the standard technique is the Single Cell Gel Electrophoresis assay (SCGE, also known as comet), what briefly consists in run nucleoids containing supercoiled loops of DNA linked to the nuclear matrix (obtained by lysing cells with detergent and high salt levels) by electrophoresis. Then, it results in structures resembling comets with both a ‘head’ (supercoiled intact DNA) and a ‘tail’ (nicked and fragmented DNA), fragments that can migrate. In the end, the intensity

of the comet tail relative to the head reflects the number of DNA breaks. However, this method allows just a few samples each time[124]. One another hand, there is another very used and very well- established technique to measure SSB, immunofluorescence. The protocol consists briefly in fix cell, incubate them with antibodies against proteins that participate in DNA Damage, like H2A.X. This protein becomes phosphorylated H2A.X during strand breaks lesion and it can be detected by fluorescence microscopy if it is conjugated to a fluorophore, and it is considered the most sensitivity and specificity compared to other assays[125,126]. The following **Table 2** resumes some of the most used methods.

Table 2: Techniques used to measure DNA Damage. Taken from Gonzalez-Hunt et al.[127]

Lesion	Assay	Description	Reference
Nuclear DNA			
Base lesions/AP sites	LC-MS/MS (and similar approaches)	Detects specific lesions by providing structural information. Highly sensitive and specific; requires high amounts of DNA, not for basal measurements.	[70]
	Lesion-specific immunoassays	Uses antibodies raised against lesion of interest. Low detection and specificity. E.g.: Enzyme-linked immunoassays (ELISA), radioimmunoassays (RIA)	[21–23]
	Southern blot analysis	Processes lesion of interest with glycosylase, then detects DNA bands via southern blot and compare signal. Requires large amounts of DNA and extensive preprocessing.	[24,25]
	ELISA-like with aldehyde reactive probe (ARP)	Reacts with aldehyde in abasic sites, detected via biotin-avidin interaction. Low sensitivity.	[30,31]
Strand breaks	Comet assay and derivatives	Single cell electrophoresis, broken DNA separates from intact DNA forming a comet. Low throughput.	[33]
	Immunofluorescence	Uses antibodies against proteins in the DNA damage response that can be found in the vicinity of double strand breaks, such as γH2A.X. Low sensitivity, possible false positives.	[71]
Varied	PCR-based assays	Calculates lesion frequency for damage capable of stalling a polymerase during PCR or resulting in less amplification. Low coverage of the genome. No information on specific lesion type.	[27,32,49]
Mitochondrial DNA			
Abasic sites	ARP immunofluorescence	Reacts with aldehyde in abasic sites, colocalization of signal with mitochondria can be visualized with immunohistochemistry. Low throughput.	[32]
Varied	PCR-based assays	Calculates lesion frequency for damage capable of stalling a polymerase during PCR or resulting in less amplification. Almost full coverage of the mitochondrial genome. No information on specific lesion type.	[27,32,49]

Since the current work of cytotoxicity studies is part of a larger project that aims to study the ability of these compounds to reverse DNA Damage caused by oxidative stress, it is later planned to induce DNA Damage in neuronal cells using the bleomycin model, which mainly induces type SB damage, and then measure DNA Damage levels caused by oxidative stress levels using the ϒH2A.X immunofluorescence detection method.

1.4. Pyrazoles

1.4.1. Introduction to Pyrazoles

Pyrazole belongs to a class of heterocyclic compounds consisting of an heteroaromatic five-membered ring containing two nitrogen atoms in adjacent positions (1 and 2 positions) and three carbons, which are also identified by the name "1,2-diazole"[128,129]. Due to rapid interconversion in solution, *N*-unsubstituted pyrazoles may present three identical and non-separable tautomers, the 1*H*-pyrazole (**I**), 3*H*-pyrazole (**II**) and 4*H*-pyrazole (**III**). Moreover, three partially reduced forms may also exist, called pyrazolines or dihydropyrazoles, namely 2,3-dihydro-1*H*-pyrazole (**IV**), 4,5-dihydro-1*H*-pyrazole (**V**) and 4,5-dihydro-3*H*-pyrazole (**VI**), and the pyrazolidine (**VII**), which are fully saturated pyrazoles[129] (**Figure 3**).

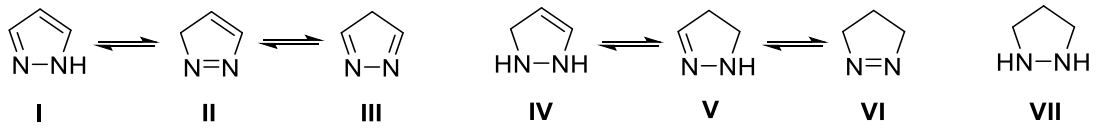

Figure 3: Structures of pyrazole tautomers (**I**, **II**, **III**), pyrazolines **(IV**, **V**, **VI**) and pyrazolidine (**VII**)

Pyrazoles are seldom found in nature, which may be due to the difficulty of the formation of N-N bond by living organisms[130]. However, a high interest has existed over the years regarding the synthesis of pyrazole derivatives, since these compounds have a wide range of applications, especially in drug discovery and medicine[131]. This type of compounds were synthesized firstly by Knorr in 1883, when he synthesized a pyrazole derived compound, pyrazolone[132]. Pyrazolone is the keto derivative of pyrazole[133]. Starting from pyrazolone, antipyrine was quickly discovered and approved for use. In 1884, antipyrine was already used to treat pain, inflammation and fever[134] and, from this moment on, attention was focused on pyrazoles and their derivatives due to their great pharmacologic potential.

Several biological activities are recognized for pyrazole-type compounds, namely analgesic, anti-inflammatory (COX-2 inhibitors), anticancer, anxiolytic, antidepressant, anti-pyretic, antimicrobial, antifungal, antiviral, antioxidant, and neuroprotective activities[135]. In fact, pyrazoles are the active ingredients of already marketed drugs such as celecoxib, antipyrine, phenylbutazone, novalgine, ramifenazone, apixaban, fipronil,

rimonabant, pyrazofurin among others[135–139]. In sum, pyrazoles are considered key structures in medicinal chemistry due to their varied biological activities, and they appear to be safe as they are active ingredients of several already marketed drugs.

Within the scope of this work, the antioxidant and neuroprotective activities of pyrazoles are particularly relevant and will be addressed in the following sections.

1.4.2. Pyrazoles to Counteract Oxidative Stress

Pyrazole is an important pharmacophore in the development of antioxidants to counteract oxidative stress. As recently reviewed by Silva et al.[140], several examples of pyrazoles alone or combined with other pharmacophores have shown high antioxidant activity. Among these examples, pyrazoles that present in their structure one or more styryl groups stand out, as they are more identical, in structural terms, to the compounds that will be studied in this work. This is the case of 3,5-bis(styryl)pyrazoles (**VIII**), curcumin analogues, that are well-known for their antioxidant activity (**Figure 4**). Some derivatives possess superior activity to that of curcumin in DPPH, ferric reducing antioxidant power (FRAP), and β-carotene bleaching assays[141]. Compared with 3,5-bis(4-hydroxy-3-methoxystyryl)pyrazole (**VIIIa**) (EC_{50} = 14 ± 0.18 μmol), curcumin presented lower inhibition of DPPH$^{\bullet}$ radical (102 mmol), (half maximal effective concentration (EC_{50}) = 40 ± 0.06 μmol)). The presence of hydroxy and methoxy groups on the terminal phenyl rings is benefic for the antioxidant capacity. Moreover, the 3,5-bis(styryl)pyrazole **CNB-001** has shown interesting results in studies related to neuroprotection and Alzheimer's disease. It was able to restore membrane homeostasis disrupted after brain trauma, being a promising compound for therapeutic use in the treatment of Parkinson's disease[142]. In combination with tissue plasminogen activator, **CNB-001** is efficient in the treatment of stroke[143]. Compound (**VIIIa**) acted as inhibitor of β-amyloid secretion and protein kinases involved in neuronal excitotoxicity[144]. Some analogues of pyrazole **VIIIa** also displayed good inhibition of γ-secretase activity, tau aggregation, and/or affinity to fibrillar Aβ42[145].

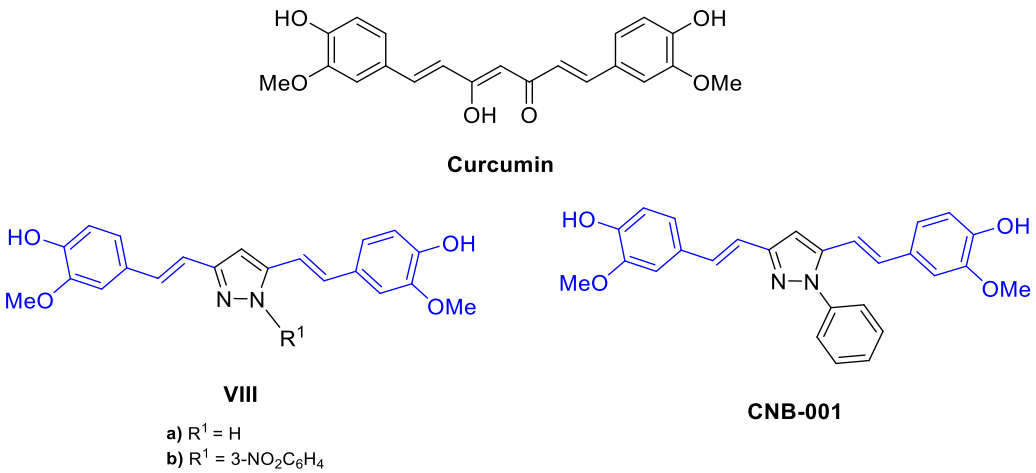

Figure 4: Structures of **curcumin**, 3,5-bis(styryl)pyrazoles (**VIII**) and **CNB-001** that possess antioxidant and neuroprotective activities (styryl groups detached in blue)

1.4.3. Pyrazoles to Counteract DNA Damage

The repair of DNA damage is a complex process that is based on pathways to remedy specific types of damage to DNA, which include the damage induced by oxidative stress. Different DNA damage response inhibitors have been developed through the years. However, in what concerns to pyrazoles, there are only a few studies reported in the literature. One of these studies, demonstrated the DNA repair ability of Niraparib (**Figure 5**), a pyrazole that behaves as a PARP1/2 inhibitor. The involvement of PARP1 in the recognition and repair of DNA damage is well-established[146]. Niraparib detects single-strand DNA breaks and synthesizes a poly(ADP-ribose) chain (PAR) to recruit repair proteins[147].

The nucleotide excision repair (NER) is an incredibly versatile pathway and remedies DNA bulky adduct damage and requires the activity of more than 30 individual proteins and complexes. It relies on four essential steps: recognition, incision/excision, resynthesis and ligation. The pyrazole X-80 (**Figure 5**) is a XPA protein inhibitor that displayed reasonable potency in fluorescence polarization DNA binding assays, and in cancer therapy, for example, this compound may enhance the action of platinum-derived chemotherapeutic drugs[148].

Studies with in cultured human blood lymphocytes demonstrated that Celecoxib (**Figure 5**) protects from ionizing radiation effects that cause oxidative stress, DNA damage and chromosome abbreviations on normal cells[149].

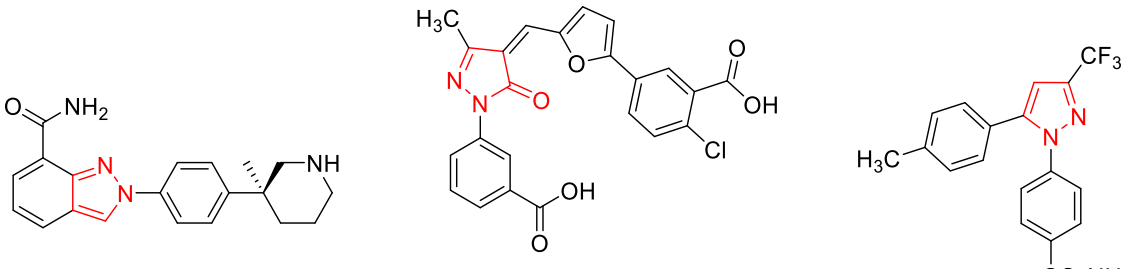

Figure 5: Drugs that have the ability to repair DNA damage and possess a pyrazole nucleus in its structure (detached in red)

1.5. Aim of the work

Despite the already known biological activities of styrylpyrazoles[150,151], their interesting physicochemical properties, such as tautomerism, isomerism[152,153] conjugation extension, due to the presence of the styryl (2-arylvinyl) group, as well as the rich chemistry related to their synthesis and transformation, this type of pyrazole has rarely been studied. Previous studies revealed that two families of pyrazoles the (*E*)-3(5)-(2-hydroxyphenyl)-4-styryl-1*H*-pyrazoles and (*E*)-3(5)-(2-hydroxyphenyl)-5(3)-styryl-1*H*-pyrazoles (**Figure 6**) possess good $ABTS^{+\bullet}$ and $NO^{\bullet}$ radicals scavenging activity (data not yet published), especially the compounds of the first family. These results may be indicative of the potential of these compounds as good antioxidant agents.

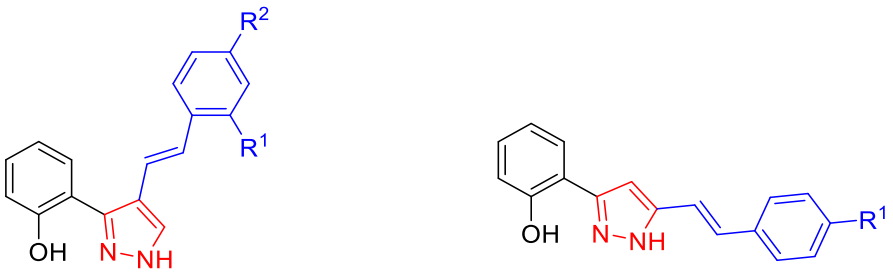

R^1 = H, Cl, OMe; R^2 = H, CF_3

(*E*)-3(5)-(2-hydroxyphenyl)-4-styryl-1*H*-pyrazoles

R^1 = H, Cl, OMe

(*E*)-3(5)-(2-hydroxyphenyl)-5(3)-styryl-1*H*-pyrazoles

Figure 6: Pyrazoles that have shown promising antioxidant activity in previous studies. Styryl groups detached in blue and pyrazole nucleus detached in red. Adapted from Correia et al.[154]

Based on these previous results, this work aims to evaluate the potential of a series of pyrazoles of the above-mentioned families (**Figure 7**) to counteract oxidative stress and consequent DNA damage, conditions thar are underlying neurodegeneration. Among the selected pyrazoles for this study, two of them possess a long alkyl chain of ten carbons linked to the N1-nitrogen or 2'-oxygen atoms. The introduction of this chain allows to modulate the physicochemical properties of these compounds in order to increase the lipophilicity. This seems to be a crucial feature to make the compounds more able to cross the blood brain barrier envisaging their application in the treatment of neurodegenerative diseases.

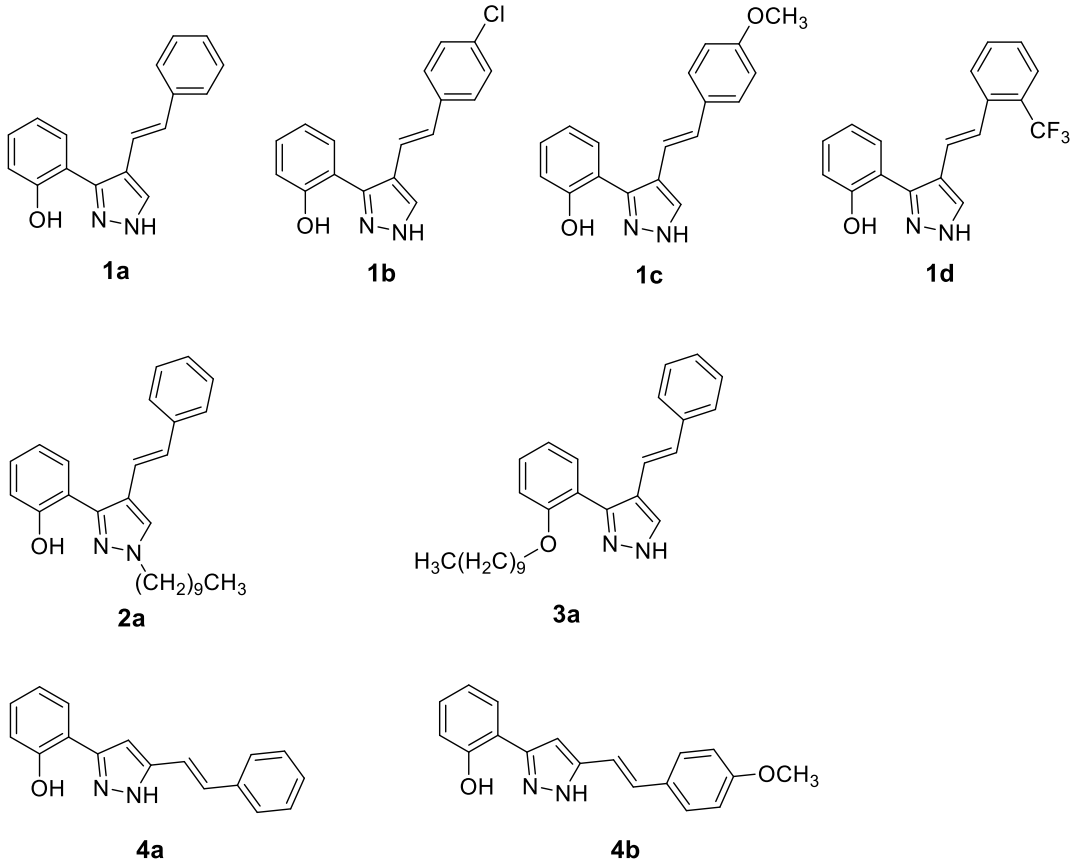

Figure 7: (*E*)-4-Styrylpyrazoles (**1a-1d** (Group 1), **2a** and **3a** (Group 2)) and (*E*)-5(3)-styrylpyrazoles (**4a**,**4b** (Group 3**)**) studied in this work.

Knowing the properties that are already recognized for this type of compounds and taking into account the global concern about the advancement of this type of diseases that is already foreseen in a near future, this work intended to be the first step of a pioneering investigation that aims to evaluate the potential of these pyrazole-derived compounds as drugs to tackle neurodegenerative diseases. In this sense, it is extremely

important to know more about these compounds' safety, so this work intends to evaluate their toxicity to human cells. Therefore, the specific goals of this work are:

- ✓ Synthesize some of the selected pyrazoles (**1c**, **2a**, **3a**, **4a** and **4b**) and structurally characterize them by nuclear magnetic resonance spectroscopy and mass spectrometry in order to confirm their structure and purity. Pyrazoles **1a**, **1b** and **1d** were already available in the laboratory in sufficient amount for this study.
- ✓ Evaluate the pyrazoles' cytotoxicity using HeLa cells and different concentrations of the eight different pyrazoles for cell viability tests based on resazurin assay. We chose to use human cells, to work closely to our ultimate goal reality, which is to be drugs for human use, but we chose at the same time to use simple handling cells, to be easier to perform this preliminary kind of tests with many compounds that intend to function as a preliminary selection of the most promising ones.
- ✓ Evaluate the pyrazole's cytotoxicity using the same cells for intracellular levels of ϒH2A.X protein quantification in order to enrich and better clarify the results obtained from cell viability tests, ensuring that the compounds that we will consider to be no cytotoxic in resazurin assays won't really be causing any kind of hidden damage, namely in the genetic material. For that, we will apply the SDS-Page technique to separate proteins from the cells previously analyzed, and we will detect and quantify the DNA damage marker protein by Western-blotting.
- ✓ Establish structure-activity relationship studies based on the results obtained in the biological assays and identify the safer and more active compounds and chemical groups. This knowledge will motivate, in the chemistry field, inspiration for design new molecules containing these kinds of seemingly promising structures and, in the biological field, the continuation of more advanced studies with the most promising compounds.

CHAPTER 2

SYNTHESIS AND STRUCTURAL CHARACTERIZATION OF STYRYLPYRAZOLES

CHAPTER 2: SYNTHESIS AND STRUCTURAL CHARACTERIZATION OF STYRYLPYRAZOLES

2.1. Preamble

In this work, two families of styrylpyrazoles have been studied: (*E*)-3(5)-(2-hydroxyphenyl)-4-styryl-1*H*-pyrazoles and (*E*)-3(5)-(2-hydroxyphenyl)-5(3)-styryl-1*H*-pyrazoles (see **Figure 7**, section 1.5). In this chapter we will describe the nomenclature of these compounds and the synthetic strategies followed for their preparation, their structural characterization, as well as the fully detailed experimental protocols.

2.2. Nomenclature

The nomenclature adopted for the styrylpyrazoles **1a-d**, **2a**, **3a** and **4a**,**b** represented in **Figure 7** does not follow the IUPAC rules. The numbering of the structure starts at the pyrazole ring, with the number 1 being assigned to the NH or to the substituted nitrogen and the number 2 being assigned to the other nitrogen atom, and so on. The 2'-hydroxyl group is a substituent group which is attached to the 3 or 5 position of the pyrazole. Note that in the case of N1 non-substituted asymmetric styrylpyrazoles there may be two tautomers so that the position where the 2'-hydroxyphenyl group is attached can be the 3 or 5 position (**Figure 2**). The carbons of this substituent group are numbered from 1' to 6' with the 2'-position being that to which the hydroxy (for compounds **1a-d**, 2a and **4a**,**b**) or decyloxy (for compound **3a**) group is attached. Also due to the fact that two tautomers are possible, in pyrazoles **4a**,**b** the styryl group, which is also considered a substituent, may be attached at the 3 or 5 position (**Figure 8**). The carbons of the aromatic ring of the styryl group are numbered from 1" to 6" and the carbons of the exocyclic double bond are numbered as α and β. Both compounds have the designation (*E*)- that precedes the name of the compound and indicates the trans configuration of the Cα=Cβ double bond. Thus, compounds **1a-d**, and **2a** are derivatives of (*E*)-3(5)-(2-hydroxyphenyl)-4-styryl-1*H*-pyrazoles, compound **3a** is named as (*E*)-3(5)-(2-

decyloxyphenyl)-4-styryl-1*H*-pyrazole, and compounds **4a**,**b** are derivatives of (*E*)-3(5)-(2-hydroxyphenyl)-5(3)-styryl-1*H*-pyrazoles.

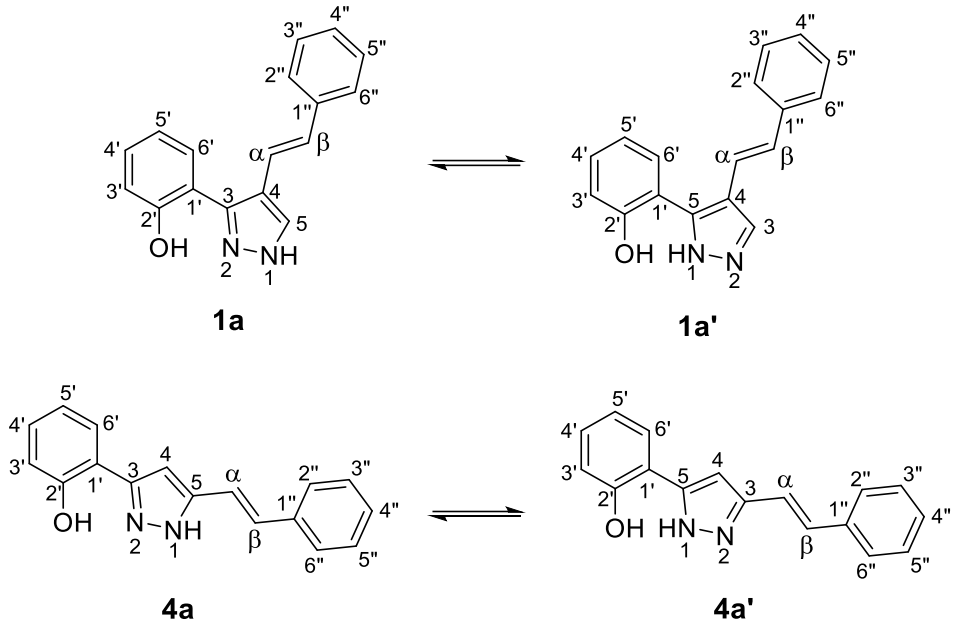

Figure 8: Structure, numbering system and tautomers of (*E*)-3(5)-(2-hydroxyphenyl)-4-styryl-1*H*-pyrazoles (**1a** and **1a'**) and (***E***)-3(5)-(2-hydroxyphenyl)-5(3)-styryl-1*H*-pyrazoles (**4a** and **4a'**)

2.3. Synthesis Strategies

Among the compounds studied in this work, only compounds **1c**, **2a**, **3a**, **4a** and **4b** were synthesized. The remaining compounds **1a**, **1b** and **1d** were already available in the laboratory in sufficient amount and high purity degree for the studies to be carried out.

In this section, will be described the synthetic methods used for the preparation of the above-mentioned compounds.

2.3.1. Synthesis of (*E*)-3(5)-(2-hydroxyphenyl)-4-styryl-1*H*-pyrazoles 1c, 2a and 3a

Compounds **1c, 2a** and **3a** belong to the family of (*E*)-3(5)-(2-hydroxyphenyl)-4-styryl-1*H*-pyrazoles. Compound **1c** was synthesized in two steps (**Scheme 1**). Following a method previously reported by Silva et al.[155], in the first step, 4-oxo-4*H*-chromene-3-

carbaldehyde (**5**) (or 3-formylchromone) undergoes a Knoevenagel condensation with 4-methoxyphenylacetic acid **6a** in dry pyridine, at 120 ºC, using potassium *tert*-butoxide as base, to give the (*E*)-3-(4-methoxystyryl)-4*H*-chromen-4-one (**7a**). In the second step, the 3-strylchromone **7a** reacts with hydrazine hydrate in methanol, at room temperature, to give the (*E*)-3(5)-(2-hydroxyphenyl)-4-(4-methoxystyryl)-1*H*-pyrazole (**1c**)[156,157].

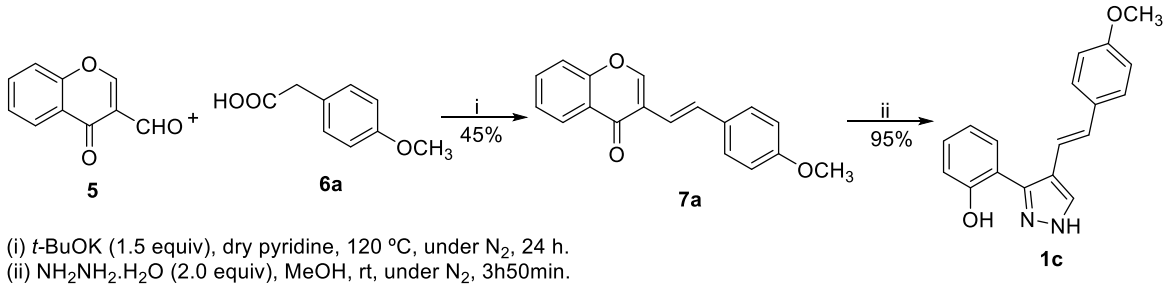

Scheme 1*:* Steps for **1c** synthesis

Compounds **2a** and **3a** were obtained in three steps (**Scheme 2**). First, the Knoevenagel condensation of 4-oxo-4*H*-chromene-3-carbaldehyde (**5**) with phenylacetic acid **6b** gave the (*E*)-3-styryl-4*H*-chromen-4-one (**7b**). The reaction of compound **7b** with hydrazine hydrate in methanol, at room temperature, gave the (*E*)-3(5)-(2-hydroxyphenyl)-4-styryl-1*H*-pyrazole (**1a**), in very good yield. Then, pyrazole **1a** underwent an alkylation reaction with 1-bromodecane to give the (*E*)-1-decyl-3(5)-(2-hydroxyphenyl)-4-styryl-1*H*-pyrazole (**2a**), in 60% yield, which results from the alkylation at the NH of the pyrazole ring. It is noteworthy that another product was obtained, in low yield, which corresponds to the (*E*)-3(5)-[(2-decyloxy)phenyl]-4-styryl-1*H*-pyrazole (**3a**).

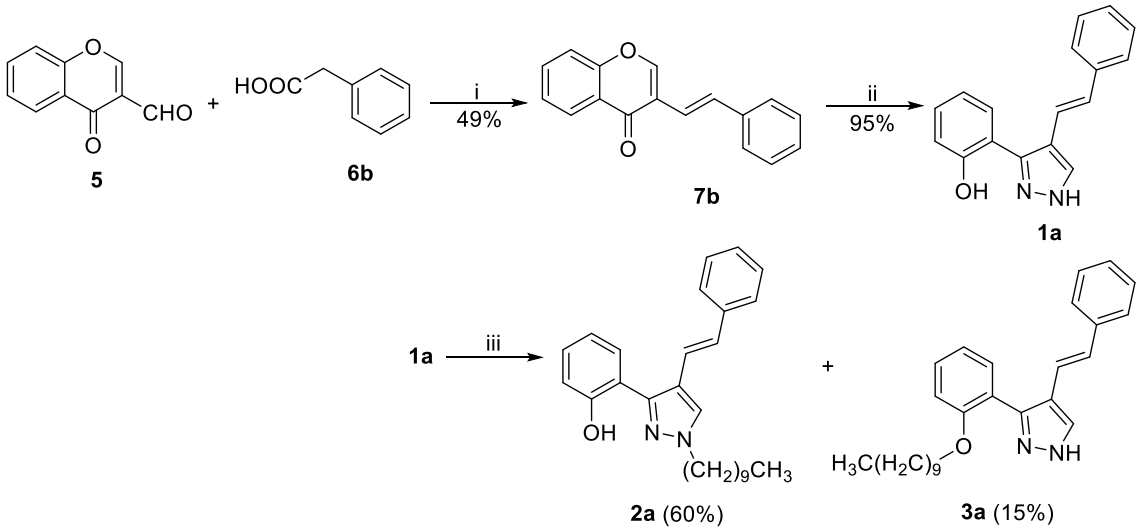

(i) *t*-BuOK (1.5 equiv), dry pyridine, 120 ºC, under N_2, 24 h.
(ii) $NH_2NH_2.H_2O$ (2.0 equiv), MeOH, rt, under N_2, 3h50min.
(iii) 1-Bromodecane (1.5 equiv), K_2CO_3 (3.0 equiv), acetone p.a, reflux, 24 h.

Scheme 2*:* Steps for **2a**, **3a** synthesis.

2.3.2. Synthesis of (*E*)-3(5)-(2-hydroxyphenyl)-5(3)-styryl-1*H*-pyrazoles

The synthesis of (*E*)-3(5)-(2-hydroxyphenyl)-5(3)-styryl-1*H*-pyrazoles **4a** and **4b** was performed following a method previously described by Silva et al.[158] The method involves three steps (**Scheme 3**). In the first step, a Steglich esterification of 2'-hydroxyacetophenone **8** with the appropriate cinnamic acid **9a,b** in a chlorinated solvent, dichloromethane, at room temperature, in the presence of dicyclohexylcarbodiimide (DCC) and 4-pyrrolidinopyridine (4-PPy) for 6 days, gives the corresponding 2-acetylphenyl cinnamates **10a,b**.[158]In this work, only the 2-acetylphenyl cinnamate **10a** was prepared. In the next step, the 2-acetylphenyl cinnamate was converted into the corresponding (*E*)-1-(2-hydroxyphenyl)-5-phenylpent-4-ene-1,3-dione (**11a**) by a Baker-Venkataraman rearrangement in strong basic conditions. Finally, the reaction of (*E*)-1-(2-hydroxyphenyl)-5-phenylpent-4-ene-1,3-dione (**12a**) and (*E*)-1-(2-hydroxyphenyl)-5-(4-methoxyphenyl)pent-4-ene-1,3-dione (**12b**) (prepared from corresponding 2-acetylphenyl cinnamate **11b**) with hydrazine hydrate in methanol afforded the corresponding (*E*)-3(5)-(2-hydroxyphenyl)-5(3)-styryl-1*H*-pyrazoles **4a** and **4b** in low yields.

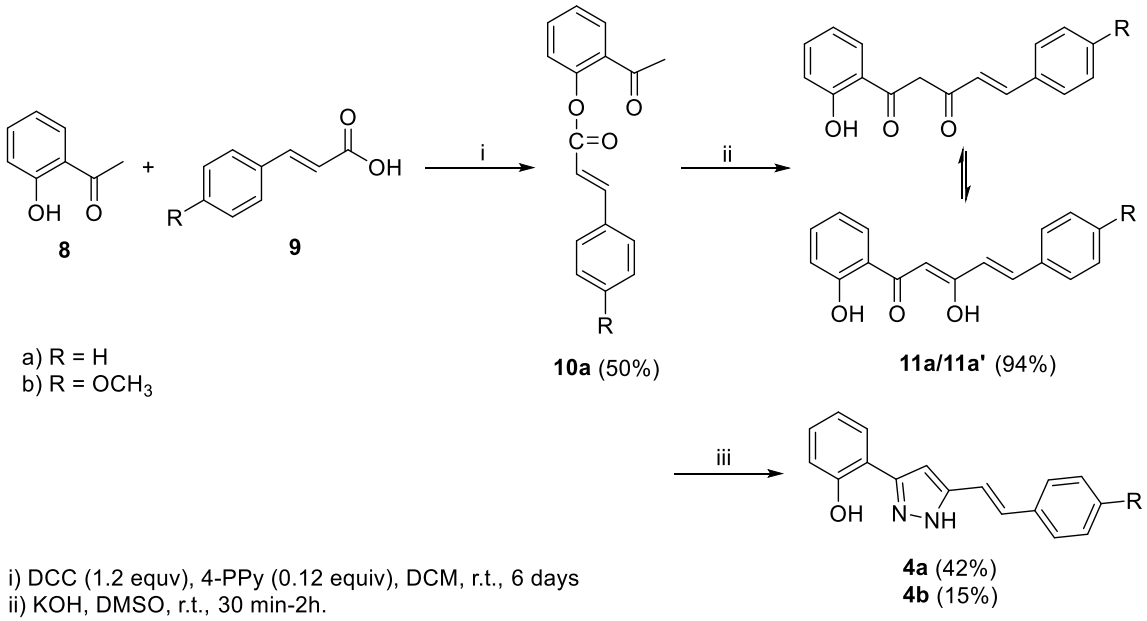

Scheme 3*:* Steps for **4a**, **4b** synthesis

2.4. Structural Characterization

In this section, it will be briefly discussed the main characteristics observed in the NMR spectra of the synthesized styrylpyrazoles. We will start with the analysis of the spectra of (*E*)-3(5)-(2-hydroxyphenyl)-4-(4-methoxystyryl-1*H*-pyrazole) **1c** as a representative compound of the (*E*)-3(5)-(2-hydroxyphenyl)-4-styryl-1*H*-pyrazoles' family, and then we will present the main features of the NMR spectra of compounds **2a** and **3a**. Finally, we will discuss the main features of the NMR spectra of (*E*)-3(5)-(2-hydroxyphenyl)-5(3)-styryl-1*H*-pyrazole **4a**, as an example of the (*E*)-3(5)-(2-hydroxyphenyl)-5(3)-styryl-1*H*-pyrazoles' family.

2.4.1. Structural characterization of (*E*)-3(5)-(2-hydroxyphenyl)-4-styryl-1*H*-pyrazoles 1a and 1c

The (*E*)-3(5)-(2-hydroxyphenyl)-4-styryl-1*H*-pyrazole **1a** is already reported in the literature[159] and herein it was characterized by ^{1}H NMR. In **Figure 9** and **Figure 10**, it was represented the ^{1}H NMR spectra of (*E*)-3(5)-(2-hydroxyphenyl)-4-(4-

methoxystyryl)-1*H*-pyrazole **1c**, where it possible to observe the singlet due to the resonance of the protons of the methoxy group at δ_H = 3.84 ppm. Other important features in the ^{1}H NMR spectra of the pyrazoles **1a** and **1c** are: i) the signal due to the resonance of H-5 that appears as a singlet at δ_H = 7.82–7.84 ppm; ii) the vinylic protons H-α at δ_H = 7.02–7.16 ppm and H-β at δ_H = 6.84–6.90 ppm. The values of the olefinic coupling constants ($^3J_{H\alpha -H\beta}$ = 16.2–16.4 Hz) confirm the *trans* configuration of the exocyclic double bond. The resonance of the 2'-O<u>H</u> proton is also a typical signal of these compounds. However, due to its nature, a labile proton, in some cases it may be not observed in the ^{1}H NMR spectrum. This fact explains why this signal was not observed for compounds **1a** and **1c**. In the ^{1}H NMR spectra of compound **1c** it was also possible to observe two doublets in the aromatic region, at δ_H = 7.41 (J = 8.8 Hz) and δ_H = 6.91 (J = 8.8 Hz) respectively, corresponding to the resonances of H-2",6" and H-3",5" of the *para*-substituted ring (4"-OCH_3). The protons H-3",5" appear at lower frequencies than H-2",6" due to the protecting effect of the methoxy groups in the *ortho*-positions. Two double doublets were observed corresponding to the resonances of H-6' and H-3' at δ_H = 7.64 ppm and δ_H = 7.07 ppm, the second occurring at lower frequency due to the protecting effect of the hydroxy group at the *ortho* position. The signal corresponding to the resonance of H-4' was observed at δ_H = 7.27 ppm, as double doublet of doublets due to the coupling of this proton with the vicinal protons H-3' and H-5' and the coupling at longer distance with H-6' ($^4J_{H4'-H6'}$ = 1.6 Hz).

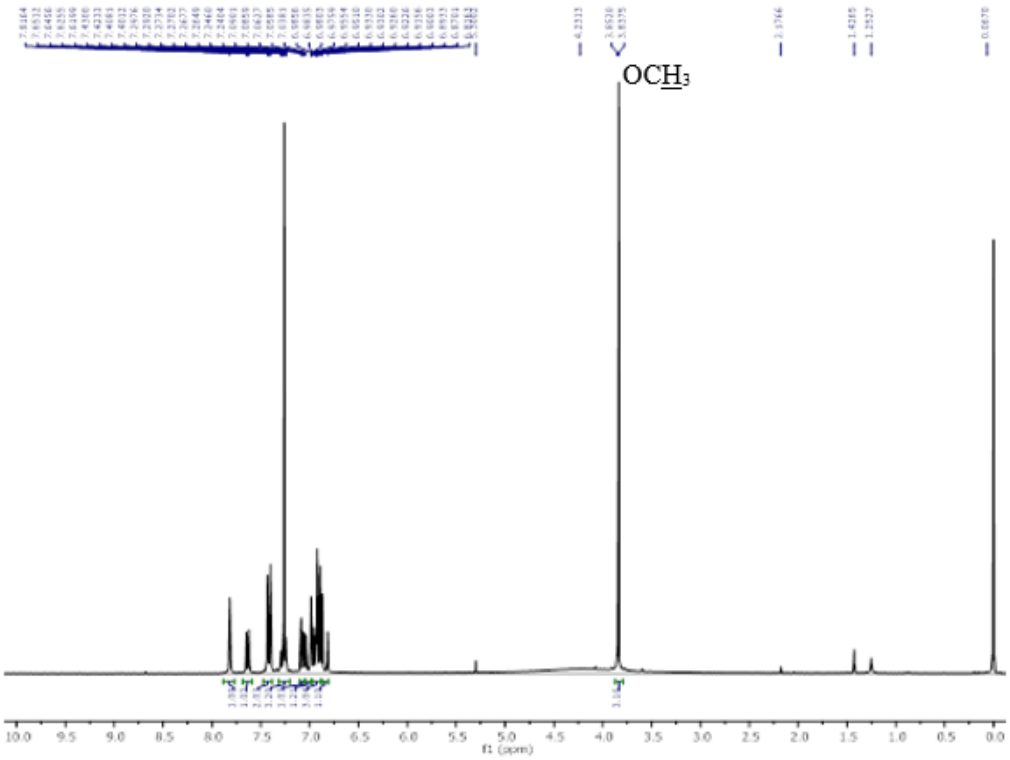

Figure 9: [1]H NMR spectrum of (*E*)-3(5)-(2-hydroxyphenyl)-4-(4-methoxystyryl)-1*H*-pyrazole **1c** (300.13 MHz, $CDCl_3$)

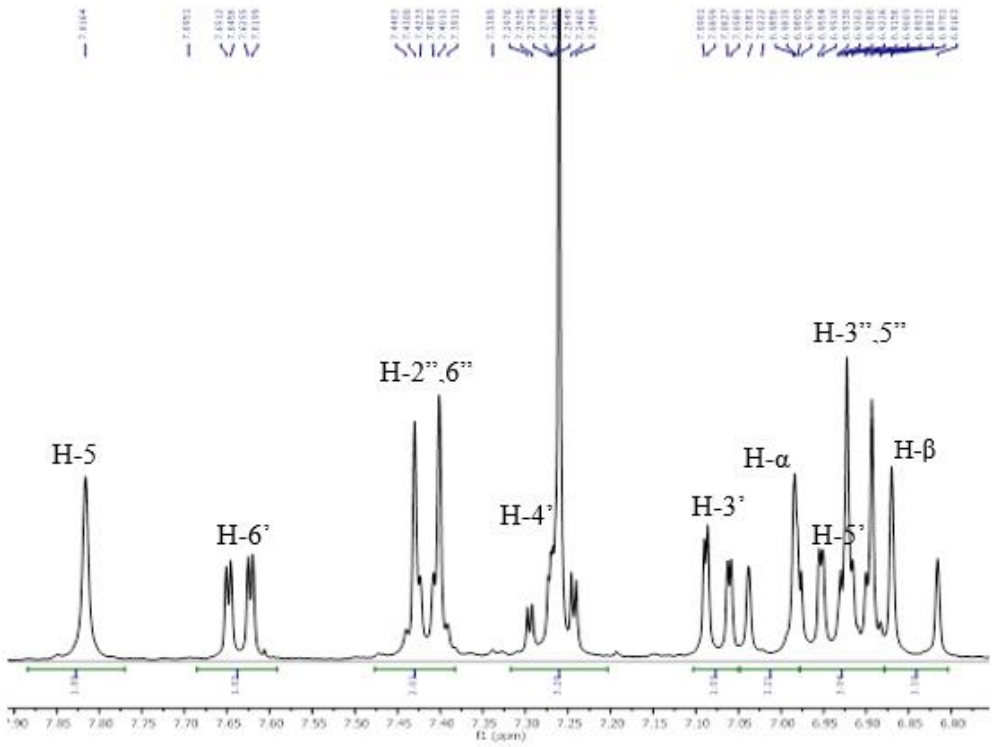

Figure 10: Expansion of the [1]H NMR spectrum of (*E*)-3(5)-(2-hydroxyphenyl)-4-(4-methoxystyryl)-1*H*-pyrazole **1c** (300.13 MHz, $CDCl_3$)

2.4.2. Structural characterization of (*E*)-1-decyl-3-(2-hydroxyphenyl)-4-styryl-1*H*-pyrazole 2a and (*E*)-3(5)-[(2-decyloxy)phenyl]-4-styryl-1*H*-pyrazole 3a

The main characteristics of the NMR spectra of styrylpyrazoles **2a** and **3a (Figure 11**), which allow to distinguish them from the precursor pyrazole **1a**, are the resonances due to the protons and carbons of the long chain linked to the nitrogen (for compound **2a**) or oxygen (for compound **3a**) atoms, which appear in the aliphatic region of the spectra, as shown in **Figures 12** and **Figure 13**. The structural characterization of these compounds is already described in the literature[151]. The comparison of our characterization data with those reported in the literature (**Table 3** and **Table 4**) confirmed the correct assignment of the signals and consequently the structure of the synthesized compounds.

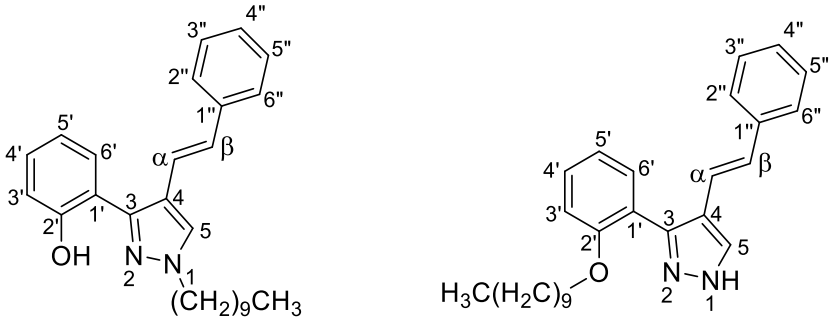

Figure 11: Structures and numbering of styrylpyrazoles **2a** and **3a** (isomers)

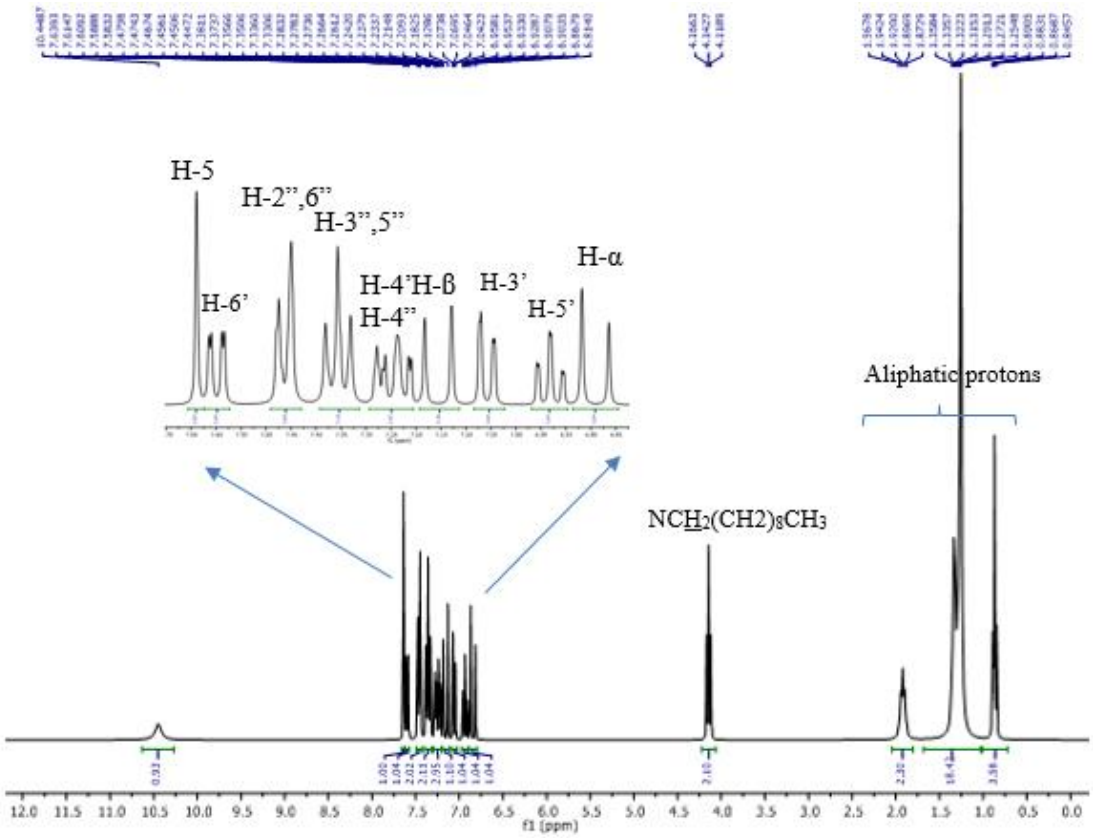

Figure 12: ^{1}H NMR spectrum of (*E*)-1-decyl-3(5)-(2-hydroxyphenyl)-4-styryl-1*H*-pyrazole **2a** (300.13 MHz, $CDCl_3$)

Table 3: Comparison of ^{1}H NMR chemical shifts (δ in ppm), multiplicity and coupling constants (J in Hz) of compounds **2a** and **3a** with the values reported in the literature

Compounds / **Signal**	**2a**	**2a** (Lit.)[151]	**3a**	**3a** (Lit.)[151]
N<u>H</u>	---	---	---	---
H-5	7.64, s	7.56, s	7.90, s	7.57, s
2'-O<u>H</u>	10.45, s	10.50, s	---	---
H-3'	7.06, dd, *J* 8.2, 1.3 Hz	7.07, dd, *J* 8.2, 1.2 Hz	6.99-7.11, m	7.07, dd, *J* 8.2, 1.1 Hz
H-4'	7.29 – 7.20, m	7.19-7.25, m	7.18-7.25, m	7.21-7.25, m
H-5'	6.93, dt, *J* 7.7, 1.3 Hz	6.92, ddd, *J* 7.6, 7.5, 1.2 Hz	6.99-7.11, m	6.92, ddd *J* 7.6, 7.5, 1.1 Hz
H-6'	7.60, dd, *J* 7.7, 1.7 Hz	7.60, dd, *J* 7.6, 1.5 Hz	7.52, dd, *J* 7.6, 1.7 Hz	7.60, dd *J* 7.6, 1.6 Hz
H-α	7.16, d, *J* 16.2 Hz	7.14, d, *J* 16.2 Hz	6.94, d, *J* 16.3 Hz	7.14, d, *J* 16.2 Hz
H-β	6.84, d *J* 16.2 Hz	6.81, d, *J* 16.2 Hz	6.99-7.11, m	6.81, d, *J* 16.2 Hz
H-2",6"	7.46, d *J* 7.1 Hz	7.44, d *J* 7.1 Hz	7.41-7.47, m	7.44, d, *J* 7.4 Hz
H-3",5"	7.35, dd, *J* 7.8, 7.3 Hz	7.33, dt, *J* 7.1, 7.0 Hz	7.27-7.41, m	7.33, dt, *J* 7.8, 7.4 Hz
H-4"	7.20 – 7.29, m	7.19-7.25, m	7.27-7.41, m	---
X-C<u>H</u>$_2$(CH$_2$)$_8$CH$_3$	4.14, t, *J* 7.1 Hz	4.06, t, *J* 6.9 Hz	4.06, t, *J* 6.6 Hz,	4.07, t, *J* 7.0 Hz
X-CH$_2$C<u>H</u>$_2$(CH$_2$)$_7$CH$_3$	1.92, quint, *J* 7.4 Hz	1.87, quint, *J* 6.9 Hz	1.81, quint, *J* 6.7 Hz	1.87, quint *J* 7.0 Hz
X-CH$_2$CH$_2$(C<u>H</u>$_2$)$_7$CH$_3$	1.03 -1.68, m	1.25-1.29, m	1.24-1.45, m	1.24-1.30, m
X-(CH$_2$)$_9$C<u>H</u>$_3$	0.87, t, *J* 6.7 Hz	0.87, t, *J* 6.7 Hz	0.87, t, *J* 6.6 Hz	0.87, t, *J* 7.0 Hz

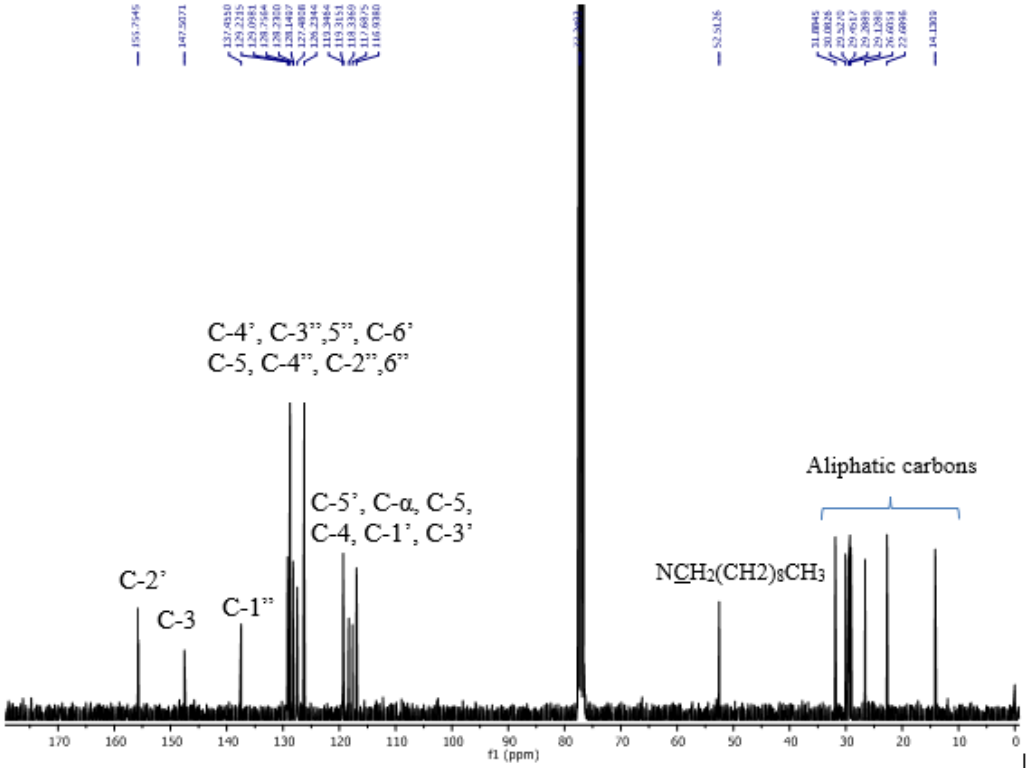

Figure 13: ^{13}C NMR spectrum of (*E*)-1-decyl-3(5)-(2-hydroxyphenyl)-4-styryl-1*H*-pyrazole **2a** (75.47 MHz, $CDCl_3$)

Table 4: Comparison of ^{13}C NMR chemical shifts (δ in ppm) of compounds **2a** and **3a** with the values reported in the literature

Compounds / **Signal**	**2a**	**2a** (Lit.)[151]	**3a**	**3a** (Lit.)[151]
C-3	147.3	147.3	137.8	137.8
C-4	118.3	118.2	118.2	118.2
C-5	128.15	128.06	137.1	137.2
C-1’	117.7	117.6	118.0	118.1
C-2’	155.8	155.7	156.1	156.0
C-3’	116.9	116.8	112.6	112.5
C-4’	129.1	129.0	129.8	129.8
C-5’	119.4	119.2	121.1	121.1
C-6’	128.23	128.09	130.7	130.6
C-α	119.3	119.1	120.1	120.1
C-β	129.2	129.1	128.0	127.9
C-1”	137.5	137.3	136.3	136.3
C-2”,6”	126.2	126.1	126.1	126.0
C-3”,5”	128.8	128.6	128.6	128.6
C-4”	127.5	127.3	127.1	127.1
X-$\underline{C}H_2(CH_2)_8CH_3$	52.5	52.3	68.9	68.9
X-$(CH_2)_7\underline{C}H_2CH_2CH_3$	31.9	31.8	31.9	31.9
X-$CH_2\underline{C}H_2(CH_2)_7CH_3$	30.1	30.0	29.2	29.52
X-$(CH_2)_3(\underline{C}H_2)_4(CH_2)_2CH_3$	29.1, 29.3, 29.53, 29.45	29.0, 29.2, 29.36, 29.43	29.3, 29.5, 29.5, 29.7	29.2, 29.3, 29.48, 29.52
X-$(CH_2)_2\underline{C}H_2(CH_2)_6CH_3$	26.6	26.5	26.1	26.1
X-$(CH_2)_8\underline{C}H_2CH_3$	22.7	22.6	22.6	22.7
X-$(CH_2)_9\underline{C}H_3$	14.1	14.1	14.1	14.1

X- = N (for compound **2a**) or O (for compound **3a**)

2.4.3. Structural characterization of (*E*)-3(5)-(2-hydroxyphenyl)-5(3)-styryl-1*H*-pyrazoles 4a and 4b

Although the (*E*)-3(5)-(2-hydroxyphenyl)-5(3)-styryl-1*H*-pyrazoles **4a** and **4b** (**Figure 14**) were synthesized in this work, its structural characterization is already reported in the literature and therefore it will not be discussed in detail. However, it is important to refer that the signals observed in the ^{1}H NMR spectra of compound **4a** and **4b (Figure 15** and **Figure 16**) present the ^{1}H NMR spectrum of compound **4a**, as an example, correspond to those reported in the literature thus confirming the structures of these compounds (**Table 5**). It is noteworthy that pyrazoles **1a** and **1c** can be distinguished from pyrazoles **4a** and **4b** based on the singlets due to the resonances of H-5 (for **1a,1c**) and of H-4 (for **4a, 4b**) which appear at different frequencies, being the former assigned at higher frequency values because it is linked to a carbon that is directly linked to a nitrogen atom. Moreover, in the ^{1}H NMR spectrum of compound **4a** it was possible to observe two broad singlets at 10.79 ppm and 10.13 ppm due to the resonances of the 2'-OH and NH protons.

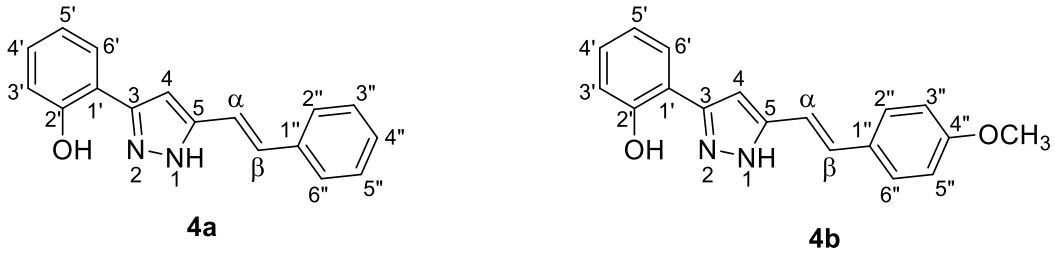

Figure 14: Structures and numbering of styrylpyrazoles **4a** and **4b**

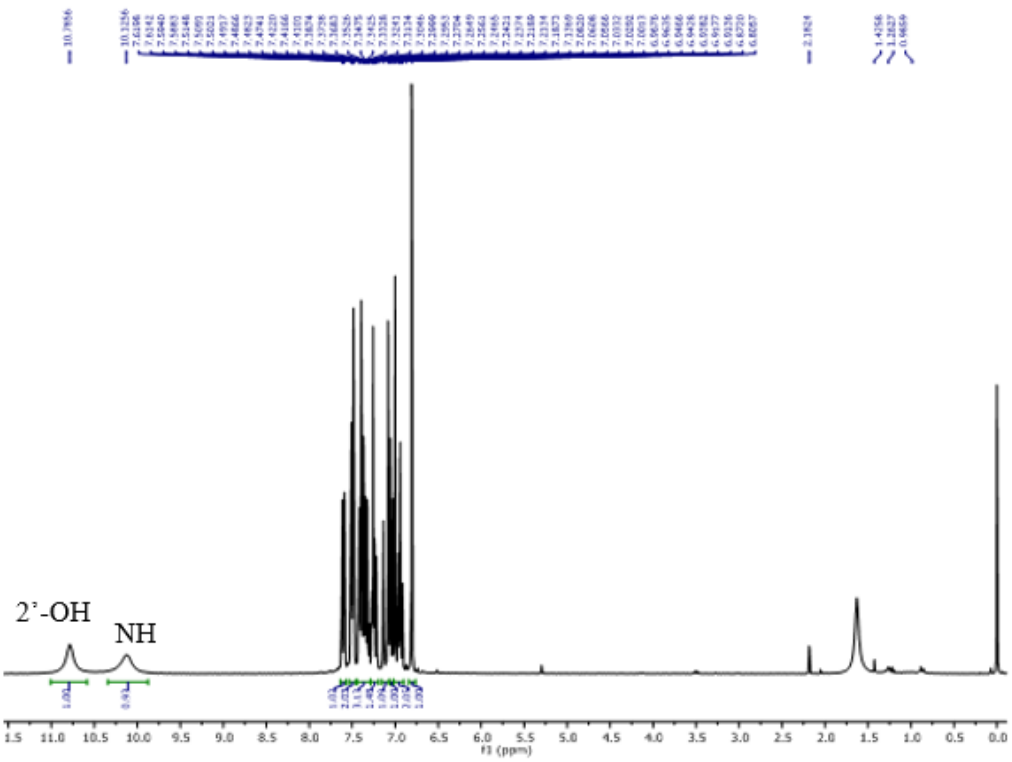

Figure 15: ^{1}H NMR spectrum of (*E*)-3(5)-(2-hydroxyphenyl)-5(3)-styryl-1*H*-pyrazole **4a** (300.13 MHz, $CDCl_3$)

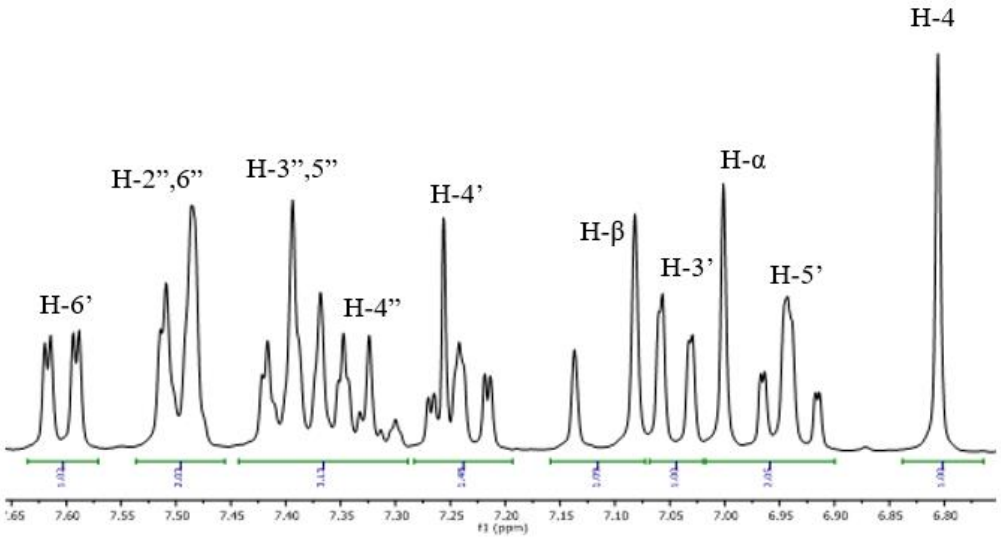

Figure 16: Expansion of the ^{1}H NMR spectrum of (*E*)-3(5)-(2-hydroxyphenyl)-5(3)-styryl-1*H*-pyrazole **4a** (300.13 MHz, $CDCl_3$)

Table 5: Comparison of ^{1}H NMR chemical shifts (δ in ppm), multiplicity and coupling constants (J in Hz) of compounds **4a** and **4b** with the values reported in the literature

Signal	**4a**	**4a** (Lit.)[156]	**4b**	**4b** (Lit.)[156]
N<u>H</u>	10.13, br s	10.10, br s	---[a]	10.04, br s
H-4	6.81, s	6.78, s	6.93, s	6.76, s
2'-O<u>H</u>	10.79, br s	10.78, br s	---[a]	10.83, br s
H-3'	7.04, dd, *J* 8.2, 1.2 Hz	7.04, dd, *J* 8.0, 1.2 Hz	7.03-7.08, m	7.04, dd, *J* 8.4, 1.2 Hz
H-4'	7.27 – 7.21, m	7.24, ddd, *J* 7.6, 8.0, 1.6 Hz	7.21-7.27, m	7.24, dt, *J* 8.4,1.6 Hz
H-5'	6.94, dt, *J* 7.5, 1.2 Hz	6.94, dt, *J* 7.6, 1.2 Hz	6.76-6.80, m	6.93, ddd, *J* 7.3, 8.1, 1.2 Hz
H-6'	7.60, dd *J* 7.8, 1.7 Hz	7.61, dd, *J* 7.7, 1.6 Hz	7.60, dd, *J* 7.7, 1.6 Hz	7.60, dd, *J* 7.3, 1.6 Hz
H-α	6.97, d, *J* 16.5 Hz	6.98, d, *J* 16.5 Hz	6.83, d, *J* 16.3 Hz	6.83, d, *J* 16.6 Hz
H-β	7.11, d, *J* 16.5 Hz	7.12, d, *J* 16.5 Hz	7.06, d, *J* 16.3 Hz	7.05 d, *J* 16.6 Hz
H-2",6"	7.46-7.54, m,	7.51, dd, *J* 8.4, 1.3 Hz	7.43, d, *J* 8.8 Hz	7.44, d, *J* 8.8 Hz
H-3",5"	7.29 – 7.44, m	7.40, t, *J* 8.4, 7.1 Hz	6.91, d, *J* 8.8 Hz	6.92, d, *J* 8.8 Hz
H-4"	7.29 – 7.44, m	7.32, tt, *J* 7.1, 1.3 Hz	---	---
4"-OC<u>H</u>$_3$	---	---	3.84, s	3.84, s

CHAPTER 3

BIOLOGICAL STUDIES

CHAPTER 3: BIOLOGICAL STUDIES

3.1. Preamble

After putting forward our hypothesis that these pyrazole compounds could reverse ND and DNA damage caused by oxidative stress and, therefore, be used in the future to formulate drugs, the first and most important step is to study their security. To this end, cytotoxicity studies were carried out for each of the eight compounds at different concentrations in Human cells. For this, cell viability tests were initially carried out in simple cell models, HeLa cells, using the Resazurin Assay method, which evaluated the metabolic viability of cells exposed to different concentrations of compound for 24 hours. After these tests, cell lysates were collected for protein analyses by SDS-Page followed by Western Blotting (WB) to confirm and enrich the cell viability results obtained in the metabolic test. This step was considered important to ensure that the cells are not only metabolically functional, but also do not show apparently hidden damages at the level of their genetic material. To this end, we proceeded to detect and quantify the ϒH2A.X protein, a biomarker of DNA damage.

3.2. Cell Assays

3.2.1. Cell Culture Maintenance

For this work, Human cell line HeLa (American Type Culture Collection (ATCC) CCL-2, Manassas, Virginia, USA) was used. Cells were cultured in 100 mm cell culture plates, in complete culture medium (DMEM Supplemented with 10% inactivated FBS and 1% antibiotic and antimycotic) and maintained in a controlled and humified atmosphere at 37 ºC and 5% CO_2. Cells were monitored daily using an inverted light microscope. Subculture procedures were made when a confluency of 80–90% was reached.

For subculture procedures, the medium was discarded, a quick wash was done with 3ml of PBS 1X, which was also discarded after, and 1ml of trypsin (0.05% Trypsin-EDTA (1X); Gibco) was added and left to float for 3 min at 37 °C. After, 3 ml of culture medium were added to the plate, the cells were resuspended and transferred to a centrifuge tube to be centrifuged for 3 min at 1000 rpm. The supernatant was discarded, cells were resuspended in a suitable amount of fresh culture medium and seeded on a new plate at an adjusted concentration for an adjusted amount of time, knowing that the number of cells approximately doubles every 24 hours.

3.2.2. Cell Counting For Experiences

For each replica of each compound, two 12-well plates (BioLite 12 Well Multidish; Thermo Fisher Scientific) were used. The applied subculture procedures were similar to the described above, except that for the experiments a specific amount of 125 000 cells was guaranteed to seed in each well. For this, it was necessary to proceed with the cell count using a glass hemocytometer and a coverslip.

This way, after centrifuge, cells were very good resuspended in a known volume and a 1:10 of that volume was transferred to a microtube to better ensure a good homogenization. Of this amount, again very well resuspended, a part was removed to a new microtube, to which were added a 1:10 ratio of Trypan Blue 0.4% (Gibco).

The hemocytometer and the coverslip were prepared. First, they were cleaned with paper towel and 70% ethanol, then the coverslip was moistened with water and slided over the chambers using slight pressure to affix it to the hemocytometer.

The cell suspension was again very well resuspended, and the two chambers of the hemocytometer were filled with it. The counting was performed in a microscope focused in the grid lines, counting all viable cells that go within the square or over its upper or left limits, and not counting the ones out or over its right or lower limits as shown in **Figure 17**. After do that for the four big squares composed of 16 smaller squares each, the same was one in the second chamber. Viable cells are distinguished from non-viable ones because they are not stained, whereas non-viable ones are intense blue stained, due to the fact that its structure is affected and allows the passage of the Trypan Blue solution into the cell. The number of viable cells existing in the known volume of one chamber

(0.1 µL) will be the average of the two chambers count. Based on this, calculations about the volume to be pipetted to seed 125 000 cells in each well were performed.

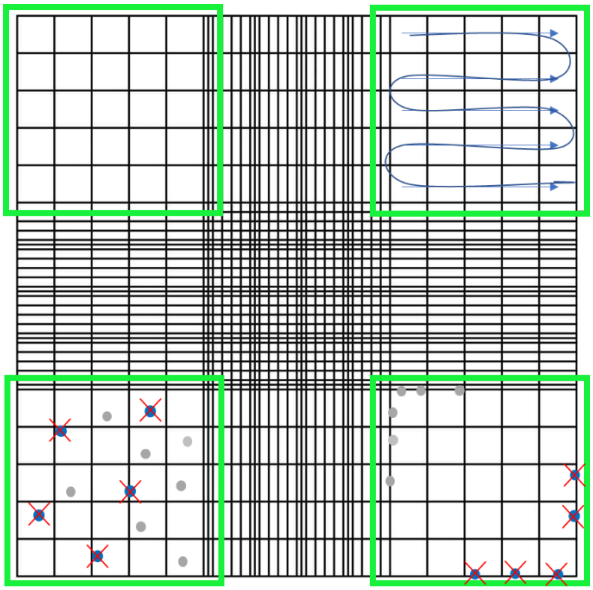

Figure 17: Representation of the hemocytometer image observed under the microscope. It is intended to show that: i) the count must be the mean of the four middle squares countings; ii) the count must be done line by line from left to right; iii) cells stained blue are not viable and should not be counted; iv) the cells in the lower and right limits of the middle frames must not be counted (and neither in the small squares, for organization, as they will be counted in the next line, ensuring that each cell is only counted once.)

In each well of the 12-well plate was placed the corresponding cell suspension volume and 450 µL of fresh medium. Cells were incubated under usual conditions for 16 h to ensure proper plate adhesion and stabilization.

3.2.3. Cell Exposure to Pyrazoles

After 16h of plating, the medium was discarded and replaced for fresh one for the respective condition. The plates were handled in the same way and as simultaneously as possible.

On the first plate, the 5 concentrations (1, 10, 20, 50 and 100 µM – these concentrations were achieved base in Carreira et al.[160] and in protocol optimizations made initially) were tested in duplicate by adding 450 µL of pyrazole's stock containing a pyrazole stock 10 mM in DMSO diluted to the respective concentration in fresh medium. On the second plate, DMSO controls were tested in duplicate for each concentration

tested in the first plate, by adding 450 µL of the respective DMSO control to each well (**Figure 18**).

DMSO was the solvent used to dissolve pyrazoles (which were in powder form) since they are organic compounds and, therefore, poorly soluble in water and very soluble in organic solvents, such as DMSO, widely used in cell culture.

This controls contained only fresh medium and DMSO in the amounts that were used to prepare the dilutions analyzed on the first plate and were intended to ensure that the values that would be obtained for viability would be due to the compound effect and not to DMSO effect, which, although increasing as the compound concentration increases (so that viable dilutions could be made), it is always up to 1%, which according to the analyzed literature should allow a normal cellular viability[161,162].

In both plates, negative controls (0 µM) were guaranteed also in duplicate by adding 450 µL of just fresh medium (**Figure 18**). These controls pretended to guarantee that the cell pool used for the experiment was in good condition, as well as to be the reference for the normal value of cell viability, with which the values obtained at the remaining concentrations would be compared later.

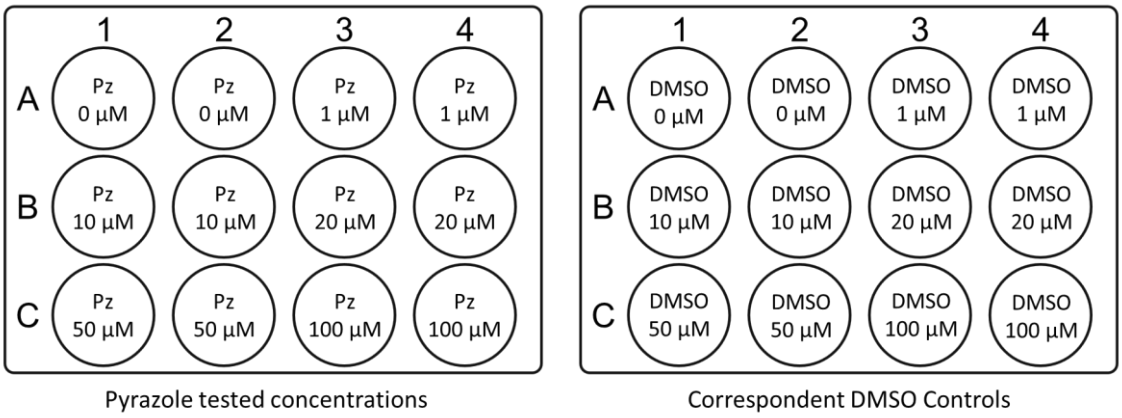

Figure 18: Organization of experimental conditions for each replica of each pyrazole: two 12-well plates with 125 000 cells/well were used. The first plate contained five concentrations of tested pyrazole (10, 20, 50 and 100 µM) and the negative control (0 µM), in duplicate, and the second plate contained the respective DMSO controls, which stands of DMSO quantities used to prepare each of the conditions of the first plate, also in duplicate. At least 3 replicas were made for each of the eight pyrazoles

After, both plates were incubated under the described conditions for 24 h. For each compound, a minimum number of 3 independent replicates was guaranteed.

3.2.4. Cell Viability Assays

Four hours before the exposure time ends, 10% of each well volume in resazurin 1% (50 µL for a final volume of 500 µL) was added to every well and the plates were maintained in the same conditions until the exposure time is reached, protected from the light. After that, medium samples, three from each condition, were collected and transferred to a 96-well plate kept in the dark. The plate was analysed by spectrophotometry in an absorbance plate reader (Infinite M200, Tecan) at 570 and 600 nm.

This resazurin assay[163] is based on the metabolic mediated reduction by living and viable cells of the oxidized blue colored resazurin (or just resazurin) that absorbs at 600 nm to a pink colored reduced resazurin product (also called resorufin) that absorbs at 570 nm. This happens because living cells maintain a reducing environment within their cytoplasm and mitochondria, when dehydrogenase enzymes catalyze reduction reactions like this (**Figure 19**)[164,165]. This way, cell viability values can be determined by measuring these two values of absorbance, being that the more viable cells there are in the experiment the more conversion of resazurin to resorufin occurred, so the number of metabolically viable cells will be directly proportional to the absorbance of resorufin value and inversely proportional to the absorbance of resazurin value.

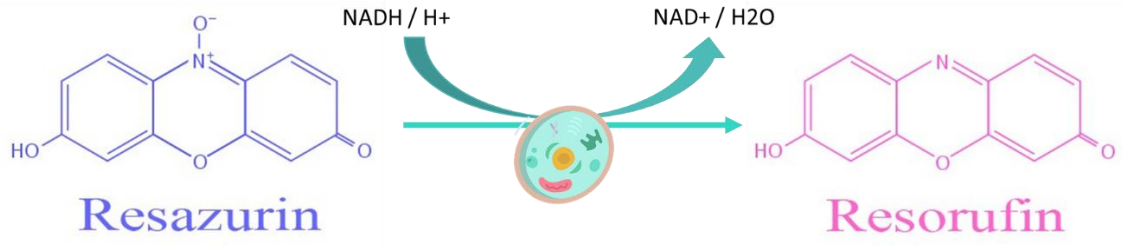

Figure 19: Conversion of resazurin (blue) to resofurin (pink), in a viable cell, that underlies the function of this cell viability assay widely used in human cells. When cells are metabolically viable, a reaction of reduction of resazurin to resofurin catalyzed by different oxidoreductase enzyme systems that use NAD(P)H as the primary electron donor takes place in mitochondria

After measuring the absorbance, viability was calculated by making a quotient between the absorbance of reduced resazurin (or resazurin) (at 600 nm) and the absorbance of resofurin (at 570 nm) for each condition, including negative controls and DMSO controls. The cell viability obtained values were expressed in arbitrary units. The

value corresponding to the quotient made for the negative control received the value of 100% and the others were calculated regarding this.

3.3. SDS-Page

3.3.1. Cell Lysates Collection

After viability tests were performed, the remaining cells in the 12-well were washed with PBS, collected to microtubes identified for each condition and subjected to centrifugation at 1000 rpm for 3 min. Then, the medium was discarded, the pellet was washed in PBS, which was discarded after another centrifugation, and HeLa cells were lysed by resuspension in hot SDS 1% solution and maintained in ice. Then samples were then boiled at 90 ◦C for 10 min, sonicated in IKA LABORTECHNIK U200S Control equipment for 10 s (0.5 cycles, 60% amplitude) and maintained in ice.

3.3.2. Protein Quantification

Total protein concentration was quantified using the Pierce Bicinchoninic Acid (BCA) protein assay kit (Pierce^{TM} BCA Protein Assay Kit; Thermo Scientific) according to the manufacturer's instructions.

3.3.3. Samples Setting

After determining the protein concentration present in each lysate sample, the final preparation of the samples to be analyzed by SDS-page was performed. For this purpose, new microtubes were identified and for each sample, the volume needed to contain 30 µg of protein, the amount of protein that we define as the ideal one to our gel running, was added to the respective microtube, prefacing with 1% SDS to a volume of 75 µL. SDS allows to denature proteins, separate isolated polypeptide chains, and conferee a negative charge to the sample.

Blanks and markers, with no protein, were also prepared. Blanks contained only SDS 1% (75 µL) and markers contained SDS 1% and protein marker in 75 µL final volume also (72 µL of SDS 1% added in this step and 3 µL of protein marker added later).

After, it was added LB 4X to all the samples in a 1:4 proportion, that is 25 mL to a 100 mL final volume, our defined loading volume. LB contain β-mercaptoethanol, a reagent with antioxidation properties that here has the function of reducing the disulfide bonds of the proteins in the sample, and glycerol, that here has the function of force sample enter onto the running gel. It also contains bromophenol blue, that allows to visually follow the samples running.

Then, samples were homogenized, boiled for 5 min, and left to cool. 3 mL of protein marker (Precision Plus Protein^{TM} Standards, Dual Color, Bio-Rad) were added at this point to the respective microtube and homogenized. The samples were all subjected to spin-down to be applied onto the gel with capillary tips.

3.2.4. Gels Preparation

Separating Gel

Protein separation was done by vertical acrylamide gel electrophoresis using a gradient gel between 5% and 20% of acrylamide, which allows the separation of proteins with a wide range of molecular weights. The function of acrylamide is, after polymerization, to allow the formation of a mesh with variable pore that will sort of filter the proteins according to their size to separate them. This will occur by the action of an electric field since acrylamide has also conductive capabilities.

For each gel, a 5% acrylamide and a 20% acrylamide solution were prepared, which were then mixed using a mixer in a stir plate with a magnet and introduced into the 1.5 mm thick glass system to polymerize. It is necessary to previously assemble all the electrophoresis system and wash the system and the mixer with distilled water.

The first solution was prepared mixing 9.29 mL of distilled H_2O, 3.75 mL of LGB and 1.875 mL of acrylamide, and the second one mixing 3.67 mL of distilled H_2O, 3.75 mL of LGB and 7.5 mL of acrylamide. LBG, containing Tris, has the function of supplying electrons to allow the formation of electrical current in the vat.

The last step was adding 75 µL of APS 10X and 7.5 µL of TEMED to each of the solutions and immediately place them in their respective mixer column, open the system and allowing that the space between the glasses to be filled with this gradient mixture. The gel should be left to polymerize for about 1h protected from oxygen.

These two reagents (APS and TEMED) are the last to be added because they are responsible for starting to catalyze the reaction that will result in the gel polymerization, and this starts to happen immediately after the addition. APS works as a source of free radicals and TEMED as a stabilizer.

Stacking Gel

After the upper gel (where the separation of proteins will take place) was polymerized, the top gel was prepared, which has the function of concentrating proteins in a thin line so that they can enter the separation gel at the same time.

To prepare each stacking gel, a 3.5% solution of acrylamide was prepared mixing 6.92 mL of H_2O, 0.88 mL of acrylamide, 2 mL of UGB and 100 µL of SDS 10%. UBG, containing Tris, has the function of supplying electrons to allow the formation of electrical current in the vat.

Lastly, it was added 100 µL of APS 10% and 10 µL of TEMED and the solution was placed on top of the already polymerized gel inside the system. Then, a 15-well 1.5 mm-thick comb was placed, and the gel was left to polymerize for about 30 min covered from the oxygen.

3.2.5. Eletrophoresis

After loading the samples into the gel wells, the gels system was placed in a vertical electrophoresis vat containing running buffer, and the positive and negative electrodes were connected to the respective terminals and to the power supply, at 45mA/gel duration for about 2h30min.

During this time, the protein samples were subjected to an electric field and migrated from the negative pole to the positive pole according to their charge and their molecular weight in an inversely proportional way. In this case, as the proteins were treated with SDS and heat, they were therefore denatured and given a negative charge.

Therefore, they will only migrate according to their molecular weight. Thus, larger proteins will migrate less, while lower molecular weight proteins will migrate more.

3.2.6. Transfer

When the run front nearly reached the lower limit of the gel, the run was terminated and the protein content of the gel transferred to a nitrocellulose membrane (Amersham™ Protan™ 0.2 µM NC, Nitrocellulose Blotting Membrane, GE Healthcare Life Sciences).

For the transfer protocol, the nitrocellulose membrane was cut to the size of our gel. In a cuvette, transfer buffer was placed and the sponges, filter papers and the cut membrane were placed to hydrate. The transfer cassette was assembled (paying attention to the formation of air bubbles between the gel and the membrane that affect the normal transfer of protein between them) in the order cassette part one, sponge, filter paper, gel, membrane, filter paper, sponge, cassette part two, the cassette was closed and pasted into the transfer vat. The gel face was turned to the negative pole and the membrane face to the positive pole, so that the migration of negatively charged proteins from the gel occurred towards the membrane by action of this horizontal electric field of 200 mA for about 18 h.

3.3. Western-Blotting

3.3.1. Membranes Staining

After hydrating the nitrocellulose membrane in TBS for 10 min, it was incubated at room temperature, with shaking, for 5 min, with the Ponceau S solution, after which several washes were done with distilled water to remove non-specific bonds until the red background disappeared from membrane empty zones. The membrane was read on a Densitometer (GS-800 Calibrated Densitometer; Bio-Rad Laboratories, Inc.). Images were collected with The Discovery Series™, Quantity OneAfter, 1-D Analysis Software,

Bio-Rad Laboratories, Inc. In the end, several membrane washes were done with TBS-T 1X until the protein tags had completely disappeared.

3.3.2. Protein ϒH2AX Immunodetection

In this work, we detected the ϒH2A.X protein by the fact that, when cells are exposed to ionizing radiation or DNA-damaging chemotherapeutic agents (our case with pyrazoles), double-stranded breaks (DSBs) are generated that rapidly result in the phosphorylation of histone H2A variant H2AX. Because phosphorylation of H2AX at Ser 139 (γ-H2AX) is abundant, fast, and correlates well with each DSB, it is the most sensitive marker that we can use to evaluate DNA damage.

Starting from the hydrated membrane, this was incubated with the blocking solution for 3 hours at room temperature with shaking. Afterwards, the membrane was washed for 5 min with 1X TBS-T with shaking at room temperature. Thereafter, the membrane was incubated at room temperature and with shaking for 2 h with the mouse primary antibody to the H2AX protein. After 2 h of incubation at room temperature, the membrane remained in incubation at 4 ºC overnight with shaking. The next day, the membrane was removed to room temperature, where it was incubated for another hour with shaking. Three washes of 10 min each were performed with TBS-T 1X with shaking at room temperature, after which it was incubated with the secondary anti-mouse antibody for 1 h with shaking at room temperature. Finally, 6 washes of 10 min each were done with TBS-T 1X at room temperature and with shaking to remove unspecific bonds that might have been formed.

Finally, the membrane was drained and placed in a plastic cover to be incubated for 5 min at room temperature and protected from light with the chemiluminescent detection reagent (ECL Select™ Western Blotting Detection Reagent; Amersham™, GE Healthcare Life Sciences). Then, excess reagent was removed, and the membrane was revealed by chemiluminescence with UV light in a ChemiDoc™ Touch Imaging System and the images were collected to be analysed.

3.3.3. Protein ϒH2AX Quantification

After acquiring the ponceau staining images in the densitometer and the revealing protein images in the chemidoc, they were analyzed in the software Image Lab (Bio-Rad Laboratories, Inc., Hercules, California, USA) to achive the quantification of ϒH2A.X protein levels. For that, we used Ponceau S staining as protein loading control for data normalization and relative protein levels were calculated by comparing each pyrazole concentration levels with the control levels.

For each concentration, the intensity of each well in the ponceau image was firstly calculated (backgroup intensity was subtracted). Then, the intensity of each respective band in the revealed image was calculated (the background intensity was subtracted). Then, to normalize the results to the amount of protein loaded, a ratio was made between the blot intensity and the ponceau intensity. And finally, arbitrary units are assigned, giving the negative control a value of 1 and calculating the rest relative to it.

3.4. Statistical Analysis

Statistical analysis was performed using the GraphPad Prism 7.0 software (GraphPad Software, San Diego, California, USA) with a statistical confidence coefficient of 95% for comparisons between the cell viability for each pyrazole (**1a**, **1b**, **1c**, **1d**, **2a**, **3a**, **4a**, **4b**) in the various concentrations (1, 10, 20, 50 and 100 µM) and the cell viability for each pyrazole in the control (0 µM). Data were expressed as mean ± standard deviation (SD) of, at least, three independent experiments. Values of p-value < 0.05 were considered statistically significant.

We started by evaluating whether the samples had normal distribution with the Shapiro-wilk normality test. When the samples were normally distributed, one-way Anova tests were performed to check whether there were statistically significant differences between the various concentrations and the negative control, for each of the replicates, and the Brown–Forsyth test was performed to ensure homogeneity of sample variances. Whenever differences were found to exist, Dunn's multiple comparisons test was then applied to assess between which groups and the control such differences existed.

When the samples were not normally distributed, a Kruskal-Wallis test was performed to check whether there were statistically significant differences between the various concentrations and the negative control. Then, whenever differences were found to exist, Dunn's multiple comparisons test was then applied to assess between which groups and the control such differences existed.

3.5. Results

3.5.1. Viability Assays Results

To evaluate the cytotoxicity of the chosen pyrazole compounds on the cells, a cell viability assay was carried out based on the metabolic capacity of viable cells to reduce resazurin to resofurin as explained in **section 3.2.4**. For this purpose, HeLa cells were exposed for 24h to different concentrations of pyrazoles and, four hours before the end of the exposure time, a resazurin solution was added to the wells. At the end of the time, samples of medium from the various conditions were analyzed by spectrophotometry at 570 and 600 nm. To calculate cell viability, a quotient between the values obtained for the absorbance at 570 nm, corresponding to resofurin, and the values obtained for the absorbance at 600 nm, corresponding to resazurin, was performed for each condition. The negative control containing only cells and culture medium was assigned the arbitrary value of 100% of viability, and the cell viability of the other conditions was calculated relatively to this. At least three experiments were performed for each compound.

Simultaneously, similar experiments were carried out without containing pyrazole to ensure that in our experiments with pyrazole we were not introducing a bias factor in the results as we were using an external substance in cytotoxic amounts to prepare the compound dilutions (DMSO). The results are presented below, organized by groups of compounds (Group 1 – pyrazoles **1a**, **1b**, **1c**,**1d** – **Figure 20**; Group 2 – pyrazoles **2a**, **3a** – **Figure 21;** Group 3 – pyrazoles **4a**, **4b** – **Figure 22**).

In the first Group (**Figure 20**), we can observe in a general way that concentrations 1 µM, 10 µM, 20 µM and 50 µM do not seem to present an offense to the cells, with a small exception for compound **1d** where at 50 µM there seems to be already some

reduction in cell viability (13.85%). In this compound, and unlike the three previous ones, the decrease in cell viability seems to happen in a more progressive way as the concentration of the compound increases and it is visible soon from concentration 1 µM. At concentrations 1 µM and 10 µM, the reduction in cell viability is around 6%, increasing to 13.85% in 20 µM and to 36.19% in 100 µM, with cell viability values at the concentration 100 µM being about 64% for **1d**.

In the remaining three compounds from Group 1, cell viability is approximately 100% for concentrations 1 µM, 10 µM, 20 µM and 50 µM, differing only in the 100 µM concentration. Looking at this concentration, the most toxic compound for cells seems to be **1b**, where only 22.27% of the cells were viable after pyrazole exposure. This one is followed by compound **1a**, with 70.51% of viable cells at 100 µM, and finally, for the compound **1c,** that seems to be the least toxic, with 85.46% of viable cells in the maximum concentration.

For all the experiments, the respective summaries of DMSO controls carried out simultaneously with each experiment are presented. In all of them it is possible to observe that there are no differences in cell viability of any of the concentrations (1 µM, 10 µM, 20 µM, 50 µM and 100 µM) compared to the control (0 µM), so the DMSO quantities used in the pyrazole stocks' preparation are not affecting the cell viability of the experiments.

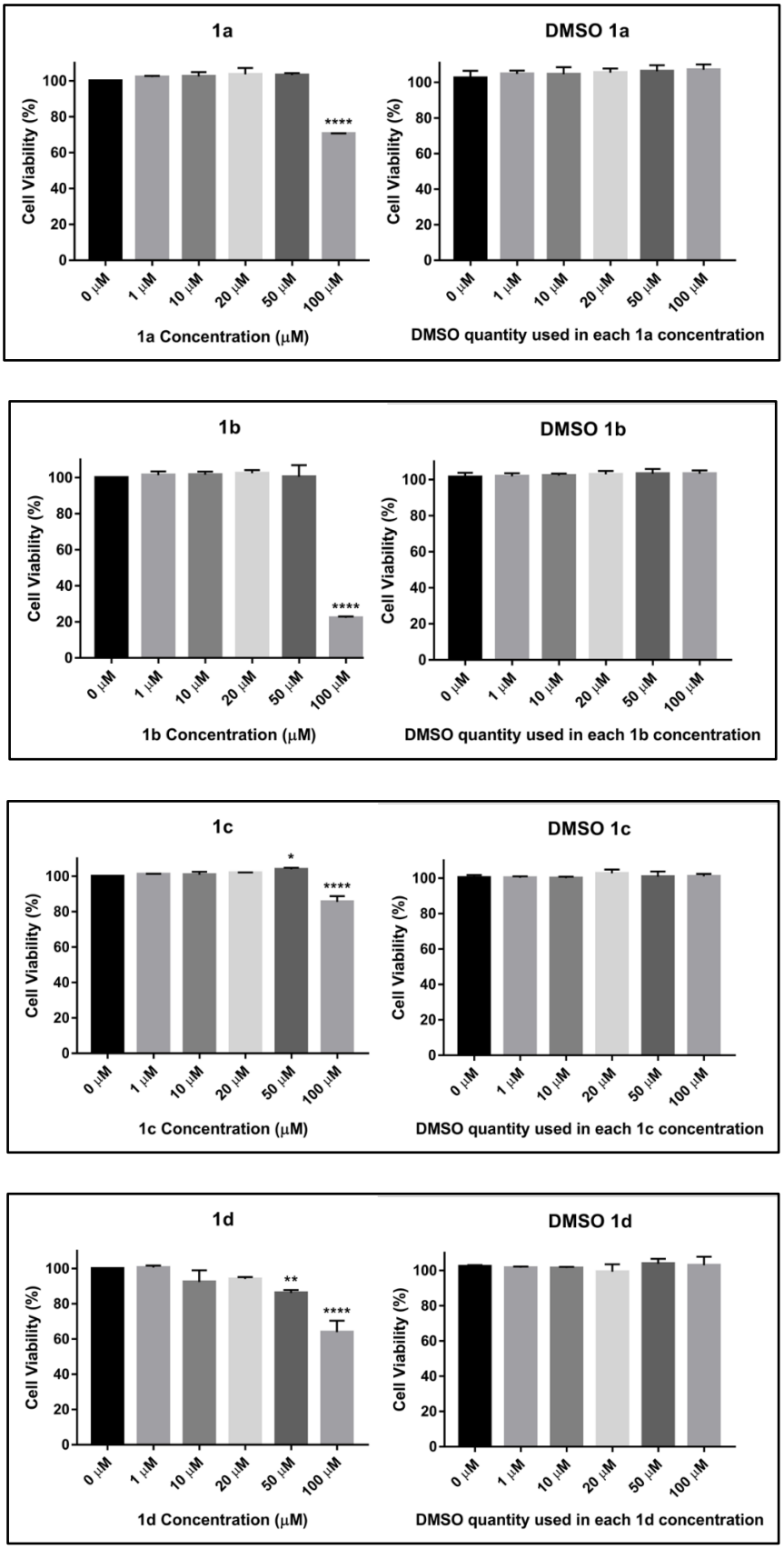

Figure 20: Results of cell viability assays with pyrazoles from Group 1, **1a**, **1b**, **1c** and **1d,** and respective DMSO controls assessed with the resazurin method. The graphs show mean values and

respective standard deviations for cell viability values. Samples size: **1a** n= 3; **1b** n=4; **1c** n=3; **1d** n=3). The graphs show mean values and respective standard deviations. Statistical analysis was performed by comparing cell viability mean values of each condition (pyrazole or DMSO) with the viability mean values of the respective negative control. All the results were normally distributed, so one-way Anova tests were performed to verify the existence of differences, and the Brown–Forsyth test was performed to ensure homogeneity of sample variances. When differences were found to exist, Dunn's multiple comparisons were then applied to assess between which groups and the control such differences existed. It is considered that * corresponds to a p-value < 0,05, ** to a p-value <0,01, *** to a p-value <0,001 and **** to a p-value < 0,0001.

Relatively to the second Group of pyrazoles including **2a** and **3a** (**Figure 21**), they present cell viability values of approximately 100% for all the concentrations, so they seem to be no cytotoxic. This way **2a** and **3a** seems to be the safest ones for human cells even in at 100 µM. The respective DMSO controls do not show either difference between groups, so the DMSO quantities used in the pyrazole stocks' preparation are not affecting the cell viability of the experiments.

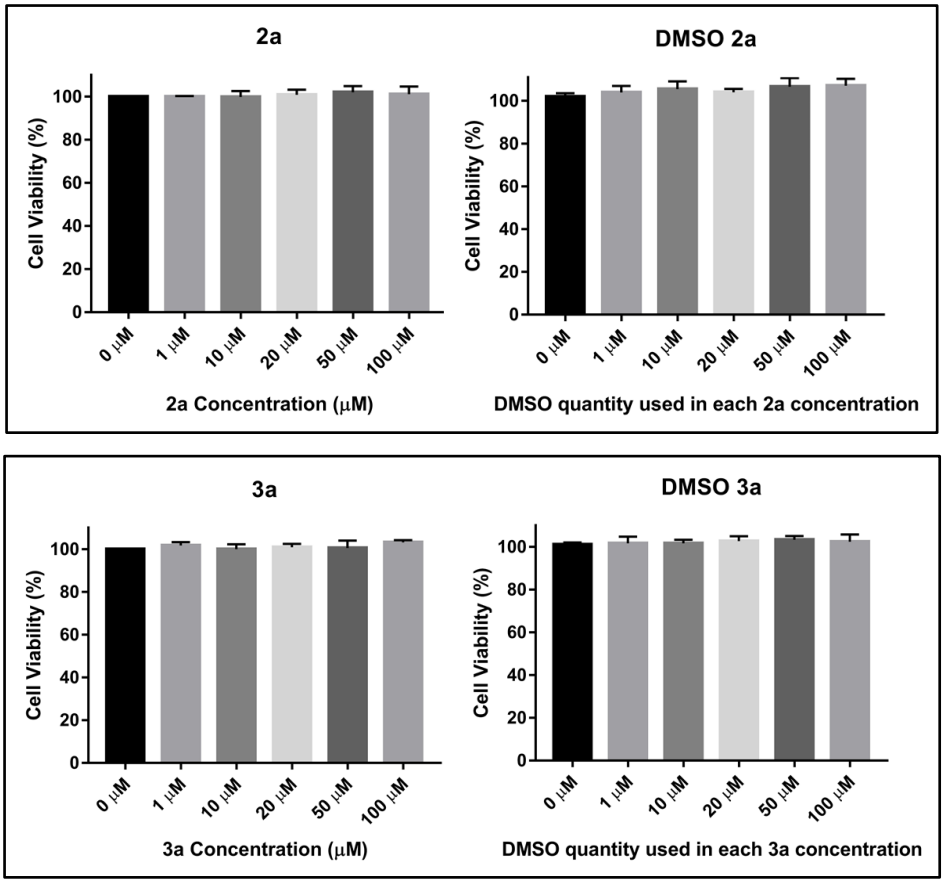

Figure 21: Results of cell viability assays with Group 2 pyrazoles, **2a** and **3a**, and respective DMSO controls assessed with the resazurin method. Samples size: **2a** n=3; **3a** n=4. The graphs show mean values and respective standard deviations. Statistical analysis was performed by comparing the cell viability mean values of each condition (pyrazole or DMSO) with the viability mean values of the respective negative control. All the results were normally distributed, so one-way Anova tests were performed to verify the existence of differences, and the Brown–Forsyth test was performed to ensure homogeneity of sample variances. When differences were found to exist, Dunn's multiple comparisons were then applied to assess between which groups and the control such differences existed. It is considered that * corresponds to a p-value < 0,05, ** to a p-value <0,01, *** to a p-value <0,001 and **** to a p-value < 0,0001.

For the third group, with pyrazoles **4a** and **4b** (**Figure 22**), it is possible to observe two different behaviors. In **4a**, it is possible to observe a progressive reduction in cell viability, similarly to what we saw previously in **1d**. We saw statistically very significant differences (p-value < 0.001 and p-value < 0.0001) earlier from 10 µM onwards. At the concentration 1µM, viability levels are 98.56%, at 10 µM 94.29%, at 20 µM 87.89%, at

50 µM 76.14% and finally at 100 µM 32.65% what represents a viability reduction of 67.35%.

On the other hand, in **4b** it is possible to observe a reducing cell viability profile like **1a**, **1b** and **1c,** where in concentrations 1 µM, 10 µM, 20 µM and 50 µM there is a viability value around 100% and the reduction only happens in concentration 100 µM. In this case, this reduction is the biggest one, being 53.41% with a viability value of 46.59%.

The DMSO controls do not show either difference between groups, so the DMSO quantities used in the pyrazole stocks' preparation are not affecting the cell viability of the experiments.

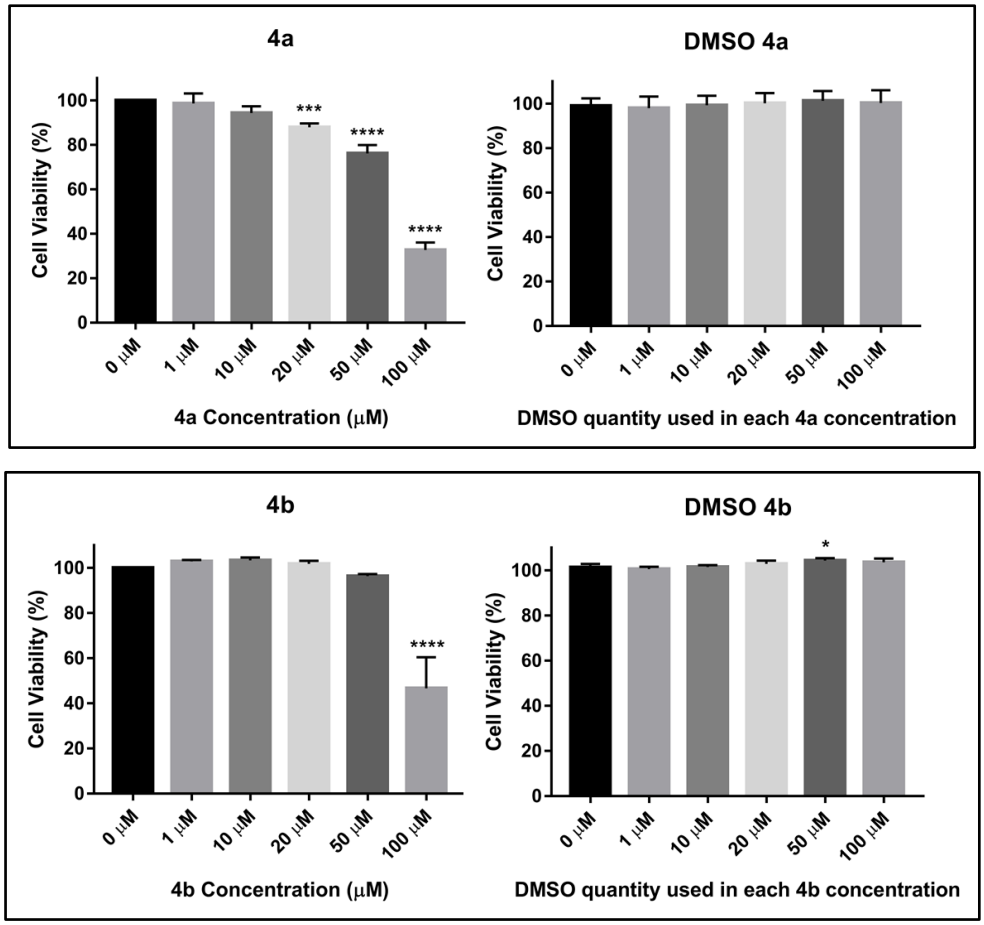

Figure 22: Results of cell viability assays with Group 3 pyrazoles, **4a** and **4b** and respective DMSO controls assessed with the resazurin method. Samples size: **4a** n=4; **4b** n=4. The graphs show mean values and respective standard deviations. Statistical analysis was performed by comparing the cell viability mean values of each condition (pyrazole or DMSO) with the viability mean values of the respective negative control. For the pyrazole experiences of **4a** and **4b** and for DMSO controls of **4a**, results were normally distributed, so one-way Anova tests were performed to verify the existence of differences, and the Brown–Forsyth test was

performed to ensure homogeneity of sample variances. When differences were found to exist, Dunn's multiple comparisons were then applied to assess between which groups and the control such differences existed. For the DMSO control values of **4a**, the were not normal so, it was performed a Kruskal-Wallis to check for differences and when differences were found to exist, Dunn's multiple comparisons test was then applied to assess between which groups and the control such differences existed. It is considered that * corresponds to a p-value < 0,05, ** to a p-value <0,01, *** to a p-value <0,001 and **** to a p-value < 0,0001.

3.5.2. Protein H2A.X quantification results

To evaluate the DNA Damage, it was evaluated intracellular protein H2A.X levels, a biomarker of DNA Damage, in particular DSBs. For this purpose, SDS-page followed by Western-Blot was performed for compounds **1a**, **1c**, **2a**, **3a** and **4b** that seemed to be the most promising, taking into account the previous results.

After the proteins had been separated by electrophoresis on an acrylamide gel, they were transferred to a nitrocellulose membrane, to which all the protein detection and quantification procedures were applied. We started by carrying out a staining with Ponceau S and acquiring the images in a transilluminator. Then, the membrane was blocked and incubated with the appropriate antibodies and reagents until it was revealed in a chemiluminescence device where the images were acquired. After analysis of the images with the BioRad software, calculations were performed to determine the concentration of H2A.X present in the samples. The negative control containing only cells and culture medium was assigned the arbitrary value of 1, and the concentration of H2A.X of the other conditions was calculated relatively to this. At least three samples were quantified for each compound.

In the first group (**Figure 23**), the bigger revelation is for compound **1a** which, in cell viability tests with resazurin seemed to be safe up to a concentration of 50 µM and only showed a drop in viability at 100 µM, while results here reveal that at 50 µM there is already DNA Damage with values roughly similar to damage values at 100 µM, about 2.3 times higher than the control. However, these differences are not statistically significant, and more replicas would be necessary to confirm these results.

Relatively to **1c**, the results seem to agree with those observed in the resazurin assays, where there was no damage to cells up to 20 µM of the compound, in 50 µM there

was already a small effect, and in 100 µM was a slightly larger effect but quite statistically significant. Here, something similar is observed, with the intracellular values of H2AX protein remaining around 1 to 1 µM, 10 µM and 20 µM, increasing slightly to 1.64 in 50 µM and then to 3 time higher with statistical significance in 100 µM.

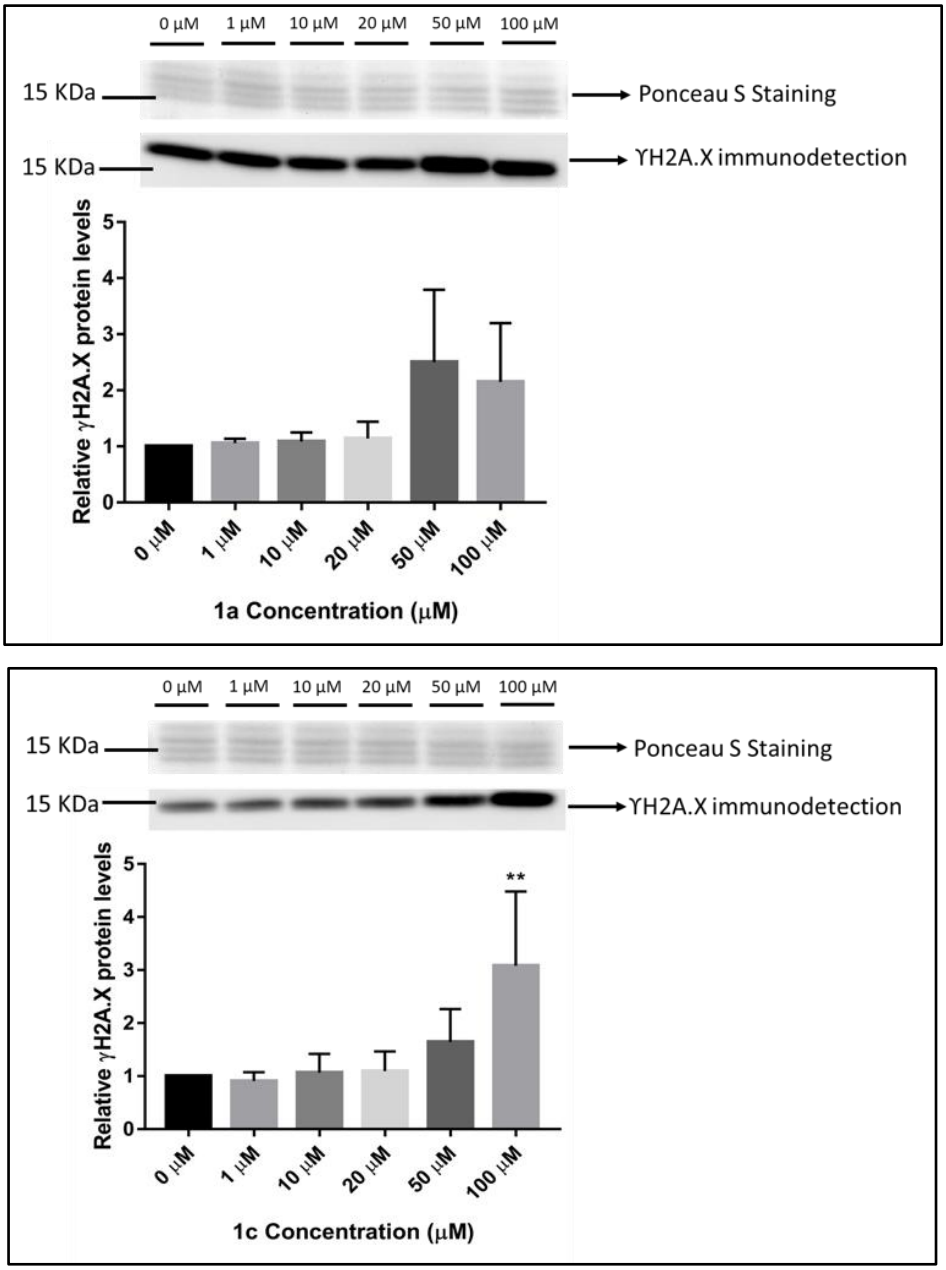

Figure 23: Results of relative ϒH2A.X protein levels assessed by Western Blotting for Group 1 pyrazoles. Samples size: **1a** n=3; **1c** n=3). The graphs show mean values and respective standard deviations. Statistical analysis was performed by comparing protein levels quantified for each concentration with the protein levels quantified for the respective negative control. For all, results were normally distributed, so one-way Anova tests were performed to verify the

existence of differences, and the Brown–Forsyth test was performed to ensure homogeneity of sample variances. When differences were found to exist, Dunn's multiple comparisons were then applied to assess between which groups and the control such differences existed. It is considered that * corresponds to a p-value < 0,05, ** to a p-value <0,01, *** to a p-value <0,001 and **** to a p-value < 0,0001

In the second group (**Figure 24**), with **2a** and **3a**, DNA damage values seem to be generally in agreement with resazurin test once that this histone values seems to be quite close to each other and it does not seem to exist differences between control values and conditions values. However, it is possible to observe a slight concentration-dependent increase of H2A.X levels, but always under 2 time higher than the control. In **2a**, values are 1.32, 1.40, 1.30, 1.76 and 1.78 and in **3a** 0.93, 1.07, 1.09, 1.41 and 1.68 for 1 µM, 10 µM, 20 µM, 50 µM and 100 µM, respectively. However, it is possible to note that, although in the resazurin assays the viability was 100% in all concentrations, here we already observe around 1.7 times more DNA damage at the concentrations 100 µM compared to the control.

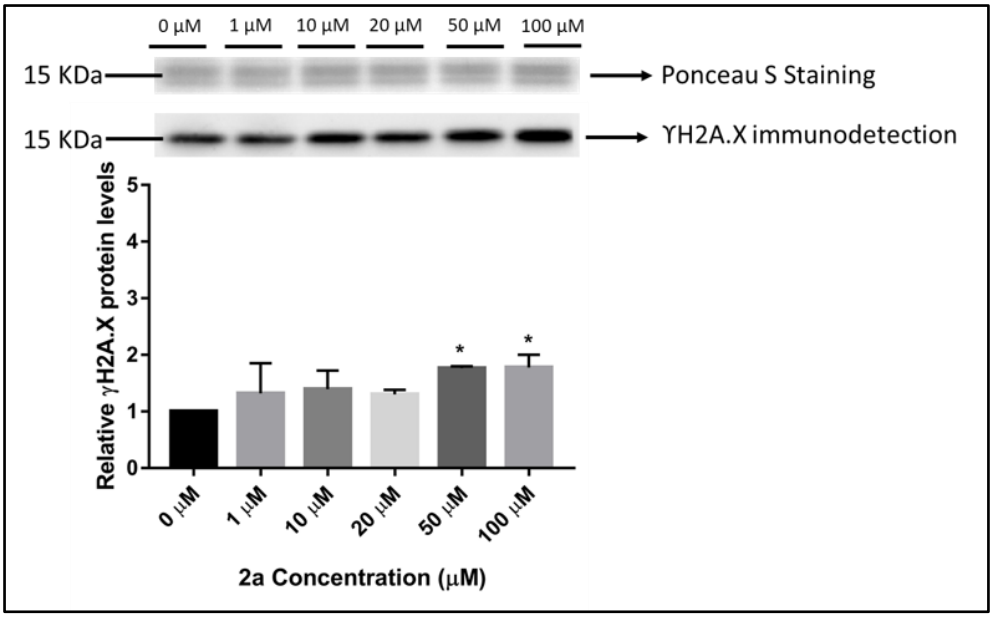

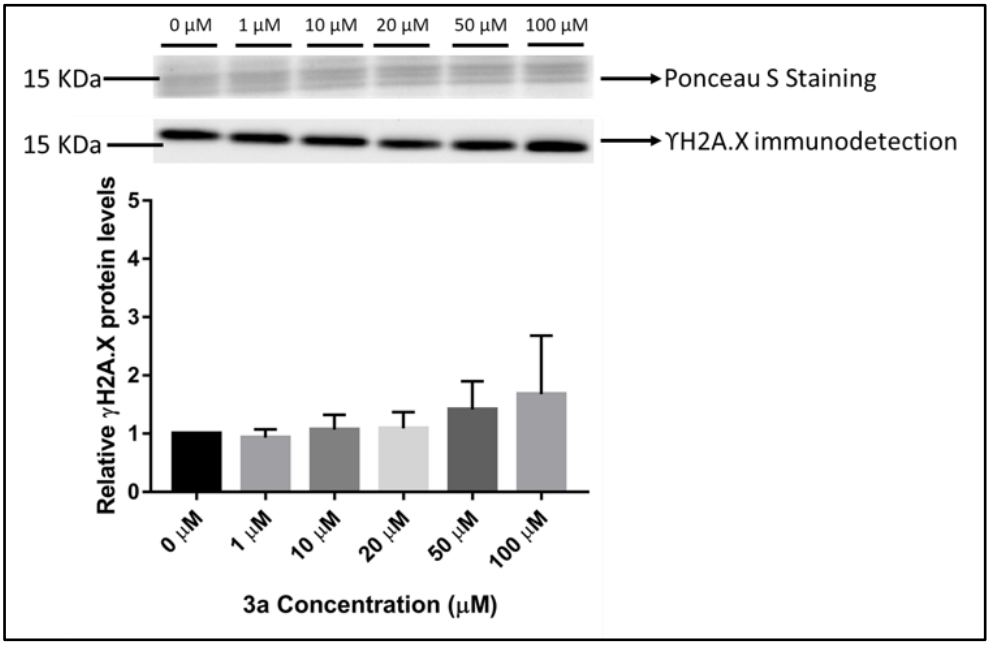

Figure 24: Results of relative ϒH2A.X protein levels assessed by Western Blotting for the second pyrazoles group. Samples size: **2a** n=3; **3a** n=3. The graphs show mean values and respective standard deviations. Statistical analysis was performed by comparing protein levels quantified for each concentration with the protein levels quantified for the respective negative control. For **2a**, results were normally distributed, so one-way Anova tests were performed to verify the existence of differences, and the Brown–Forsyth test was performed to ensure homogeneity of sample variances. When differences were found to exist, Dunn's multiple comparisons were then applied to assess between which groups and the control such differences existed. For **3a**, the results were not normal so, it was performed a Kruskal-Wallis to check for differences and when differences were found to exist, Dunn's multiple comparisons test was applied to assess between which groups and the control such differences existed. It is considered

that * corresponds to a p-value < 0,05, ** to a p-value <0,01, *** to a p-value <0,001 and **** to a p-value < 0,0001

In the third group (**Figure 25**), only compound **4b** was analyzed, which in the resazurin assay had been shown to be toxic only at 100 µM with a reduction in cell viability at this concentration around 50%. Here, looking at the results of histone quantification, we can confirm that there are only statistically significant differences in the highest concentration, but yet it is possible to observe a slight increase in the remaining ones as well. Values for H2A.X quantification are 1.20, 1.63, 2.03, 4.31 and 7.48 time for 1 µM, 10 µM, 20 µM, 50 µM and 100 µM, respectively.

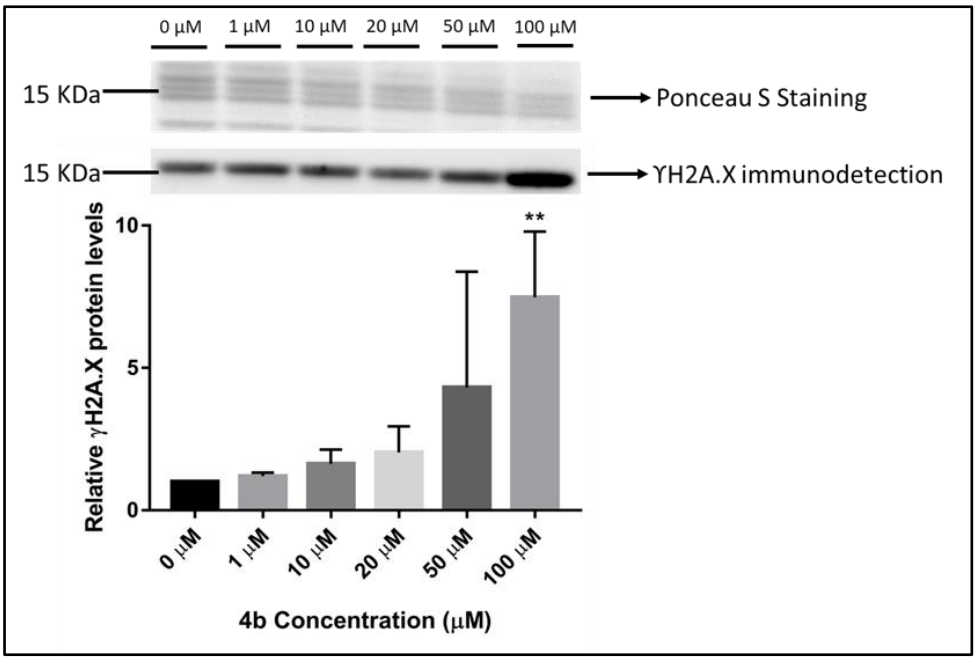

Figure 25: Results of relative ϒH2A.X protein levels assessed by Western Blotting for the third pyrazoles group, **4b**. Samples size: **4b** n=3. The graphs show mean values and respective standard deviations. Statistical analysis was performed by comparing protein levels quantified for each concentration with the protein levels quantified for the respective negative control. Results were normally distributed, so one-way Anova tests were performed to verify the existence of differences, and the Brown–Forsyth test was performed to ensure homogeneity of sample variances. When differences were found to exist, Dunn's multiple comparisons were then applied to assess between which groups and the control such differences existed. It is considered that * corresponds to a p-value < 0,05, ** to a p-value <0,01, *** to a p-value <0,001 and **** to a p-value < 0,0001.

3.6. Discussion

From cell viability tests it was possible to observe that 4-styrylpyrazoles from group 1 in general are non-cytotoxic, namely **1a**,**1b,1c**, with exception of pyrazole **1d** containing the trifluoromethyl group at the *ortho*-position that was cytotoxic at 50 µM concentration. The other derivatives **1a**,**1b,1c** showed cytotoxicity only at the 100 µM concentration, being pyrazole **1c**, that contains a methoxy group at the *para*-position, the less toxic (**Figure 26**).

The alkylated 4-styrylpyrazoles belonging to group 2 (**2a**, **3a**) were non-cytotoxic even at the higher concentration of 100 µM, so they seem to be the safest one for cells at all the tested concentrations.

Regarding the 5-styrylpyrazoles from group 3, **4a** has shown to be more cytotoxic than **4b**, which contains a methoxy group at the *para*-position. A similar behavior was observed for 4-styrylpyrazoles since compound **1c** (R =4-OCH_3) was less cytotoxic than **1a** (R = H) (**Figure 26**).

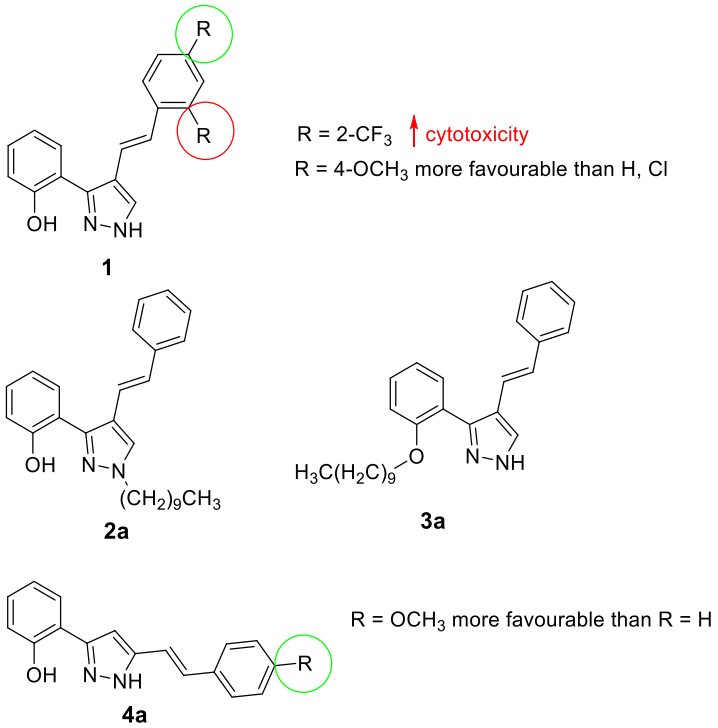

Figure 26: Structure-activity relationship studies (SARS) of the tested pyrazoles

The γH2A.X protein quantification was performed only for compounds **1a**, **1c**, **2a**, **3a** and **4b** and, in general, the quantification results agree with the results obtained in the resazurin assay, except for compound **1a** that exhibited significant DNA damage at

the 50 µM concentration while it seemed to the safe at this concentration in the resazurin method. This means that, even if the cells are metabolically viable, they may already show some damage, so it is important to carry out studies as complete as possible to prove the safety of the compounds.

For compounds **2a** and **3a** was not observed a significant DNA damage even at the higher concentration, confirming that these compounds seem to be safe for use *in vivo*. For compound **4b**, the results are in agreement with those observed in the resazurin method since the compound caused DNA damage only at the highest concentration of 100 µM.

Therefore, it was possible to observe that, although compounds **1b** and **1d** include halogenated substituents that are widely included in drugs on the market and, therefore, of proven safety, they present some toxicity at higher concentrations, especially **1d**, that exhibits trifluoromethyl in the *ortho*-position and proved to be more cytotoxic than the compounds of the same family containing other substituents in the *para*-position, or than the unsubstituted compound (**1a**).

It was also possible to observe that interesting results were obtained for compounds that contain the methoxy group in the *para*-position, **1c** and **4b**. This methoxy group, a strongly electron-donating group, had already been recognized as having antioxidant properties, so this feature may help to explain the promising results observed herein.

Finally, for groups containing alkyl chains that may contribute to increase lipophilicity and the ability to cross the blood-brain barrier (a feature that may be interesting as future drugs with action on the CNS), the results were similar for the two compounds **2a** and **3a**, despite the fact that they have substituents in different positions of the molecule, so the fact that an OH group or an NH group, both electron donors, are free to interact, does not seem to interfere with cell viability.

CHAPTER 4

CONCLUSION

CHAPTER 4: CONCLUSION

4.1. Final Conclusions

The results obtained in this study allowed to conclude that styrylpyrazoles may be promising compounds for use to counteract oxidative stress and neurodegeneration. At the end of this study, it was possible to confirm that the studied compounds present very low cytotoxicity for HeLa cells and it was also possible to identify the better substituent groups, among the studied ones, for decorating the pyrazole scaffold in order to get non-cytotoxic compounds.

The main conclusions to be drawn are: i) the toxicity of pyrazole compounds appears to be dose-dependent, occurring mainly at higher doses of the compounds; ii) 4-styrylpyrazoles appeared to be in general less cytotoxic than 5-styrylpyrazoles; iii) trifluoromethyl in the *ortho*-position (**1d**) seems to be more cytotoxic than compounds of the same family containing other substituents in the *para*-position or than the unsubstituted compound (**1a**); iv) compounds with methoxy group in the *para*-position (**1c**, **4b**) seem to be less cytotoxic than the compound with other substituent in the *ortho*-position or than the unsubstituted compound (**1a**); v) the safest compounds, since they do not shown cytotoxicity at any of the tested concentrations, are the 4-styrylpyrazoles containing carbon chains, pyrazoles **2a** and **3a**.

Finally, it is important to note that these studied doses were defined based on the literature but, as this study is preliminary, it is not possible to know whether the therapeutic doses would be above or below these toxic doses appears to be, which requires further studies to assess whether this toxicity will be important in a therapeutic context.

4.2. Future Perspectives

In the future. we consider that the follow-up of this experimental work should start by performing protein H2A.X levels quantification of the compounds that have not been performed in this work by Western blotting from the samples that have already been collected. At the same time, we also consider that should be done more Western Blot

replicas of the compounds that have already been performed, to make the results more consistent and reduce the standard deviations. Then, to strengthen the results obtained in viability tests, other proteins, namely cell integrity associated proteins, such as actin or tubulin, should also be analyzed.

Based on all these cytotoxic related results, the selection of the compounds that seem to be safer for the cells and the respective safe concentrations should be done to continue the work with it. At that moment, we also suggest changing the experimental model and starting to use a model of bigger biological relevance, such as neuronal cells.

After completing all these cytotoxicity studies, tests of the compounds' capacity to reverse oxidative stress and DNA damage that were also planned for this project should be carried out, namely induce oxidative stress in neuronal cells using hydrogen peroxide and analyze the capacity of the selected compounds to reverse that stress using the indicated commercial kit, and induce DNA damage using the bleomycin model and evaluate the recovery by ϒH2A.X levels quantification.

CHAPTER 5

EXPERIMENTAL SECTION

CHAPTER 5: EXPERIMENTAL SECTION

5.1. General

Reagents and solvents were purchased as reagent-grade and used without further purification unless otherwise stated. Melting points were determined with a Büchi melting point B-540 apparatus and are uncorrected. NMR spectra were recorded with 300 or 500 MHz [300.13 MHz (^{1}H), 75.47 MHz (^{13}C), or 500.16 MHz (^{1}H), 125.77 MHz (^{13}C)] Bruker Avance III NMR spectrometers with tetramethylsilane (TMS) as the internal reference and with $CDCl_3$ as the solvent, unless otherwise stated. Chemical shifts (δ) are quoted relative to TMS. Unequivocal ^{13}C assignments were made on the basis of 2D gHSQC (^{1}H/^{13}C) and gHMBC (delays for one-bond and long-range *J*C/H couplings were optimised for 145 and 7 Hz, respectively) experiments. Positive-ion electrospray (ESI^{+}) mass spectra were performed using a linear ion trap mass spectrometer LXQ (ThermoFinnigan, San Jose, CA). Data acquisition and analysis were performed using the Xcalibur Data System (version 2.0, ThermoFinnigan, San Jose, CA). High-mass-resolving ESI-MS were conducted in a Q-Exactive® hybrid quadrupole Orbitrap® mass spectrometer (Thermo Fisher Scientific, Bremen, Germany). The instrument was operated in positive mode, with a spray voltage at 3.0 kV and interfaced with a HESI II ion source. The analysis was performed through direct infusion of the prepared solutions at a flow rate of 10 μL min^{-1} into the ESI source and the operating conditions were as follows: sheath gas (nitrogen) flow rate 5 (arbitrary units); auxiliary gas (nitrogen) 1 (arbitrary units); capillary temperature 320°C, and S-lens rf level 50. Spectra were analyzed using the acquisition software Xcalibur ver. 4.0 (Thermo Scientific, San Jose, CA, USA).

5.2. Synthesis procedures

5.2.1. Synthesis of (*E*)-3-styryl-4*H*-chromen-4-ones

5.2.1.1. Synthesis of (E)-3-(4-methoxystyryl)-4H-chromen-4-one (7a)

A mixture of 4-oxo-4*H*-chromene-3-carbaldehyde **5** (3.45 mmol), 4-methoxyphenylacetic acid **6a** (2.87 g, 17.3 mmol) and potassium *tert*-butoxide (*t*-BuOK) (0.58 g, 5.18 mmol) in dry pyridine (30 mL) was heated at 120 ºC for 24 h. After that period, the reaction mixture was cooled to room temperature and poured into H_2O and ice (25 mL) and the pH adjusted to 2 with a solution of HCl (10%). The pale-yellow precipitate was separated by filtration, dissolved in $CHCl_3$, washed with H_2O, dried with anhydrous Na_2SO_4, and purified by column chromatography with CH_2Cl_2 as eluent. The (*E*)-3-(4-methoxystyryl)-4*H*-chromen-4-one (**7a**) was obtained in 45% yield.

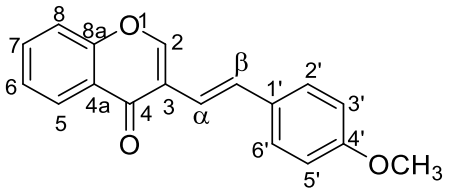

(*E*)-3-(4-Methoxystyryl)-4*H*-chromen-4-one (**7a**) (45%, 436.2mg). yellow solid. **^{1}H NMR (300.13 MHz, $CDCl_3$)** δ = 8.30 (dd, *J* = 8.0, 1.7 Hz, 1H, H-5), 8.10 (d, *J* = 0.8 Hz, 1H, H-2), 7.67 (ddd, *J* = 8.6, 7.1, 1.7 Hz, 1H, H-7), 7.55 (d, *J* = 16.0 Hz, 1H, H-β), 7.47 (d, *J* = 8.8 Hz, 2H, H-2',6'), 7.49-7.40 (m, 2H, H-6,8), 6.90 (d, *J* = 8.8Hz, 2H, H-2',6'), 6.87 (dd, *J* = 16.0, 0.8 Hz, 1H, H-α), 3.83 (s, 3H, 4'-OC<u>H</u>$_3$) ppm. **^{13}C NMR (75.47 MHz, $CDCl_3$)** δ = 176.8 (C-4), 159.5 (C-4'), 155.9 (C-8a), 152.5 (C-2), 133.5 (C-7), 131.2 (C-β), 130.2 (C-1'), 127.9 (C-2",6"), 126.3 (C-5), 125.2 (C-6), 124.1 (C-4a), 122.2 (C-3), 118.1 (C-8), 116.8 (C-α), 114.1 (C-3',5'), 55.3 (4'-O<u>C</u>H$_3$) ppm.

5.2.1.2. Synthesis of (E)-3-styryl-4H-chromen-4-one (7b)

A mixture of 4-oxo-4*H*-chromene-3-carbaldehyde **5** (600 mg, 3.45 mmol), phenylacetic acid **6b** (2.35 g, 17.3 mmol) and potassium *tert*-butoxide (*t*-BuOK) (0.58 g, 5.18 mmol) in dry pyridine (30 mL) was heated at 120 ºC for 24 h. After that period, the reaction mixture was cooled to room temperature and poured into H_2O and ice (25 mL) and the pH adjusted to 2 with a solution of HCl (10%). The pale-yellow precipitate was separated

by filtration, dissolved in $CHCl_3$, washed with H_2O, dried with anhydrous Na_2SO_4 and purified by column chromatography with CH_2Cl_2 as eluent. The (*E*)-3-styryl-4*H*-chromen-4-one was obtained in a moderate yield (49%).

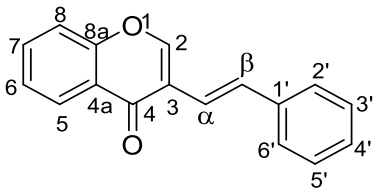

(*E*)-3-Styryl-4*H*-chromen-4-one (**7b**) (49%, 417.7 mg). mp. 163-165 ºC. (168-169 ºC, Lit.)[166].

5.2.2. Synthesis of (*E*)-3(5)-(2-hydroxyphenyl)-4-styryl-1*H*-pyrazoles

5.2.2.1. Synthesis of (E)-3(5)-(2-hydroxyphenyl)-4-styryl-1H-pyrazole (1a)

Hydrazine hydrate (0.30 mL, 3.36 mmol) was added to a solution of the (*E*)-3-styryl-4*H*-chromen-4-one (417.7 mg, 1.68 mmol) in MeOH (100 mL). The reaction mixture was stirred at room temperature, under nitrogen atmosphere until complete consumption of the starting material was observed by TLC. The mixture was then poured into $CHCl_3$ (100 mL) and washed with acidified H_2O (pH 5). The organic layer was dried over anhydrous Na_2SO4, the solvent was evaporated to dryness, and the solid residue was purified by column chromatography using $CHCl_3$ as eluent. The residue obtained after solvent evaporation was recrystallized from a mixture of CH_2Cl_2/cyclohexane.

Styrylpyrazoles **2a** and **3a** were prepared starting from pyrazole **1a** obtained in this experiment. Therefore, its full structural characterization was not performed. For biological assays was used the sample of the styrylpyrazole **1a** available in the laboratory. Melting point was determined and the sample was also analyzed by mass spectrometry.

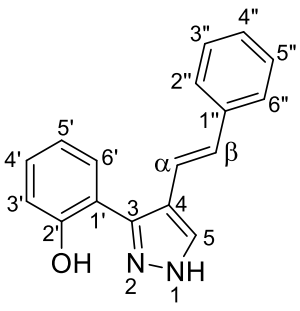

(*E*)-3(5)-(2-hydroxyphenyl)-4-styryl-1*H*-pyrazole (**1a**) (95%, 440.7 mg), light beige solid, mp. (144.5-145.0 ºC). **^{1}H NMR (300.13 MHz, $CDCl_3$)** δ = 7.84 (s, 1H, H-5), 7.62 (dd, *J* = 7.8, 1.7 Hz, 1H, H-6'), 7.52 – 7.43 (m, 2H, H-2",6"), 7.41 – 7.32 (m, 2H, H-3",5"), 7.31 – 7.23 (m, 3H, H-4',4"), 7.16 (d, *J* = 16.2 Hz, 1H, H-α), 7.08 (dd, *J* = 8.2, 1.3 Hz, 1H, H-3'), 6.96

(dt, *J* = 7.5, 1.3 Hz, 1H, H-5'), 6.90 (d, *J* = 16.2 Hz, 1H, H- β) ppm. **MS (ESI$^+$) m/z (%)**: 263.2 [(M+H)$^+$, 100]. **HRMS (ESI$^+$) m/z** calcd for $C_{17}H_{15}N_2O$, 263.1179 [M+H]$^+$; found: 263.1175.

5.2.2.2. Synthesis of (E)-3(5)-(2-hydroxyphenyl)-4-(4-methoxystyryl)-1H-pyrazole (1c)

Hydrazine hydrate (0.28 mL, 3.10 mmol) was added to a solution of the (*E*)-3-(4-methoxystyryl)-4*H*-chromen-4-one (**7a**) (431.7 mg, 1.55 mmol) in MeOH (90 mL). The reaction mixture was stirred at room temperature, under nitrogen atmosphere for 3h50min. The mixture was then poured into $CHCl_3$ (100 mL) and washed with acidified H_2O (pH 5). The organic layer was dried over anhydrous Na_2SO_4, the solvent was evaporated to dryness, and the solid residue was purified by column chromatography using $CHCl_3$ as eluent. The residue obtained after solvent evaporation was recrystallized from a mixture of CH_2Cl_2/cyclohexane.

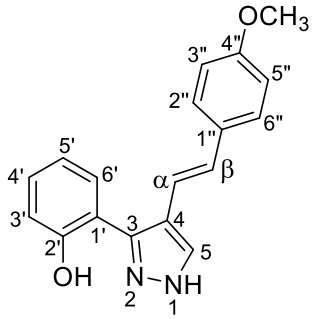

(*E*)-3(5)-(2-hydroxyphenyl)-4-(4-methoxystyryl)-1*H*-pyrazole (**1c**) (95%, 430.5 mg), white solid, mp. (157.3-157.8 °C). **^{1}H NMR (300.13 MHz, $CDCl_3$)** δ = 7.82 (s, 1H, H-5), 7.64 (dd, 1H, *J* = 7.8, 1.6 Hz, 1H, H-6'), 7.41 (d, 2H, *J* = 8.8 Hz, H-2",6"), 7.27 (ddd, *J* = 8.0, 7.7, 1.6 Hz, 1H, H-4'), 7.07 (dd, *J* = 8.2, 1.3 Hz, 1H, H-3'), 7.02 (d, *J* = 16.2 Hz, 1H, H-α), 7.05-6.98 (m, 1H, H-5'), 6.91 (d, *J* = 8.8 Hz, 2H, H-3",5"), 6.84 (d, 1H, *J* = 16.2 Hz, H-β), 3.84 (s, 3H, 4"-OC<u>H</u>$_3$) ppm. **MS (ESI$^+$) m/z (%):** 293.3 [(M+H)$^+$, 100]. **HRMS (ESI$^+$) m/z** calcd for $C_{18}H_{17}N_2O_2$, 293.1285 [M+H]$^+$; found: 293.1288.

5.2.3. Synthesis of (*E*)-3(5)-[(2-decyloxy)phenyl]-4-styryl-1*H*-pyrazole (3a)

Potassium carbonate (0.68 g, 4.92 mmol) and decyl bromide (0.51 mL, 2.40 mmol) were added to a solution of (*E*)-3(5)-(2-hydroxyphenyl)-4-styryl-1*H*-pyrazole (0.42 g, 1.60 mmol) in acetone (80 mL). The mixture was refluxed with stirring for 24 h. After, the

mixture was cooled to room temperature, the potassium carbonate was filtered off and washed with acetone (2 x 10 mL). The solvent was evaporated to dryness and the residue was taken in $CHCl_3$ and purified by thin layer chromatography using a 9:1 mixture hexane:AcOEt as eluent. Two main compounds have been isolated; the (*E*)-1-decyl-3-(2-hydroxyphenyl)-4-styryl-1*H*-pyrazole **2a** and (*E*)-3(5)-[(2-decyloxy)phenyl]-4-styryl-1*H*-pyrazole **3a** which were obtained as oils in 60% and 15% yields, respectively.

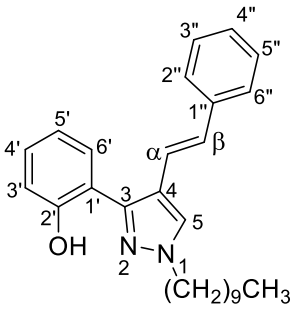

(*E*)-1-decyl-3-(2-hydroxyphenyl)-4-styryl-1*H*-pyrazole (**2a**), light beige solid, mp 56.2-57.2 (Lit 50-51ºC)[151]**. ^{1}H NMR (300.13 MHz, $CDCl_3$)** δ = 10.45 (s, 1H, 2'-OH), 7.64 (s, 1H, H-5), 7.60 (dd, *J* = 7.7, 1.7 Hz, 1H, H-6'), 7.46 (d, *J* = 7.1 Hz, 2H, H-2",6"), 7.35 (dd, *J* = 7.8, 7.3 Hz, 2H, H-3",5"), 7.29 – 7.20 (m, 2H, H-4',4"), 7.16 (d, *J* = 16.2 Hz, 1H, H-α), 7.06 (dd, *J* = 8.2, 1.3 Hz, 1H, H-3'), 6.93 (dt, *J* = 7.7, 1.3 Hz, 1H, H-5'), 6.84 (d, *J* = 16.2 Hz, 1H, H-β), 4.14 [t, *J* = 7.1 Hz, 2H, $NCH_2(CH_2)_8CH_3$], 1.92 [quint, *J* = 7.4 Hz, 2H, $NCH_2CH_2(CH_2)_7CH_3$], 1.68 – 1.03 [m, 14H, $NCH_2CH_2(CH_2)_7CH_3$], 0.87 [t, *J* = 6.7 Hz, 3H, $N(CH_2)_9CH_3$] ppm. **^{13}C NMR (75.47 MHz, $CDCl_3$)** δ = 155.8 (C-2'), 147.3 (C-3), 137.5 (C-1"), 129.2 (C-β), 129.1 (C-4'), 128.8 (C-3",5"), 128.23 (C-6'), 128.15 (C-5), 127.5 (C-4"), 126.2 (C-2",6"), 119.4 (C-5'), 119.3 (C-α), 118.3 (C-4), 117.7 (C-1'), 116.9 (C-3'), 52.5 [$NCH_2(CH_2)_8CH_3$], 31.9 [$N(CH_2)_7CH_2CH_2CH_3$], 30.1 [$NCH_2CH_2(CH_2)_7CH_3$], 29.53, 29.45, 29.3, 29.1 [$N(CH_2)_3(CH_2)_4(CH_2)_2CH_3$], 26.6 [$N(CH_2)_2CH_2(CH_2)_6CH_3$], 22.7 [$N(CH_2)_8CH_2CH_3$], 14.1 [$N(CH_2)_9CH_3$] ppm. **MS (ESI$^+$) m/z (%):** 403.4 [$(M+H)^+$, 100]. **HRMS (ESI$^+$) m/z:** calculated for $C_{27}H_{35}N_2O$, 403.2744 $[M+H]^+$; found: 403.2737.

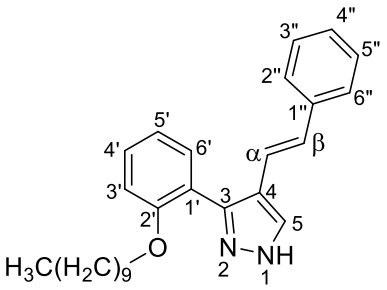

(*E*)-3(5)-[(2-decyloxy)phenyl]-4-styryl-1*H*-pyrazole (**3a**) (15%, 96.6 mg), light yellow oil[151]. **^{1}H NMR (300.13 MHz, $CDCl_3$)** δ = 7.90 (s, 1H, H-5), 7.52 (dd, *J* = 7.6, 1.7 Hz, 1H, H-6'), 7.47 – 7.41 (m, 2H, H-2",6"), 7.41 – 7.27 (m, 3H, H-3",4",5"), 7.25 – 7.18 (m, 1H, H-4'), 7.11 – 6.99 (m, 3H, H-3',5',β), 6.94 (d, *J* = 16.3 Hz, 1H, H-α), 4.06 [t, *J* = 6.6 Hz, 2H, $OCH_2(CH_2)_8CH_3$], 1.81 [quint, *J* = 6.7 Hz, 2H, $OCH_2CH_2(CH_2)_7CH_3$], 1.45-1.24 [m, 14H, $OCH_2CH_2(CH_2)_7CH_3$], 0.87 [t, *J* = 6.6 Hz,

3H, $O(CH_2)_9C\underline{H}_3$] ppm. **^{13}C NMR (75.47 MHz, $CDCl_3$)** δ = 156.1 (C-2'), 137.8 (C-3), 137.1 (C-5), 136.3 (C-1"), 130.7 (C-6'), 129.8 (C-4'), 128.6 (C-3",5"), 128.0 (C-β), 127.1 (C-4"), 126.1 (C-2",6"), 121.1 (C-5'), 120.1 (C-α), 118.2 (C-4), 118.0 (C-1'), 112.6 (C-3'), 68.9 [$O\underline{C}H_2(CH_2)_8CH_3$], 31.9 [$O(CH_2)_7\underline{C}H_2CH_2CH_3$], 29.7, 29.5, 29.5, 29.3 and 29.2 [$OCH_2\underline{C}H_2CH_2(\underline{C}H_2)_4(CH_2)_2CH_3$], 26.1 [$O(CH_2)_2\underline{C}H_2(CH_2)_6CH_3$], 22.6 [$O(CH_2)_8\underline{C}H_2CH_3$], 14.1 [$OCH_2(CH_2)_8\underline{C}H_3$] ppm. **MS (ESI$^+$) m/z (%):** 403.4 [$(M+H)^+$, 100]. **HRMS (ESI$^+$) m/z:** calculated for $C_{27}H_{35}N_2O$, 403.2744 $[M+H]^+$; found: 403.2739.

5.2.4. Synthesis of 2-acetylphenyl cinnamate (9)

To a solution of 2'-hydroxyacetophenone **8** (2 mL, 16.6 mmol) in CH_2Cl_2 (100 mL) were added cinnamic acid **9** (2.96 g, 19.9 mmol), DCC (4.12 g, 19.9 mmol) and 4-PPy (0.30 g, 1.99 mmol). The mixture was stirred at room temperature for 6 days. After that period, the reaction mixture was filtered, and the solid was washed with CH_2Cl_2. The solvent was partially evaporated, and the product was purified by column chromatography using CH2Cl2 as eluent. The 2-acetylphenyl cinnamate **10** was isolated in moderate yield.

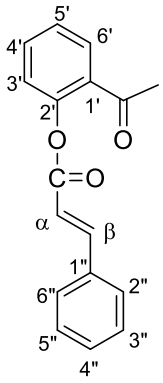

2-Acetylphenyl cinnamate (**10**), white solid (50%, 2.22 g).

This compound is an intermediate of the synthesis of pyrazole **4a** and therefore its full structural characterization was not performed.

5.2.5. Synthesis of (*E*)-1-(2-hydroxyphenyl)-5-phenylpent-4-ene-1,3-dione

To a solution of 2-acetylphenyl cinnamate **10** (2.22 g, 8.35 mmol) in DMSO (20 mL) was added potassium hydroxide (2.34 g, 41.75 mmol). The reaction mixture was stirred at room temperature under nitrogen atmosphere until complete consumption of the starting material was observed. After that period, the mixture was poured into H_2O and ice and acidified to pH = 2 with a solution of HCl (10%). The formed precipitate was filtered, dissolved in $CHCl_3$, washed with water, and dried over anhydrous Na_2SO_4. After solvent

evaporation, the (*E*)-1-(2-hydroxyphenyl)-5-phenylpent-4-ene-1,3-dione (**11a**) was isolated in very good yield.

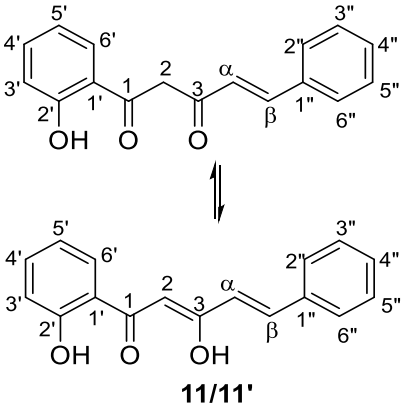

(*E*)-1-(2-hydroxyphenyl)-5-phenylpent-4-ene-1,3-dione (**11a/11a'**) (94%, 2.09 g).

This compound is an intermediate of the synthesis of pyrazole **4a** and therefore its full structural characterization was not performed.

5.2.6 Synthesis of (*E*)-3(5)-(2-hydroxyphenyl)-5(3)-styryl-1*H*-pyrazole (4a)

To a solution of (*E*)-1-(2-hydroxyphenyl)-5-phenylpent-4-ene-1,3-dione (**11a**) (2.09 g, 7.86 mmol) in MeOH (250 mL) was added hydrazine hydrate (4.38 mL, 62.9 mmol). The reaction mixture was stirred at room temperature under nitrogen atmosphere for 24 h. After that period, the reaction mixture was concentrated and then poured into $CHCl_3$ (100 mL) and washed with acidified H_2O (pH 5). The organic layer was dried over anhydrous Na_2SO_4, the solvent was evaporated, and the solid residue was purified by column chromatography using $CHCl_3$ as eluent. The residue obtained after solvent evaporation was recrystallized from a mixture of CH_2Cl_2/cyclohexane. The (*E*)-3(5)-(2-hydroxyphenyl)-5(3)-styryl-1*H*-pyrazole (**4a**) was obtained in moderate yield.

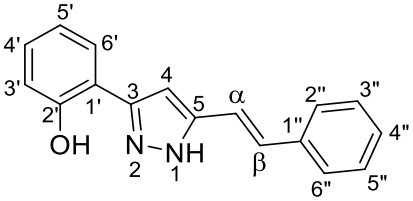

(*E*)-3(5)-(2-hydroxyphenyl)-5(3)-styryl-1*H*-pyrazole (**4a**) (42%, 865.9 mg). White cristalline solid, mp. (126.5-127.6 ºC) (Lit. 120-121 ºC)[158]. **^{1}H NMR (300.13 MHz, $CDCl_3$)** δ = 10.79 (br s, 1H, 2'-OH), 10.13 (br s, 1H, NH), 7.60 (dd, 1H, 7.8, 1.7 Hz, 1H, H-6'), 7.54 – 7.46 (m, 2H, H-2",6"), 7.44 – 7.29 (m, 3H, H-3",4",5"), 7.27 – 7.21 (m, 1H, H-4'), 7.11 (d, *J* = 16.5 Hz, 1H, H-β), 7.04 (dd, *J* = 8.2, 1.2 Hz, 1H, H-3'), 6.97 (d, *J* = 16.5 Hz, 1H, H-α), 6.94 (dt, 1H, *J* = 7.5, 1.2 Hz, H-5'), 6.81 (s, 1H, H-4) ppm. **MS (ESI$^+$)**

m/z (%): 263.2 [$(M+H)^+$, 100]. **HRMS (ESI^+) m/z:** calculated for $C_{17}H_{15}N_2O$, 263.1179 $[M+H]^+$; found: 293.1174.

5.2.7. Synthesis of (*E*)-3(5)-(2-hydroxyphenyl)-5(3)-(4-methoxystyryl)-1*H*-pyrazole (4b)

To a solution of (*E*)-1-(2-hydroxyphenyl)-5-(4-methoxyphenyl)pent-4-ene-1,3-dione (0.97 g, 3.26 mmol) in MeOH (100 mL) was added hydrazine hydrate (2.33 mL, 26.1 mmol). The reaction mixture was stirred at room temperature under nitrogen atmosphere for 24 h. After that period, the reaction mixture was concentrated and then poured into $CHCl_3$ (100 mL) and washed with acidified H_2O (pH 5). The organic layer was dried over anhydrous Na_2SO_4, the solvent was evaporated, and the solid residue was purified by column chromatography using $CHCl_3$ as eluent. The residue obtained after solvent evaporation was recrystallized from a mixture of CH_2Cl_2/cyclohexane. The (*E*)-3(5)-(2-hydroxyphenyl)-5(3)-(4-methoxystyryl)-1*H*-pyrazole (**4b**) was obtained in low yield.

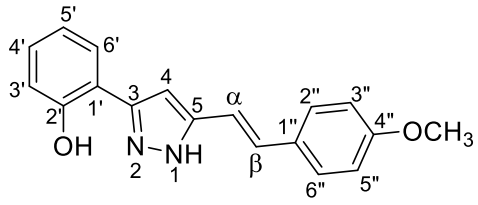

(*E*)-3(5)-(2-hydroxyphenyl)-5(3)-(4-methoxystyryl)-1*H*-pyrazole (**4b**) (15%, 147.1 mg), white solid, mp 125.1-126.3 ºC (Lit. 117-119 ºC)[158]. **^{1}H NMR (300.13 MHz, $CDCl_3$)** δ = 7.60 (dd, *J* = 7.7, 1.6 Hz, 1H, H-6'), 7.43 (d, *J* = 8.8 Hz, 2H, H-2",6"), 7.27-7.21 (m, 1H, H-4'), 7.08-7.03 (m, 1H, H-3'), 7.06 (d, *J* = 16.3 Hz, 1H, H-β), 6.93 (s, 1H, H-4), 6.91 (d, *J* = 8.8 Hz, 2H, H-3",5"), 6.83 (d, *J* = 16.3 Hz, 1H, H-α), 6.80 – 6.76 (m, 1H, H-5'), 3.84 (s, 3H, OCH_3) ppm. **^{13}C NMR (75.47 MHz, $CDCl_3$)** δ = 160.1 (C-4), 156.0 (C-2'), 152.6(C-3), 142.4 (C-5), 132.0 (C-β), 129.5 (C-4'), 128.6 (C-1"), 128.1 (C-2",6"), 126.6 (C-6'), 119.4 (C-5'), 117.1 (C-3'), 114.4 (C-3",5"), 112.1 (C- α), 99.3 (C-4), 55.4 (4"-O<u>C</u>H_3) ppm. **MS (ESI^+) m/z (%):** 293.3 $[(M+H)^+$, 100]. **HRMS (ESI^+) m/z:** calculated for $C_{18}H_{17}N_2O_2$, 293.1285 $[M+H]^+$; found: 293.1279.

5.3. Experimental data of the styrylpyrazoles 1b and 1d available in the laboratory

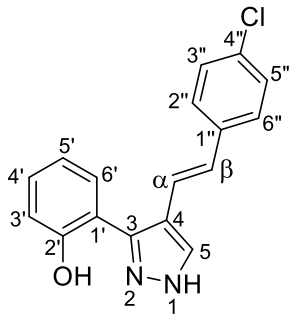

(*E*)-4-(4-chlorostyryl)-3(5)-(2-hydroxyphenyl)-1*H*-pyrazole (**1b**). White solid, mp. 170.0-170.8 ºC (Lit. 163-164 ºC)[157]. **MS (ESI$^+$) m/z (%):** 297.2 [$(M+H)^+$, ^{35}Cl, 100], 299.2 [$(M+H)^+$, ^{37}Cl, 35]. **HRMS (ESI$^+$) m/z:** calculated for $C_{17}H_{14}N_2OCl$, 297.0789 $[M+H]^+$; found: 297.0784.

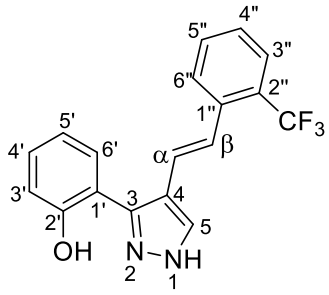

(*E*)-3(5)-(2-hydroxyphenyl)-4-(2-trifluoromethylstyryl)-1*H*-pyrazole (**1d**). Light beige solid, mp. 146.6-148.1 ºC, **MS (ESI$^+$) m/z (%):** 331.3 [$(M+H)^+$, 100]. **HRMS (ESI$^+$) m/z:** calculated for $C_{18}H_{14}N_2OF_3$, 331.1053 $[M+H]^+$; found: 331.1047.

CHAPTER 6

REFERENCES

CHAPTER 6: REFERENCES

1. Heemels M-T. Neurodegenerative diseases. Campbell P, ed. *Nat Insight*. 2016;539(7628).
2. Wyss-Coray T. Ageing, neurodegeneration and brain rejuvenation. *Nature*. 2016;539(7628):180-186. doi:10.1038/nature20411
3. Ziegler-Graham K, Brookmeyer R, Johnson E, Arrighi HM. Worldwide variation in the doubling time of Alzheimer's disease incidence rates. *Alzheimer's Dement*. 2008;4(5):316-323. doi:10.1016/J.JALZ.2008.05.2479
4. Elobeid A, Libard S, Leino M, Popova SN, Alafuzoff I. Altered proteins in the aging brain. *J Neuropathol Exp Neurol*. 2016;75(4):316-325. doi:10.1093/jnen/nlw002
5. Neumann H, Kotter MR, Franklin RJM. Debris clearance by microglia: An essential link between degeneration and regeneration. *Brain*. 2009;132(2):288-295. doi:10.1093/brain/awn109
6. Danial NN, Korsmeyer SJ. Cell Death: Critical Control Points. *Cell*. 2004;116(2):205-219. doi:10.1016/S0092-8674(04)00046-7
7. Beal MF. Mitochondrial dysfunction in neurodegenerative diseases. *Biochim Biophys Acta*. 1998;1366:211-223.
8. Lee VM-Y, Goedert M, Trojanowski JQ. Neurodegenerative Tauopathies. *Annu Rev Neurosci*. 2001;24:1121-1159.
9. Canter RG, Penney J, Tsai LH. The road to restoring neural circuits for the treatment of Alzheimer's disease. *Nature*. 2016;539(7628):187-196. doi:10.1038/nature20412
10. Abeliovich A, Gitler AD. Defects in trafficking bridge Parkinson's disease pathology and genetics. *Nature*. 2016;539(7628):207-216. doi:10.1038/nature20414
11. Barnham KJ, Masters CL, Bush AI. Neurodegenerative diseases and oxidative stress. *Nat Rev Drug Discov*. 2004;3(3):205-214. doi:10.1038/nrd1330
12. Taylor JP, Brown RH, Cleveland DW. Decoding ALS: From genes to mechanism. *Nat Insight*. 2016;539(7628):197-206. doi:10.1038/nature20413
13. Taylor JP, Hardy J, Fischbeck KH. Toxic Proteins in Neurodegenerative Disease. *Sci Compass*. 2002;296(5575):1991-1995. doi:10.1126/science.1067122

14. Mattson MP. Apoptosis in neurodegenerative disorders. *Nat Rev Mol Cell Biol*. 2000;1(2):120-129. doi:doi: 10.1038/35040009
15. Agorogiannis EI, Agorogiannis GI, Papadimitriou A, Hadjigeorgiou GM. Protein misfolding in neurodegenerative diseases. *Neuropathol Appl Neurobiol*. 2004;30(3):215-224. doi:10.1111/j.1365-2990.2004.00558.x
16. Braak H, Del Tredici K, Rüb U, De Vos RAI, Steur ENHJ, Braak E. Staging of brain pathology related to sporadic Parkinson's disease. *Neurobiol Aging*. 2003;24(2):197-211. doi:10.1016/S0197-4580(02)00065-9
17. Neumann M, Sampathu DM, Kwong LK, et al. Ubiquitinated TDP-43 in Frontotemporal Lobar Degeneration and Amyotrophic Lateral Sclerosis. *Sci Reports*. 2006;314(5796):130-133. doi:10.1126/science.1134108
18. Thal DR, Rüb U, Orantes M, Braak H. Phases of Aß-deposition in the human brain and its relevance for the development of AD. *Neurology*. 2002;58:1791-1800. doi:10.1212/WNL.58.12.1791
19. Erikson GA, Dale L. Bodian, Rueda M, et al. Whole Genome Sequencing of a Healthy Aging Cohort. *Cell*. 2016;165(4):1002-1011. doi:doi:10.1016/j.cell.2016.03.022.
20. Horvath S. DNA methylation age of human tissues and cell types. *Genome Biol*. 2013;14(10):R115. doi:10.1111/ocr.12268
21. Small SA, Schobel SA, Buxton RB, Witter MP, Barnes CA. A pathophysiological framework of hippocampal dysfunction in ageing and disease. *Nat Rev Neurosci*. 2012;12(10):585-601. doi:10.1038/nrn3085
22. Schwartz M, Shechter R. Systemic inflammatory cells fight off neurodegenerative disease. *Nat Rev Neurol*. 2010;6(7):405-410. doi:10.1038/nrneurol.2010.71
23. Hardy J, Selkoe DJ. The Amyloid Hypothesis of Alzheimer´s Disease: Progress and Problems on the Road to Therapeutics. *Sci Compass Rev Med*. 2002;297(5580):353-357.
24. Beal MF. Aging, energy, and oxidative stress in neurodegenerative diseases. *Ann Neurol*. 1995;38(3):357-366. doi:10.1002/ana.410380304
25. Pasinelli P, Brown RH. Molecular biology of amyotrophic lateral sclerosis: insights from genetics. *Nat Rev Neurosci*. 2006;7(9):710-723. doi:10.1038/nrn1971
26. Ferri CP, Prince M, Brayne C, et al. Global prevalence of dementia: a Delphi

consensus study. *Lancet*. 2005;366(9503):2112-2117. doi:10.1016/S0140-6736(05)67889-0

27. Patterson C. World Alzheimer Report 2018. The state of the art of dementia research: New frontiers. *Alzheimer's Dis Int*. 2018. doi:10.1111/j.0033-0124.1950.24_14.x
28. Du X, Wang X, Geng M. Alzheimer's disease hypothesis and related therapies. *Transl Neurodegener*. 2018;7(2):1-7. doi:10.1186/s40035-018-0107-y
29. Davies P, Maloney AJF. Selective loss of central cholinergic neurons in Alzheimer's disease. *Lancet*. 1976;25:1403. doi:10.1111/ipd.12577
30. Hardy J, Allsop D. Amyloid deposition as the central event in the aetiology of Alzheimer's disease. *Trends Pharmacol Sci*. 1991;12:383-388. doi:10.1016/0165-6147(91)90609-V
31. Frost B, Jacks RL, Diamond MI. Propagation of Tau Misfolding from the Outside to the Inside of a Cell. *J Biol Chem*. 2009;284(19):12845-12852. doi:10.1074/jbc.M808759200
32. Swerdlow RH, Khan SM. A "mitochondrial cascade hypothesis" for sporadic Alzheimer's disease. *Med Hypotheses*. 2004;63(1):8-20. doi:10.1016/j.mehy.2003.12.045
33. Martins RN, Villemagne V, Sohrabi HR, et al. Alzheimer's Disease: A Journey from Amyloid Peptides and Oxidative Stress, to Biomarker Technologies and Disease Prevention Strategies-Gains from AIBL and DIAN Cohort Studies. *J Alzheimer's Dis*. 2018;62(3):965-992. doi:10.3233/JAD-171145
34. Butterfield DA, Halliwell B. Oxidative stress, dysfunctional glucose metabolism and Alzheimer disease. *Nat Rev Neurosci*. 2019;20(3):148-160. doi:10.1038/s41583-019-0132-6
35. Bush AI, Pettingell WH, Multhaup G, et al. Rapid induction of Alzheimer Aβ amyloid formation by zinc. *Science (80-)*. 1994;265(5177):1464-1467. doi:10.1126/science.8073293
36. Osorio RS, Pirraglia E, Agüera-Ortiz LF, et al. Greater risk of Alzheimer's disease in older adults with insomnia. *J Am Geriatr Soc*. 2011;59(3):559-562. doi:10.1111/j.1532-5415.2010.03288.x
37. Mukherjee S, Mez J, Trittschuh E, et al. Genetic data and cognitively-defined late-onset Alzheimer's disease subgroups. *Mol Psichiatr*. 2019.

doi:10.1016/j.physbeh.2017.03.040

38. Hdab-Barmada M, Moossy J, Nemoto EM, Lin MR. Hyperoxia produces neuronal necrosis in the rat. *J Neuropathol Exp Neurol*. 1986;45(3):233-246.
39. Davydov BI, Drobyshev VI, Ushakov IB, Fyodorov VP. Morphological analysis of animal brain reactions to short-term hyperoxia. *Kosm Biol i Aviakosmicheskaya Meditsina*. 1988;2(2):56-62.
40. Halliwell B. Oxidative stress and neurodegeneration: where are we now? *J Neurochem*. 2006;97:1634-1658. doi:10.1111/j.1471-4159.2006.03907.x
41. Thomas DD, Ridnour LA, Isenberg JS, et al. The chemical biology of nitric oxide: Implications in cellular signaling. *Free Radic Biol Med*. 2008;45(1):18-31. doi:10.1016/j.freeradbiomed.2008.03.020
42. Martínez MC, Andriantsitohaina R. Reactive Nitrogen Species: Molecular Mechanisms and Potential Significance in Health and Disease. *Antioxidants Redox Signal*. 2009;11(3):669-702. doi:10.1089/ars.2007.1993
43. Dröge W. Free Radicals in the Physiological Control of Cell Function. *Physiol Rev*. 2002;82:47-95. doi:10.1152/physrev.00018.2001
44. Sies H. *Oxidative Stress: Introductory Remarks*. Pergamon Press Inc.; 1985. doi:10.1016/b978-0-12-642760-8.50005-3
45. Sies H. Biochemistry of Oxidative Stress. *Angew Chem Int Ed Engl*. 1986;25:1058-1071. doi:https://doi.org/10.1002/ange.19860981203
46. Sies H. Redox Biology Oxidative stress: a concept in redox biology and medicine. *Redox Biol*. 2015;4:180-183. doi:10.1016/j.redox.2015.01.002
47. Sies H. Strategies of antioxidant defense. *Eur J Biochem*. 1993;215:213-219.
48. Sies H. Strategies of antioxidant defense: relations to oxidative stress. *Signal Mech*. 1995;H 92.
49. Gandhi S, Abramov AY. Mechanism of Oxidative Stress in Neurodegeneration. *Oxid Med Cell Longev*. 2012. doi:10.1155/2012/428010
50. Trachootham D, Alexandre J, Huang P. Targeting cancer cells by ROS-mediated mechanisms: a radical therapeutic approach? *Nat Rev Drug Discov*. 2009;8(7):579-591. doi:10.1038/nrd2803
51. Andersen JK. Oxidative stress in neurodegeneration: cause or consequence? *Nat Rev Neurosci*. 2004. doi:10.1038/nrn1434
52. Shukla V, Mishra SK, Pant HC. Oxidative Stress in Neurodegeneration. *Adv*

Pharmacol Sci. 2011. doi:10.1155/2011/572634

53. Paravicini TM, Touyz RM. Redox signaling in hypertension. *Cardiovasc Res*. 2006;71:247-258. doi:10.1016/j.cardiores.2006.05.001
54. Haigis MC, Yanker BA. The Aging Stress Response. *Mol Cell*. 2010;40(2):333-344. doi:10.1016/j.molcel.2010.10.002.The
55. Halliwell B. Antioxidants and human disease: A general introduction. *Nutr Rev*. 1997;55:S44-S49. doi:10.1111/j.1753-4887.1997.tb06100.x
56. Sies H. *Oxidative Stress*. London: Academic Press; 1985.
57. Neilly PJD, Kirk SJ, Gardiner KR, Rowlands BJ. The L-arginine/nitric oxide pathway - Biological properties and therapeutic applications. *Ulster Med J*. 1994;63(2):193-200.
58. Moretti M, Rodrigues ALS. Ascorbic acid as an antioxidant and applications to the central nervous system. *Pathology*. 2020:159-167. doi:10.1016/b978-0-12-815972-9.00015-9
59. Vincent HK, Innes KE, Vincent KR. Oxidative stress and potential interventions to reduce oxidative stress in overweight and obesity. *Diabetes, Obes Metab*. 2007;9(6):813-839. doi:10.1111/J.1463-1326.2007.00692.X
60. Colton CA, Gilbert DL. Production of superoxide anions by a CNS macrophage, the microglia. *FEBS Lett*. 1987;223(2):284-288. doi:10.1016/0014-5793(87)80305-8
61. Nagappan PG, Chen H, Wang DY. Neuroregeneration and plasticity: A review of the physiological mechanisms for achieving functional recovery postinjury. *Mil Med Res*. 2020;7(30):1-16. doi:10.1186/s40779-020-00259-3
62. Pisoschi AM, Pop A, Iordache F, Stanca L, Predoi G, Serban AI. Oxidative stress mitigation by antioxidants - An overview on their chemistry and influences on health status. *Eur J Med Chem*. 2021;209(112891). doi:10.1016/j.ejmech.2020.112891
63. Gutteridge JMC. Invited review free radicals in disease processes: A compilation of cause and consequence. *Free Rad Res Comms*. 1993;19(3):141-158. doi:10.3109/10715769309111598
64. Halliwell B. Free radicals, antioxidants, and human disease: curiosity, cause, or consequence? *Lancet*. 1994;344:721-724.
65. Galasko DR, Peskind E, Clark CM, et al. Antioxidants for Alzheimer disease: A

randomized clinical trial with cerebrospinal fluid biomarker measures. *Arch Neurol*. 2012;69(7):836-841. doi:10.1001/archneurol.2012.85

66. Moosavian SP, Arab A, Paknahad Z, Moradi S. The effects of garlic supplementation on oxidative stress markers: A systematic review and meta-analysis of randomized controlled trials. *Complement Ther Med*. 2020;50(102385). doi:10.1016/j.ctim.2020.102385
67. Kim KH, Lee D, Lee HL, Kim CE, Jung K, Kang KS. Beneficial effects of Panax ginseng for the treatment and prevention of neurodegenerative diseases: past findings and future directions. *J Ginseng Res*. 2018;42(3):239-247. doi:10.1016/j.jgr.2017.03.011
68. Qin S, Huang L, Gong J, et al. Meta-analysis of randomized controlled trials of 4 weeks or longer suggest that curcumin may afford some protection against oxidative stress. *Nutr Res*. 2018;60(76):1-12. doi:10.1016/j.nutres.2018.08.003
69. Chiu HF, Venkatakrishnan K, Wang CK. The role of nutraceuticals as a complementary therapy against various neurodegenerative diseases: A mini-review. *J Tradit Complement Med*. 2020;10(5):434-439. doi:10.1016/j.jtcme.2020.03.008
70. Uddin S, Al Mamun A, Kabir T, et al. Neuroprotective role of polyphenols against oxidative stress-mediated neurodegeneration. *Eur J Pharmacol*. 2020;886(173412). doi:10.1016/j.ejphar.2020.173412
71. Ringman JM, Frautschy SA, Teng E, et al. Oral curcumin for Alzheimer's disease: Tolerability and efficacy in a 24-week randomized, double blind, placebo-controlled study. *Alzheimer's Res Ther*. 2012;4(5):43. doi:10.1186/alzrt146
72. Buettner GR. Spin Trapping - Electron-Spin-Resonance Parameters of Spin Adducts. *Free Radic Bio Med*. 1987;3(4):259-303.
73. Sies H. Hydrogen peroxide as a central redox signaling molecule in physiological oxidative stress: Oxidative eustress. *Redox Biol*. 2017;11:613-619. doi:10.1016/j.redox.2016.12.035
74. Product Data Sheet Product Data Sheet - ROS-ID® Total ROS detection kit. 2013. https://docs.rs-online.com/0501/0900766b81290203.pdf.
75. Barbosa KBF, Costa NMB, Alfenas RDCG, De Paula SO, Minim VPR, Bressan J. Estresse oxidativo: Conceito, implicações e fatores modulatórios. *Rev Nutr*. 2010;23(4):629-643. doi:10.1590/S1415-52732010000400013

76. Peterson CL, Laniel MA. Histones and histone modifications. *Curr Biol*. 2004;14(14):546-551. doi:10.1016/j.cub.2004.07.007
77. Ciccia A, Elledge JS. The DNA Damage Response: Making it safe to play with knives. *Mol Cell*. 2010;40(2):179-204. doi:10.1016/j.molcel.2010.09.019.
78. Cooper GM. The Nuclear Envelope and Traffic between the Nucleus and Cytoplasm - The Cell - NCBI Bookshelf. In: Sinauer Associates, ed. *The Cell: A Molecular Approach*. 2nd ed. Sunderland (MA); 2000. https://www.ncbi.nlm.nih.gov/books/NBK9927/. Accessed February 28, 2022.
79. Alberts B, Johnson A, Lewis J, Raff M, Roberts K, Walter P. The Cell: A Molecular Approach. In: Garland Sciences, ed. *Molecular Biology of the Cell*. 4nd ed. New York; 2002.
80. Hoeijmakers JHJ. DNA Damage, Aging, and Cancer. *N Engl J Med*. 2009;361(15):1475-1485.
81. Lindahl T, Barnes DE. Repair of endogenous DNA damage. *Cold Spring Harb Symp Quant Biol*. 2000;65:127-133. doi:10.1101/sqb.2000.65.127
82. Nakamura J, Swenberg JA. Endogenous apurinic/apyrimidinic sites in genomic DNA of mammalian tissues. *Cancer Res*. 1999;59(11):2522-2526.
83. Rothkamm K, Krüger I, Thompson LH, Löbrich M. Pathways of DNA Double-Strand Break Repair during the Mammalian Cell Cycle. *Mol Cell Biol*. 2003;23(16):5706-5715. doi:10.1128/MCB.23.16.5706-5715.2003
84. D'Adda FDF, Reaper PM, Clay-Farrace L, et al. A DNA damage checkpoint response in telomere-initiated senescence. *Nature*. 2003;426(6963):194-198. doi:10.1038/NATURE02118
85. Shimizu I, Yoshida Y, Suda M, Minamino T. DNA damage response and metabolic disease. *Cell Metab*. 2014;20(6):967-977. doi:10.1016/J.CMET.2014.10.008
86. Turgeon M-O, Perry NJS, Poulogiannis G. DNA Damage, Repair, and Cancer Metabolism. *Front Oncol*. 2018;8. doi:10.3389/fonc.2018.00015
87. Sinha RP, Häder D-P. UV-induced DNA damage and repair: a review. *Photochem Photobiol Sci*. 2002;1(4):225-236. doi:10.1039/b201230h
88. Rastogi RP, Richa, Kumar A, Tyagi MB, Sinha RP. Molecular Mechanisms of Ultraviolet Radiation-Induced DNA Damage and Repair. *J Nucleic Acids*. 2010:1-32. doi:10.4061/2010/592980

89. Sachs RK, Chen PL, Hahnfeldt PJ, Hlatky LR. DNA damage caused by ionizing radiation. *Math Biosci*. 1992;112(2):271-303. doi:10.1016/0025-5564(92)90028-U

90. Leadon SA. Repair of DNA damage produced by ionizing radiation: A minireview. *Semin Radiat Oncol*. 1996;6(4):295-305. doi:10.1016/S1053-4296(96)80025-7

91. Awang N. Genotoxic Effects on buccal Cells of Workers Exposed to Fogging Sprays during Fogging Operation. *Biomed J Sci Tech Res*. 2017;1(5). doi:10.26717/BJSTR.2017.01.000433

92. Sopian NA, Jalaludin J, Bakar SA, Hamedon TR, Latif MT. Exposure to particulate pahs on potential genotoxicity and cancer risk among school children living near the petrochemical industry. *Int J Environ Res Public Health*. 2021;18(5):1-21. doi:10.3390/IJERPH18052575

93. Morrison A, Johnson AL, Johnston LH, Sugino A. Pathway correcting DNA replication errors in Saccharomyces cerevisiae. *EMBO J*. 1993;12(4):1467-1473. doi:10.1002/j.1460-2075.1993.tb05790.x

94. Mitra S, Boldogh I, Izumi T, Hazra TK. Complexities of the DNA base excision repair pathway for repair of oxidative DNA damage. *Environ Mol Mutagen*. 2001;38(2-3):180-190. doi:10.1002/em.1070

95. Boyce KJ, Wang Y, Verma S, Shakya VPS, Xue C, Idnurm A. Mismatch repair of DNA replication errors contributes to microevolution in the pathogenic fungus Cryptococcus neoformans. *MBio*. 2017;8(3). doi:10.1128/MBIO.00595-17

96. Kunkel TA, Erie DA. Eukaryotic Mismatch Repair in Relation to DNA Replication. *Annu Rev Genet*. 2015;49:291-313. doi:doi:10.1146/annurev-genet-112414-054722

97. Caldecott KW. Single-strand break repair and genetic disease. *Nat Rev Genet*. 2008;9(8):619-631. doi:10.1038/nrg2380

98. Anindya R. Single-stranded DNA damage: Protecting the single-stranded DNA from chemical attack. *DNA Repair (Amst)*. 2020;87(102804). doi:10.1016/j.dnarep.2020.102804

99. Scully R, Panday A, Elango R, Willis NA. DNA double-strand break repair-pathway choice in somatic mammalian cells. *Nat Rev Mol Cell Biol*. 2019;20(11):698-714. doi:10.1038/S41580-019-0152-0

100. Imran SAM, Yazid MD, Cui W, Lokanathan Y. The intra- and extra-telomeric role

of trf2 in the dna damage response. *Int J Mol Sci*. 2021;22(9900). doi:10.3390/ijms22189900

101. B. Alberts, A. Johnson, J. Lewis, M. Raff, K. Roberts PW. *Molecular Biology of the Cell, 4th Ed., Garland, New York, NY, USA*.; 2002.
102. E.C. Friedberg, G.C. Walker, W. Siede, R.D. Wood, R.A. Schultz TE. DNA Repair and Mutagenesis, 2nd ed., ASM Press, Washington, DC, USA,. *2006*.
103. Sharma S. Age-related nonhomologous end joining activity in rat neurons. *Brain Res Bull*. 2007;73(1-3):48-54. doi:10.1016/j.brainresbull.2007.02.001
104. Chatterjee N, Walker GC. Mechanisms of DNA damage, repair, and mutagenesis. *Environ Mol Mutagen*. 2017;58(5):235-263. doi:10.1002/em.22087
105. Li GM. Mechanisms and functions of DNA mismatch repair. *Cell Res*. 2008;18(1):85-98. doi:10.1038/CR.2007.115
106. Krokan HE, Bjørås M. Base excision repair. *Cold Spring Harb Perspect Biol*. 2013;5(4):1-22. doi:10.1101/CSHPERSPECT.A012583
107. Spivak G. Nucleotide excision repair in humans. *DNA Repair (Amst)*. 2015;36:13-18. doi:10.1016/J.DNAREP.2015.09.003
108. Wright WD, Shah SS, Heyer WD. Homologous recombination and the repair of DNA double-strand breaks. *J Biol Chem*. 2018;293(27):10524-10535. doi:10.1074/JBC.TM118.000372
109. Rondeau S, Vacher S, De Koning L, et al. ATM has a major role in the double-strand break repair pathway dysregulation in sporadic breast carcinomas and is an independent prognostic marker at both mRNA and protein levels. *Br J Cancer*. 2015;112(6):1059-1066. doi:10.1038/bjc.2015.60
110. Maréchal A, Zou L. DNA damage sensing by the ATM and ATR kinases. *Cold Spring Harb Perspect Biol*. 2013;5(9):1-17. doi:10.1101/cshperspect.a012716
111. Mohammad M-A-A, Darband SG, Kaviani M, et al. DNA damage response and repair in colorectal cancer: Defects, regulation and therapeutic implications. *DNA Repair (Amst)*. 2018;69:34-52. doi:10.1016/j.dnarep.2018.07.005
112. Beal MF. Does impairment of energy metabolism result in excitotoxic neuronal death in neurodegenerative illnesses? *Ann Neurol*. 1992;31(2):119-130. doi:10.1002/ANA.410310202
113. Scandalios JG. Oxidative stress responses - what have genome-scale studies taught us? *Genome Biol*. 2002;3(7). doi:10.1186/GB-2002-3-7-REVIEWS1019

114. Yun HY, Dawson VL, Dawson TM. Neurobiology of Nitric Oxide. *Crit Rev trade Neurobiol*. 1996;10(3-4):291-316. doi:10.1615/CRITREVNEUROBIOL.V10.I3-4.20

115. Emerit J, Edeas M, Bricaire F. Neurodegenerative diseases and oxidative stress. *Biomed Pharmacother*. 2004;58(1):39-46. doi:10.1016/j.biopha.2003.11.004

116. Madabhushi R, Pan L, Tsai LH. DNA damage and its links to neurodegeneration. *Neuron*. 2014;83(2):266-282. doi:10.1016/j.neuron.2014.06.034

117. Moura M De, Houten B Van. Mechanisms of DNA Damage, Repair, and Mutagenesis. *Environ Mol Mutagen*. 2017;58:235-263. doi:10.1002/em

118. Andreazza AC, Frey BN, Valvassori SS, et al. DNA damage in rats after treatment with methylphenidate. *Prog Neuro-Psychopharmacology Biol Psychiatry*. 2007;31(6):1282-1288. doi:10.1016/J.PNPBP.2007.05.012

119. Liu HG, Wang Y, Lian L, Xu LH. Tributyltin induces DNA damage as well as oxidative damage in rats. *Environ Toxicol*. 2006;21(2):166-171. doi:10.1002/TOX.20170

120. Angelis KJ, Velemínský J, Rieger R, Schubert I. Repair of bleomycin-induced DNA double-strand breaks in Vicia faba. 1989;212(2):155-157. doi:10.1016/0027-5107(89)90066-3

121. Cadet J, Davies KJA, Medeiros MH, Di Mascio P, Wagner JR. Formation and repair of oxidatively generated damage in cellular DNA. *Free Radic Biol Med*. 2017;107:13-34. doi:10.1016/j.freeradbiomed.2016.12.049

122. Cadet J, Douki T, Ravanat JL. Measurement of oxidatively generated base damage in cellular DNA. *Mutat Res Mol Mech Mutagen*. 2011;711(1-2):3-12. doi:10.1016/J.MRFMMM.2011.02.004

123. Ide H, Kow YW, Chen B-X, Erlanger BF, Wallace SS. Antibodies to oxidative DNA damage: Characterization of antibodies to 8-oxopurines. *Cell Biol Toxicol*. 1997;13:405-417.

124. Ostling O, Johanson KJ. Microelectrophoretic study of radiation-induced DNA damages in individual mammalian cells. *Biochem Biophys Res Commun*. 1984;123(1):291-298. doi:10.1016/0006-291X(84)90411-X

125. Tu WZ, Li B, Huang B, et al. γH2AX foci formation in the absence of DNA damage: Mitotic H2AX phosphorylation is mediated by the DNA-PKcs/CHK2 pathway. *FEBS Lett*. 2013;587(21):3437-3443.

doi:10.1016/J.FEBSLET.2013.08.028

126. Rybak P, Hoang A, Bujnowicz L, et al. Low level phosphorylation of histone H2AX on serine 139 (γH2AX) is not associated with DNA double-strand breaks. *Oncotarget*. 2016;7(31):49574-49587. doi:10.18632/ONCOTARGET.10411
127. Gonzalez-Hunt CP, Wadhwa M, Sanders LH. DNA damage by oxidative stress: Measurement strategies for two genomes. *Curr Opin Toxicol*. 2018;7:87-94. doi:10.1016/j.cotox.2017.11.001
128. Katritzky AR, Rees CW. Comprehensive Heterocyclic Chemistry. *Compr Heterocycl Chem*. 2009;1-7:1-7180. doi:10.1016/C2009-0-15932-9
129. Aggarwal R, Kumar V, Kumar R, Singh SP. Approaches towards the synthesis of 5-aminopyrazoles. *Beilstein J Org Chem*. 2011;7:179-197. doi:10.3762/bjoc.7.25
130. Kumar V, Aggarwal R, Tyagi P, Singh SP. Synthesis and antibacterial activity of some new 1-heteroaryl-5-amino-4- phenyl-3-trifluoromethylpyrazoles. *Eur J Med Chem*. 2005;40(9):922-927. doi:10.1016/j.ejmech.2005.03.021
131. Kumar V, Kaur K, Gupta GK, Gupta AK, Kumar S. Developments in Synthesis of the Anti-inflammatory Drug, Celecoxib: A Review. *Recent Pat Inflamm Allergy Drug Discov*. 2013;7(2):124-134. doi:10.2174/1872213X11307020004
132. Knorr L,. Einwirkung von Acetessigester auf Hydrazinchinizin derivative. *Chem. Ber*. 1883; 17:546-552.
133. Wiley RH, Wiley P. *Chemistry of Heterocyclic Compounds: Pyrazolones, Pyrazolidones, and Derivatives*. Vol 20. Wiley, New York: John Wiley & Sons, Inc.; 1964. doi:10.1002/9780470186817
134. Knorr L. *Chem. Ber*. 1884;17(546):2032.
135. Khan MF, Alam MM, Verma G, Akhtar W, Akhter M, Shaquiquzzaman M. The therapeutic voyage of pyrazole and its analogs: A review. *Eur J Med Chem*. 2016;120:170-201. doi:10.1016/j.ejmech.2016.04.077
136. Faria JV, Vegi PF, Miguita AGC, dos Santos MS, Boechat N, Bernardino AMR. Recently reported biological activities of pyrazole compounds. *Bioorganic Med Chem*. 2017;25(21):5891-5903. doi:10.1016/j.bmc.2017.09.035
137. Ansari A, Ali A, Asif M, Shamsuzzaman. Review: biologically active pyrazole derivatives. *New J Chem*. 2016;41(1):16-41. doi:10.1039/c6nj03181a
138. Küçükgüzel G, ŞenkardeŞ S. Recent advances in bioactive pyrazoles. *Eur J Med Chem*. 2015;97(1):786-815. doi:10.1016/j.ejmech.2014.11.059

139. Kumar V, Kaur K, Gupta GK, Sharma AK. Pyrazole containing natural products: Synthetic preview and biological significance. *Eur J Med Chem*. 2013;69:735-753. doi:10.1016/j.ejmech.2013.08.053
140. Gomes PMO, Ouro PMS, Silva AMS, Silva VLM. Styrylpyrazoles: Properties, Synthesis and Transformations. *Molecules*. 2020;25(24):5886. doi:10.3390/molecules25245886
141. Sherin DR, Rajasekharan KN. Mechanochemical Synthesis and Antioxidant Activity of Curcumin-Templated Azoles. *Arch Pharm (Weinheim)*. 2015;348(12):908-914. doi:10.1002/ardp.201500305
142. Sharma S, Ying Z, Gomez-Pinilla F. A pyrazole curcumin derivative restores membrane homeostasis disrupted after brain trauma. *Exp Neurol*. 2010;226(1):191-199. doi:10.1016/J.EXPNEUROL.2010.08.027
143. Lapchak PA, Boitano PD. Effect of the Pleiotropic Drug CNB-001 on Tissue Plasminogen Activator (tPA) Protease Activity in vitro: Support for Combination Therapy to Treat Acute Ischemic Stroke. *J Neurol Neurophysiol*. 2014;5:214-219. doi:10.4172/2155-9562-5-1000214
144. Das J, Pany S, Panchal S, Majhi A, Rahman GM. Binding of isoxazole and pyrazole derivatives of curcumin with the activator binding domain of novel protein kinase C. *Bioorg Med Chem*. 2011;19(21):6196-6202. doi:10.1016/J.BMC.2011.09.011
145. Narlawar R, Pickhardt M, Leuchtenberger S, et al. Curcumin-Derived Pyrazoles and Isoxazoles: Swiss Army Knives or Blunt Tools for Alzheimer's Disease? *ChemMedChem*. 2008;3(1):165-172. doi:10.1002/CMDC.200700218
146. Gavande NS, Vandervere-Carozza PS, Hinshaw HD, et al. DNA repair targeted therapy: the past or future of cancer treatment? *Pharmacol Ther*. 2016;160:65-83. doi:10.1016/j.pharmthera.2016.02.003.DNA
147. Stover EH, Konstantinopoulos PA, Matulonis UA, Swisher EM. Biomarkers of response and resistance to DNA repair targeted therapies. *Clin Cancer Res*. 2016;22(23):5651-5660. doi:10.1158/1078-0432.CCR-16-0247
148. Neher TM, Shuck SC, Liu J, Zhang J-T, Turchi JJ. Identification of novel small molecule inhibitors of the XPA protein using in silico based screening. *ACS Chem Biol*. 2010;5(10):953-965. doi:10.1021/cb1000444
149. Hosseinimehr SJ, Fathi M, Ghasemi A, Shiadeh SNR, Pourfallah TA. Celecoxib

mitigates genotoxicity induced by ionizing radiation in human blood lymphocytes. *Res Pharm Sci*. 2017;12(1):82-87. doi:10.4103/1735-5362.199051

150. Datar P, Deokule T. Development of Thiadiazole as an Antidiabetic Agent - A Review. *Mini-Reviews Med Chem*. 2014;14(2):136-153. doi:10.2174/1389557513666140103102447
151. Silva VLM, Silva AMS, Pinto DCGA, et al. Synthesis and pharmacological evaluation of new (E)- and (Z)-3-aryl-4-styryl-1H-pyrazoles as potential cannabinoid ligands. *Arkivoc*. 2010;2010(10):226-247. doi:10.3998/ark.5550190.0011.a19
152. Perevalov VP, Baryshnenkova LI, Sheban G V., et al. Spectral peculiarities of isomeric trans-styrylpyrazoles. 1990;8:1061-1064.
153. Garg V, Kumar P, Verma AK. Chemo-, regio-, and stereoselective n-alkenylation of pyrazoles/ benzpyrazoles using activated and unactivated alkynes. *J Org Chem*. 2017;82(19):10247-10262. doi:10.1021/acs.joc.7b01746
154. Correia C, Braga S, Cardoso S, Silva A, Silva V. Antioxidant activity of (styryl)pyrazoles and preliminary structure-activity relationship studies. In: *XXIV Encontro Luso-Galego de Química, Faculdade de Ciências Da Universidade Do Porto, 21-23 Novembro de 2018, Porto, QS16*.
155. Silva VLM, Silva AMS, Pinto DCGA, Cavaleiro JAS, Patonay T. Condensation of chromone-3-carboxaldehyde with phenylacetic acids: An efficient synthesis of (E)-3-styrylchromones. *Synlett*. 2004;15:2717-2720. doi:10.1055/s-2004-835660
156. Silva VLM, Silva AMS, Pinto DCGA, Cavaleiro JAS, Elguero J. Novel (E)- and (Z)-3(5)-(2-hydroxyphenyl)-4-styrylpyrazoles from (E)- and (Z)-3-styrylchromones: the unexpected case of (E)-3(5)-(2-hydroxyphenyl)-4-(4-nitrostyryl)pyrazoles. *Tetrahedron Lett*. 2007;48(22):3859-3862. doi:10.1016/j.tetlet.2007.03.147
157. Silva VLM, Silva AMS, Pinto DCGA, Cavaleiro JAS, Elguero J. Synthesis of (E)- and (Z)-3(5)-(2-hydroxyphenyl)-4-styrylpyrazoles. *Monatshefte fur Chemie*. 2009;140(1):87-95. doi:10.1007/s00706-008-0002-9
158. Silva VLM, Silva AMS, Pinto DCGA, Cavaleiro JAS, Elguero J. 3(5)-(2-Hydroxyphenyl)-5(3)-styrylpyrazoles: Synthesis and diels - Alder transformations. *European J Org Chem*. 2004;3(21):4348-4356. doi:10.1002/ejoc.200400407
159. Silva VLM. Síntese e transformação de 5-estiril-3-(2-hidroxifenil)pirazóis. 2002.

Dissertação de Mestrado. Universidade de Aveiro.

160. Carreira ARF, Pereira DM, Andrade PB, et al. Novel styrylpyrazole-glucosides and their dioxolo-bridged doppelgangers: Synthesis and cytotoxicity. *New J Chem*. 2019;43(21):8299-8310. doi:10.1039/c9nj01021a
161. Timm M, Saaby L, Moesby L, Hansen EW. Considerations regarding use of solvents in in vitro cell based assays. *Cytotechnology*. 2013;65(5):887-894. doi:10.1007/s10616-012-9530-6
162. Chen X, Thibeault S. Effect of DMSO concentration, cell density and needle gauge on the viability of cryopreserved cells in three dimensional hyaluronan hydrogel. *Proc Annu Int Conf IEEE Eng Med Biol Soc EMBS*. 2013:6228-6231. doi:10.1109/EMBC.2013.6610976
163. Fields RD, Lancaster M V. Dual-attribute continuous monitoring of cell proliferation/cytotoxicity. *Am BiotechLab*. 1993;11(4):48-50.
164. Zalata AA, Lammer Tijn N, Christophe A, Comhaire FH. The correlates and alleged biochemical background of the resazurin reduction test in semen. *Int J Androl*. 1998;21(5):289-294. doi:10.1046/j.1365-2605.1998.00126.x
165. Ramussen E. Use of fluorescent redox indicators to evaluate cell proliferation and viability. *In Vitr Mol Toxicol*. 1999;12(1):47-58.
166. Sandulache A, Silva AMS, Pinto DCGA, Almeida LMPM, Cavaleiro JAS. Wittig reactions of chromone-3-carboxaldehydes with benzylidenetriphenyl phosphoranes: A new synthesis of 3-styrylchromones. *New J Chem*. 2003;27(11):1592-1598. doi:10.1039/b303554a

APPENDIX

APPENDIX

Appendix 1 - Reagents Preparation for Biological Studies (Chapter 3)

1.1. Reagents For cell Assays

PBS 1X: Each pack of BupH Modified Dulbecco's Phosphate Buffered Saline Packs (Thermo Fisher Scientific) was dissolved in 500ml deionized water, filtered in a laminar flow chamber with a 0.2µm pore filter and stored at 4°C.

Complete Culture Medium: In a flow chamber, to Dulbecco's modified Eagle medium (DMEM (1X)); Gibco) was added 10% inactivated fetal bovine serum (FBS; Gibco) and 1% antibiotic and antimycotic (Gibco), and then it was stored at 4ºC.

Pyrazoles' Stocks: For each of the eight pyrazoles, a 10 mM stock in DMSO (Dimethyl Sulfoxide for cell culture; Panreac AppliChem, ITW Reagents) was prepared and stored at 4°C. Diverse tested concentrations were prepared from this stock by dilution in fresh culture medium to obtain the required concentrations 10, 20, 50 and 100µM.

DMSO Controls Stocks: The DMSO percentage present in each of the final conditions explained above was calculated. DMSO Control Stocks were prepared with such percentages of DMSO (Dimethyl Sulfoxide for cell culture; Panreac AppliChem, ITW Reagents) in fresh culture medium (without pyrazole), namely 0.01%, 0.1%, 0.2%, 0.5% and 1%, respectively for 10, 20, 50 and 100 µM of pyrazole conditions.

Resazurin 1% Solution: 0.1mg/ml of resazurin sodium salt (Sigma Aldrich) was dissolved in PBS 1X, pH was adjusted to 7.40, the solution was filtered in a laminar flow chamber with a 0.2µm pore filter (Fisherbrand) and stored at 4°C.

1.2. Reagents For SDS-Page

SDS 10%: Dissolve 0.1 g of SDS for each 1 ml of distilled water. Store at room temperature.

SDS 1%: Dilute the above solution in distilled water in a 1:10 ratio. Store at room temperature.

APS 10%: Dissolve 0.1 g of APS for each 1 ml of distilled water. Store at room temperature for up to a week or freeze.

Tris 1M: For 1 L dissolve 121.2 g of Tris base in distilled water, adjust pH to 6.8 and store at 4ºC.

Tris-Glycine 10X: For 1 L dissolve 30.3g of Tris 250 mM and 144.1 g of Glycine 1.92 M in distilled water and store at 4ºC (the pH should be 8.3 and no adjustment is required).

Lower Gel Buffer (LGB) 4X: For 1 L, dissolve 181.65g of Tris in a part of distilled water until complete dissolution, then adjust the volume to 1 L and the pH to 8.9, and store at 4°C.

Upper Gel Buffer (UGB) 4X: For 1L, dissolve 75.69 g of Tris in a part of distilled water until complete dissolution, then adjust the volume to 1 L and the pH to 6.8, and store at 4°C.

Loading Buffer (LB) 4X: For 10 mL of the LB solution, mix 2.5 mL of Tris 1M, 4.0 mL of glycerol, 1 mg of bromophenol blue, 0.8 g of SDS, 2 ml of β-mercaptoethanol in distilled water until 10 mL.

Running Buffer: For 1 L, mix 100 mL of Tris-glycine 10X and 10 mL SDS 10% and adjust the volume with distilled water to 1 L.

Transfer Buffer: For 1 L, mix 100 mL of Tris-glycine 10 X and 200 mL of methanol and adjust the volume with distilled water to 1 L.

1.3. Reagents For Western-Blotting

Block Solution: Dissolve 1g of BSA (Albumin Bovine Fraction V (BSA), nzytech) in 20 mL of TBS-T 1X.

Antibodies:

- **Primary antibody anti-ϒH2AX**: Dissolve 0.6 g of BSA in 20 mL of TBS-T 1X (3% BSA) and add 4 µL (1:500) of monoclonal mouse antibody Anti-Phospho-Histone H2AX (S139), Millipore, Thermo Fisher Scientific.
- **Secondary antibody anti-mouse**: Dissolve 1 g of powdered milk in 20 mL of TBS-T 1X (5% powered milk) and add 2 µL (1:10 000) of horseradish peroxidase-conjugated (HRP) secondary antibody anti-mouse (Cell Signaling Technology).

Ponceau S Solution: For a 100 mL final volume, dissolve 0.1 g of Ponceau S in distilled water, add 5 mL of glacial acetic acid, and complete with more distilled water to adjust the volume to 100 mL.

TBS 10X: For 1L, dissolve 12.11 g of Tris and 87.66 g of sodium chloride (NaCl) in distilled water, adjust pH to 8.0 and store at 4°C.

TBS-T 10X: For 1L, dissolve 12.11 g of Tris 1M and 87.66 g of sodium chloride (NaCl) in distilled water, add 10 mL (0.01%) of Tween-20, adjust pH to 8.0 and store at 4°C.